

# PHOSPHOKETOLASE - A MECHANISTIC UPDATE

Dissertation for the award of the degree  
"Doctor rerum naturalium"  
of the Georg-August-University Göttingen

submitted by

FABIENNE LIBUDA

born in Ostercappeln

Göttingen 2017

## **Members of the Thesis Committee**

Prof. Dr. Kai Tittmann (Reviewer)

Department of Molecular Enzymology  
Georg-August-Universität Göttingen

Prof. Dr. Ralf Ficner (Reviewer)

Department of Molecular Structural Biology  
Georg-August-Universität Göttingen

Prof. Dr. Ricardo Mata

Department of Computational Chemistry  
and Biochemistry  
Georg-August-Universität Göttingen

## **Members of the extended Examination Board**

Dr. Fabian Commichau

Department of General Microbiology  
Georg-August-Universität Göttingen

Dr. Manfred Konrad

Department of Enzyme Biochemistry  
Max Planck Institute for Biophysical Chemistry  
Göttingen

Prof. Dr. Holger Stark

Department of Structural Dynamics  
Max Planck Institute for Biophysical Chemistry  
Göttingen

Date of oral examination: 30. November 2017

Hereby I declare that the thesis entitled "Phosphoketolase - A mechanistic update" is my own work that was prepared with no other sources and aids than quoted. This thesis, or parts thereof, have not been submitted elsewhere for any academic award or qualification.

Göttingen, 30.09.2017

Fabienne Libuda

## Contents

<b>Abbreviations</b>	<b>10</b>
<b>Abstract</b>	<b>12</b>
<b>1 Introduction</b>	<b>14</b>
1.1 Biological relevance of phosphoketolase . . . . .	14
1.2 Phosphoketolase - A thiamine diphosphate-dependent enzyme . . . . .	18
1.2.1 Catalytic properties of thiamine diphosphate . . . . .	18
1.2.2 Thiamine diphosphate-dependent enzymes - Catalytic principles and structural features . . . . .	21
1.2.3 Thiamine diphosphate-dependent enzymes in biocatalysis . . . . .	23
1.3 Structure and reaction mechanism of phosphoketolase . . . . .	26
1.4 Acetyl-thiamine diphosphate as critical intermediate of enzymatic reactions . . . . .	30
1.5 Phosphoketolase and Transketolase - Similarities and differences . . . . .	31
1.6 Objective . . . . .	35
<b>2 Material and Methods</b>	<b>37</b>
2.1 Materials . . . . .	37
2.2 Molecular biology methods . . . . .	43
2.2.1 Preparation of chemical competent <i>E. coli</i> strains . . . . .	43
2.2.2 Transformation of plasmid DNA into <i>E. coli</i> . . . . .	43
2.2.3 Preparation of frozen storage cultures . . . . .	43
2.2.4 Isolation of plasmid DNA . . . . .	43
2.2.5 Site-directed mutagenesis . . . . .	44
2.2.6 Agarose gel electrophoresis . . . . .	44
2.2.7 Determination of DNA concentration . . . . .	44
2.2.8 Sequencing of plasmid DNA . . . . .	45
2.3 Protein production, purification and analysis . . . . .	45
2.3.1 Production of recombinant <i>B. breve</i> XFPK in <i>E. coli</i> . . . . .	45
2.3.2 Purification of recombinant XFPK . . . . .	45
2.3.3 Determination of protein concentration . . . . .	46
2.3.4 Sodium dodecyl sulfate polyacrylamide gel electrophoresis (SDS-PAGE) . . . . .	46



---

2.4	Biophysical methods . . . . .	47
2.4.1	UV-Vis spectroscopy . . . . .	47
2.4.2	Secondary structure analysis by circular dichroism spectroscopy . . . . .	47
2.4.3	Analysis of covalent reaction intermediates by <sup>1</sup> H-NMR spectroscopy . . . . .	47
2.5	Kinetic Methods . . . . .	48
2.5.1	Steady-state kinetic analysis . . . . .	48
2.5.2	Transient kinetic analysis using stopped-flow absorbance spectroscopy . . . . .	49
2.5.3	Steady-state analysis of the hydrolysis side reaction . . . . .	51
2.6	Analysis of carboligation products by gas chromatography-mass spectrometry . . . . .	53
2.7	Detection of transketolase activity . . . . .	54
<b>3</b>	<b>Results</b>	<b>56</b>
3.1	Spectroscopic analysis of reaction intermediates in the phosphoketolase reaction cycle . . . . .	56
3.2	Analysis of the AcThDP UV-Vis absorbance spectrum . . . . .	59
3.3	Kinetic analysis of the phosphoketolase reaction . . . . .	62
3.3.1	Development of a direct steady-state assay for phosphoketolase activity . . . . .	62
3.3.2	Transient kinetic analysis of AcThDP formation . . . . .	64
3.3.3	Transient kinetic analysis of AcThDP depletion . . . . .	68
3.3.4	pH-dependence of the phosphoketolase reaction . . . . .	70
3.4	Histidine 553 as catalyst for the tautomerization reaction? . . . . .	73
3.5	Carboligation side reactions in phosphoketolase . . . . .	75
3.5.1	Reaction of AcThDP with electrophilic acceptor substrates . . . . .	75
3.5.2	Analysis of ligation products by GC-MS . . . . .	77
3.5.3	Quantification of ligation products by GC-MS . . . . .	82
3.5.4	Testing of alternative aldehyde acceptors . . . . .	83
3.6	Generation and analysis of a "transketolase-like" phosphoketolase variant . . . . .	86
3.6.1	Characterization of XFPK <sub>N549D</sub> . . . . .	87
3.6.2	Characterization of XFPK <sub>Y501F/N549D</sub> and XFPK <sub>E437L/Y501F/N549D</sub> . . . . .	90
<b>4</b>	<b>Discussion</b>	<b>94</b>
4.1	New insights into the catalytic mechanism of phosphoketolase reveal coupling of tautomerization and acetyl-transfer by substrate-assisted catalysis . . . . .	94
4.2	Phosphoketolase exhibits carboligase activity . . . . .	105

---

4.3	Amino-acid exchanges between the active sites of phosphoketolase and transketolase do not account directly for their different catalytic activities . . . . .	111
4.4	Conclusion and outlook . . . . .	116
	<b>Appendix</b>	<b>119</b>
	<b>References</b>	<b>126</b>
	<b>Acknowledgment</b>	<b>126</b>
	<b>Curriculum vitae</b>	<b>128</b>

## List of Figures

1	Phosphoketolase reaction . . . . .	14
2	Schematic representation of the phosphoketolase pathway and the fructose 6-phosphate shunt . . . . .	16
3	Phosphoketolase based metabolic engineering strategy . . . . .	17
4	Chemical structure of thiamine diphosphate . . . . .	19
5	Activation mechanism of thiamine diphosphate . . . . .	20
6	General reaction mechanism of ThDP-dependent enzymes . . . . .	22
7	Formation of 2-hydroxyketones by ThDP-dependent enzymes . . . . .	24
8	Carboligation reactions catalyzed by ThDP-dependent enzymes . . . . .	25
9	Reaction mechanism of phosphoketolase . . . . .	27
10	Structure of <i>B. breve</i> phosphoketolase monomer and active site . . . . .	29
11	Phosphoketolase active site with bound reaction intermediates . . . . .	30
12	Different fates of the $\alpha$ -carbanion/enamine intermediate in phosphoketolase and transketolase . . . . .	32
13	Structure alignment of phosphoketolase and transketolase active sites . . . . .	33
14	Exemplary progress curve of AcThDP absorbance . . . . .	53
15	Schematic representation of the coupled transketolase activity assay . . . . .	54
16	UV-Vis absorbance spectrum of phosphoketolase in its resting state and after substrate addition . . . . .	57
17	Analysis of covalent ThDP-intermediates in phosphoketolase . . . . .	58
18	pH-dependence of the AcThDP absorbance band . . . . .	60
19	pH-dependence of the AcThDP absorbance band in the phosphoketolase variants XFPK <sub>E156Q</sub> and XFPK <sub>N549D</sub> . . . . .	61
20	Steady-state kinetic analysis of the phosphoketolase reaction . . . . .	63
21	Steady-state kinetic analysis of the phosphoketolase reaction depending on phosphate concentration . . . . .	64
22	Transient kinetic analysis of AcThDP formation in phosphoketolase. . . . .	66
23	Kinetic analysis of the hydrolytic side reaction . . . . .	67
24	Transient kinetic analysis of AcThDP depletion . . . . .	68
25	Testing of alternative nucleophilic acceptor substrates . . . . .	69
26	pH-dependent steady-state kinetic analysis of the phosphoketolase reaction . . . . .	70

27	pH-dependent transient kinetic analysis of AcThDP formation and depletion . . .	72
28	Investigation on the catalytic role of His553 . . . . .	74
29	Schematic representation of a potential ligation reaction between enolate-AcThDP and an aldehyde acceptor . . . . .	75
30	Absorbance spectra of AcThDP after addition of aldehyde acceptor substrates . .	76
31	Potential ligation reactions of phosphoketolase reaction intermediates with formalde- hyde . . . . .	78
32	Detection of 3-hydroxypropionic acid by GC-MS . . . . .	79
33	Detection of dihydroxyacetone by GC-MS . . . . .	80
34	GC-MS analysis of <sup>13</sup> C-labeled ligation products . . . . .	81
35	Analysis of F6P conversion in presence of formaldehyde by GC-MS . . . . .	83
36	Potential acceptor substrates for phosphoketolase catalyzed carboligation reactions	84
37	Active site environment of AcThDP in phosphoketolase . . . . .	85
38	GC-MS product analysis of XFPK <sub>H64S</sub> . . . . .	86
39	UV-Vis absorbance spectrum of XFPK <sub>N549D</sub> after substrate addition . . . . .	87
40	Steady-state kinetic analysis of XFPK <sub>N549D</sub> . . . . .	88
41	Transient kinetic analysis of AcThDP formation and depletion in XFPK <sub>N549D</sub> . .	89
42	UV-Vis absorbance spectra of XFPK <sub>Y501F/N549D</sub> and XFPK <sub>E437L/Y501F/N549D</sub> . .	91
43	Transient kinetic analysis of AcThDP formation in XFPK <sub>Y501F/N549D</sub> . . . . .	92
44	Transient kinetic analysis of AcThDP depletion in XFPK <sub>Y501F/N549D</sub> . . . . .	93
45	Kinetic parameters of the phosphoketolase reaction . . . . .	99
46	Active site of <i>B. breve</i> phosphoketolase in complex with phosphate . . . . .	102
47	Suggested mechanism for enol-keto tautomerization of AcThDP . . . . .	103
48	Novel carboligase activity in ThDP-dependent enzymes . . . . .	107
49	Nucleophilic reaction intermediates in aldolases and phosphoketolase . . . . .	108
50	Possible applications of phosphoketolase in organic synthesis . . . . .	110
51	Phosphate binding site of <i>B. breve</i> phosphoketolase . . . . .	113
52	Different orientation of a substrate channel loop in PK and TK . . . . .	116
53	Aminoacid sequence of the recombinant <i>B. breve</i> phosphoketolase . . . . .	119
54	SDS-PAGE analysis of purified XFPK <sub>WT</sub> and variants . . . . .	120
55	UV-Vis absorbance spectra of phosphoketolase with alternative substrates . . . .	120
56	Erythrose 4-phosphate calibration curve . . . . .	121

---

57	Calibration curves for quantification of carboligation products . . . . .	121
58	Progression of AcThDP absorbance over time . . . . .	122
59	Depletion of the AcThDP absorbance after mixing with formaldehyde . . . . .	122
60	Analysis of F6P conversion by GC-MS . . . . .	123
61	Exemplary progress curve of AcThDP formation in XFPK <sub>N549D</sub> . . . . .	124
62	Far-UV CD spectra of phosphoketolase wild type and "transketolase-like" variants	124
63	Phosphoketolase activity of XFPK <sub>Y501F/N549D</sub> . . . . .	125

## List of Tables

1	Macroscopic kinetic constants of the phosphoketolase reaction at different pH . .	71
2	Total amounts of carboligation products . . . . .	82

## Abbreviations

**AcThDP** acetyl-thiamine diphosphate

**ADP** adenosine diphosphate

**Asn** asparagine

**Ala** alanine

**Asp** aspartate/aspartic acid

**ATP** adenosine triphosphate

**BAL** benzaldehyde lyase

**BFD** benzoylformate decarboxylase

***B. breve*** *Bifidobacterium breve*

***B. longum*** *Bifidobacterium longum*

**CD** circular dichroism

**DHEThDP** ( $\alpha,\beta$ -dihydroxyethyl)-thiamine diphosphate

**DMSO** dimethyl sulfoxid

**DNA** deoxyribonucleic acid

**E4P** erythrose 4-phosphate

***E. coli*** *Escherichia coli*

**EDTA** ethylenediaminetetraacetic acid

**F6P** fructose 6-phosphate

**G3P** glyceraldehyde 3-phosphate

**GC-MS** gas chromatography coupled to mass spectrometry

**Gln** glutamine

**Glu** glutamate/glutamic acid

**HEPES** 4-(2-Hydroxyethyl)piperazine-1-ethanesulfonic acid

**His** histidine

**His<sub>6</sub>-tagged** hexa-histidine tagged

- IPTG** isopropyl- $\beta$ -D-thiogalactopyranoside
- LpPOX** pyruvate oxidase from *Lactobacillus plantarum*
- PFOR** pyruvate:ferredoxin oxidoreductase
- NAD** nicotinamide adenine dinucleotide
- NiNTA** Ni<sup>2+</sup> nitrilotriacetic acid
- NMR** nuclear magnetic resonance
- OD<sub>600</sub>** optical density at 600 nm
- PCR** polymerase chain reaction
- PDC** pyruvate decarboxylase
- PIPES** piperazine-N,N'-bis(2-ethanesulfonic acid)
- PMSF** phenylmethane sulfonyl fluoride
- R5P** ribose 5-phosphate
- rpm** revolutions per minute
- SDS-PAGE** sodium dodecyl sulfate polyacrylamide gel electrophoresis
- SEC** size exclusion chromatography
- S7P** sedoheptulose 7-phosphate
- ThDP** thiamine diphosphate
- TK** transketolase
- Tris** tris(hydroxymethyl)aminomethane
- Tyr** tyrosine
- UV-Vis** ultraviolet and visible fraction of electromagnetic radiation
- X5P** xylulose 5-phosphate
- XFPK** xylulose 5-phosphate/fructose 6-phosphate phosphoketolase

## Abstract

The thiamine diphosphate (ThDP)-dependent enzyme phosphoketolase catalyzes the phosphorytic cleavage of fructose-6-phosphate and/or xylulose 5-phosphate under the generation of the high-energy metabolite acetyl phosphate, as such playing a key role in the metabolism of lactic acid bacteria and *bifidobacteria*. Phosphoketolase shows remarkable similarity to the prominent ThDP-dependent enzyme transketolase and catalyzes as only known ThDP-dependent enzyme a dehydration of its central  $\alpha$ -carbanion/enamine intermediate.

Thanks to a small number of structural and functional studies, the phosphoketolase catalytic mechanism is fairly well characterized. Dehydration of the  $\alpha$ -carbanion/enamine cofactor adduct ( $\alpha,\beta$ -dihydroxyethyl)-thiamine diphosphate (DHETThDP) produces an enol-acetyl-ThDP intermediate that needs to undergo tautomerization to the corresponding keto-tautomer before a nucleophilic attack from the second substrate phosphate leads to product formation.

In this thesis, a detailed analysis of the phosphoketolase reaction by kinetic and spectroscopic techniques was carried out with special emphasis on the mechanism of acetyl-thiamine diphosphate (AcThDP) tautomerization and the underlying chemical state of the post-dehydration intermediate as well as potential carboligase side reactivity of the enzyme. The obtained results provide new insights into the phosphoketolase reaction mechanism that suggest a mechanistic update for the enol-keto-tautomerization of the post-dehydration intermediate AcThDP, give new information on the similarities and differences of phosphoketolase and transketolase and led to the discovery of a novel ThDP-catalyzed C-C bond forming side reaction.

Identification of a distinct UV-Vis absorbance signal associated to the phosphoketolase reaction intermediate AcThDP provided the basis for a transient kinetic analysis of individual steps of the phosphoketolase reaction. Additionally, a direct steady-state assay was established that allowed determination of kinetic parameters for the phosphoketolase main reaction as well as for the off-pathway hydrolysis of AcThDP to acetate that occurs in absence of the acyl-acceptor substrate phosphate. The detailed kinetic examination revealed that the rate of enol-keto tautomerization of AcThDP is increased by the presence of the acyl-acceptor substrate phosphate. Together with results from spectroscopic and computational analysis of the phosphoketolase reaction, this suggest a mechanism in which phosphate acts as substrate catalyst in the tautomerization from enol- to keto-AcThDP. Direct catalytic involvement of phosphate provides coupling of the final



acyl-transfer to the preceding tautomerization which avoids formation of the hydrolysis-susceptible keto-AcThDP intermediate in the absence of an acceptor substrate.

The proposed mechanism for AcThDP tautomerization implies formation of an enolate-AcThDP intermediate. Presence of this intermediate could be confirmed by trapping the enolate in a carbonylation reaction with formaldehyde. The side reaction between phosphoketolase bound enolate-AcThDP and the aldehyde acceptor represents a novel type of ThDP-catalyzed C-C bond forming reaction as it not originates from the central  $\alpha$ -carbanion/enamine intermediate.

Generation of a "transketolase-like" phosphoketolase variant could not induce transketolase activity, but showed the importance of three phosphoketolase-specific active site residues for the phosphoketolase reaction mechanism.

# 1 Introduction

## 1.1 Biological relevance of phosphoketolase

Phosphoketolase activity was first described in the 1950s, when HEATH *et al.* observed cleavage of xylulose 5-phosphate (X5P) to acetyl phosphate and glyceraldehyde 3-phosphate (G3P) by an enzyme purified from *Lactobacillus pentosus*<sup>1</sup>. Since then, the ThDP-dependent enzyme is recognized as a key enzyme in the carbohydrate catabolism of diverse microorganisms and is regarded as promising candidate for biotechnological applications.

The THIAMINE DIPHOSPHATE DEPENDENT ENZYME ENGINEERING DATABASE (TEED)<sup>2</sup> hosts over 2000 putative phosphoketolase sequences occurring predominantly in bacteria and some eukaryotes<sup>3</sup>. Characterization has focused on enzymes from *lactobacillaceae* and *bifidobacteria*, but phosphoketolase activity is also described for other bacteria, yeast and fungi. Phosphoketolase catalyzes the formation of acetyl phosphate from the phosphate sugars fructose 6-phosphate (F6P) or xylulose 5-phosphate and inorganic phosphate under the generation of erythrose 4-phosphate (E4P) or glyceraldehyde 3-phosphate, respectively (Figure 1). It is part of the heterofermentative lactic acid fermentation pathway and plays a key role in the fructose 6-phosphate shunt of *bifidobacteria*.

In lactic acid bacteria, energy generation is mainly provided through fermentation of monosaccharides yielding lactate (homofermentative lactic acid fermentation) or lactate together with acetate, ethanol and CO<sub>2</sub> (heterofermentative lactic acid fermentation). While homofermentative

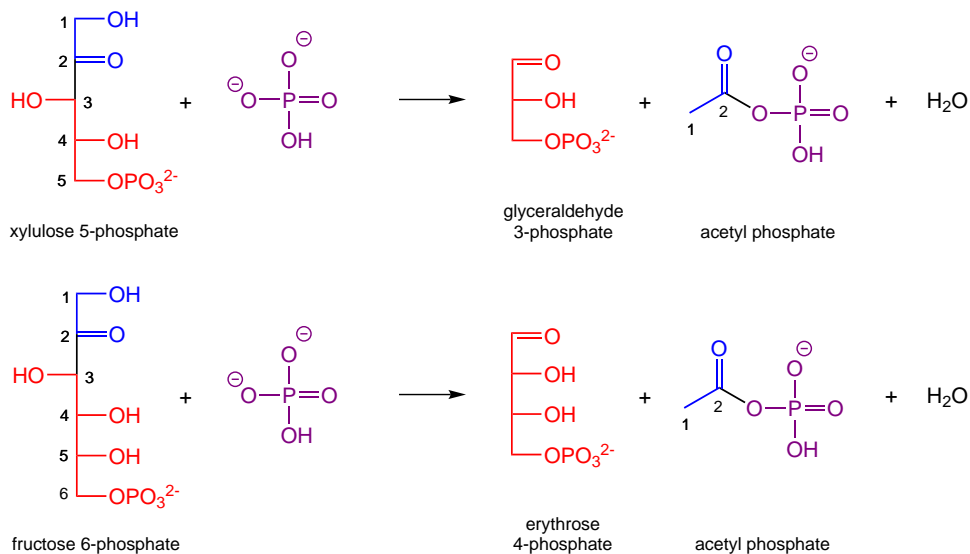


**Figure 1: Phosphoketolase reaction.** Phosphoketolase catalyzes the phosphorolytic cleavage of F6P or X5P to an aldose phosphate and acetyl phosphate. Figure adapted from TITTMANN, 2014<sup>4</sup>.

lactic acid bacteria metabolize hexose sugars via the EMBDEN-MEYERHOF-PARNAS pathway and the action of lactate dehydrogenase, obligate heterofermentative lactic acid bacteria lack the enzyme aldolase and bypass glycolysis by a variant of the pentose phosphate pathway, also known as phosphoketolase pathway<sup>5</sup> (Figure 2A). In the key step of this metabolic pathway, phosphoketolase catalyzes the phosphorolytic cleavage of X5P, which is derived from a pentose 5-phosphate through isomerization in the oxidative phase of the pentose phosphate pathway. The resulting G3P is converted to pyruvate and subsequently reduced to lactate. The energy rich second product acetyl phosphate is either used for direct generation of adenosine triphosphate (ATP) by acetate kinase or is reduced to ethanol. This pathway yields only one mole of ATP from one mole of the hexose sugar. Energy yield is increased to two equivalents ATP when pentoses are used as energy source (Figure 2A, dotted path).

*Bifidobacteria* have evolved a unique metabolic pathway for degradation of hexoses, referred to as fructose 6-phosphate phosphoketolase pathway or bifid shunt that requires catalytic activity of phosphoketolase<sup>6</sup>. In the bifid shunt two moles glucose are converted into two moles of lactate and three moles of acetate, providing an energy yield of 2.5 moles ATP per mole glucose (Figure 2B)<sup>7,8</sup>. As crucial part of the bifid shunt, phosphoketolase catalyzes the cleavage of F6P to E4P and acetyl phosphate. Together with a second molecule glucose, E4P is converted into two molecules X5P by transketolase and transaldolase, two enzymes of the non-oxidative pentose phosphate pathway. X5P is cleaved into G3P and acetyl phosphate, again catalyzed by phosphoketolase. As in heterofermentative lactic acid fermentation, G3P is converted to pyruvate and reduced to lactate. In a final step, acetate kinase transfers the phosphate group of acetyl phosphate to ADP yielding ATP<sup>9</sup>.

Apart from its physiological role, the catalytic activity of phosphoketolase has recently found application in metabolic engineering approaches. Biotechnological production of fuels or feedstock chemicals from renewable sources, non-food biomass or atmospheric CH<sub>4</sub> and CO<sub>2</sub> using engineered microbial strains is becoming increasingly popular as alternative to petroleum based production processes. A key precursor for the biosynthetic production of such products is acetyl-CoA<sup>10</sup>. However, generation of acetyl-CoA from sugars through the EMBDEN-MEYERHOF-PARNAS pathway and pyruvate decarboxylation bears the problem of carbon loss in form of CO<sub>2</sub>. Utilization of recombinant phosphoketolase pathways enables bypassing of pyruvate decarboxylation, thereby increasing the carbon conversion efficiency of the engineered strains<sup>11</sup>.

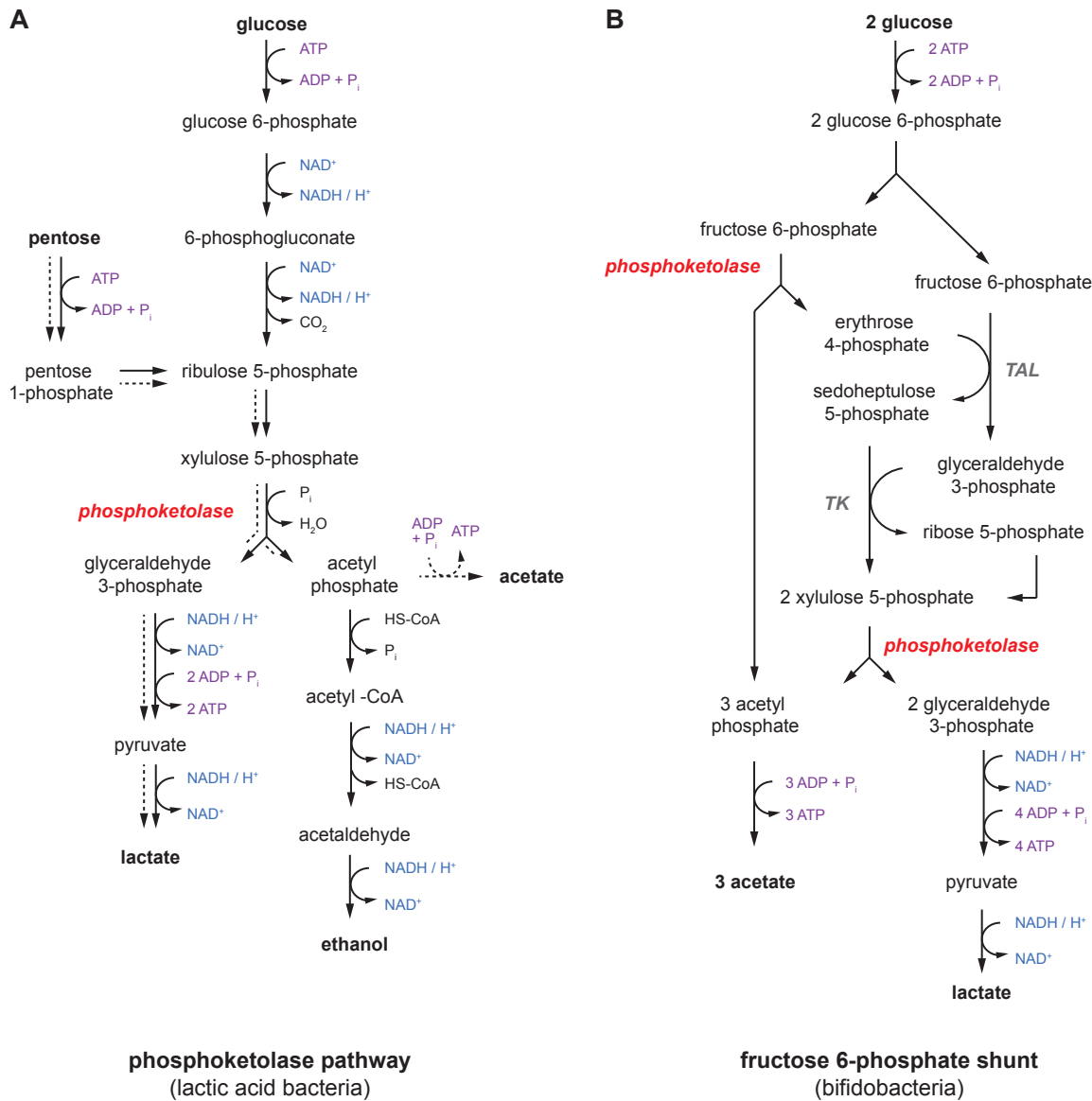


**Figure 2: Schematic representation of the phosphoketolase pathway and the fructose 6-phosphate shunt.** (A) The phosphoketolase pathway is utilized for fermentation of monosaccharides by heterofermentative lactic acid bacteria. Fermentation of hexose sugars yields acetate, ethanol and lactate under the generation of one mole ATP per mole glucose. Fermentation of pentoses to lactate and acetate increase the energy yield to two mole ATP (dotted path). (B) In the F6P shunt of *bifidobacteria* hexose sugars are converted to acetate and lactate under the generation of 2.5 moles ATP per mole glucose. (*TK*=transketolase, *TAL*=transaldolase, *NAD*=nicotinamide adenine dinucleotide)

A general phosphoketolase-based metabolic engineering strategy is shown in Figure 3. Acetyl phosphate is derived in a sequence of non-oxidative carbon rearrangement reactions and subsequently converted into acetyl-CoA by the actions of acetate kinase and acetyl-CoA synthase or phosphotransacetylase. Similar synthetic phosphoketolase pathways have successfully been used to increase rates of ethanol and acetate fermentation in yeast<sup>12,13</sup>, to improve the yield of biotechnologically produced L-glutamic acid<sup>14</sup> or for the production of fatty acid ethyl esters<sup>15</sup>, polyhydroxybutyrate<sup>16</sup> or polyketides<sup>17</sup>. Recently, BOGORAD *et al.* published a phosphoketolase dependent synthetic metabolic pathway termed "non-oxidative glycolysis" that allows ATP-independent, carbon conserving conversion of sugars or sugar phosphates into C2 metabolites<sup>18</sup>. The same group succeeded to construct a synthetic pathway for one-carbon fixation that involves the action of phosphoketolase<sup>19</sup>.

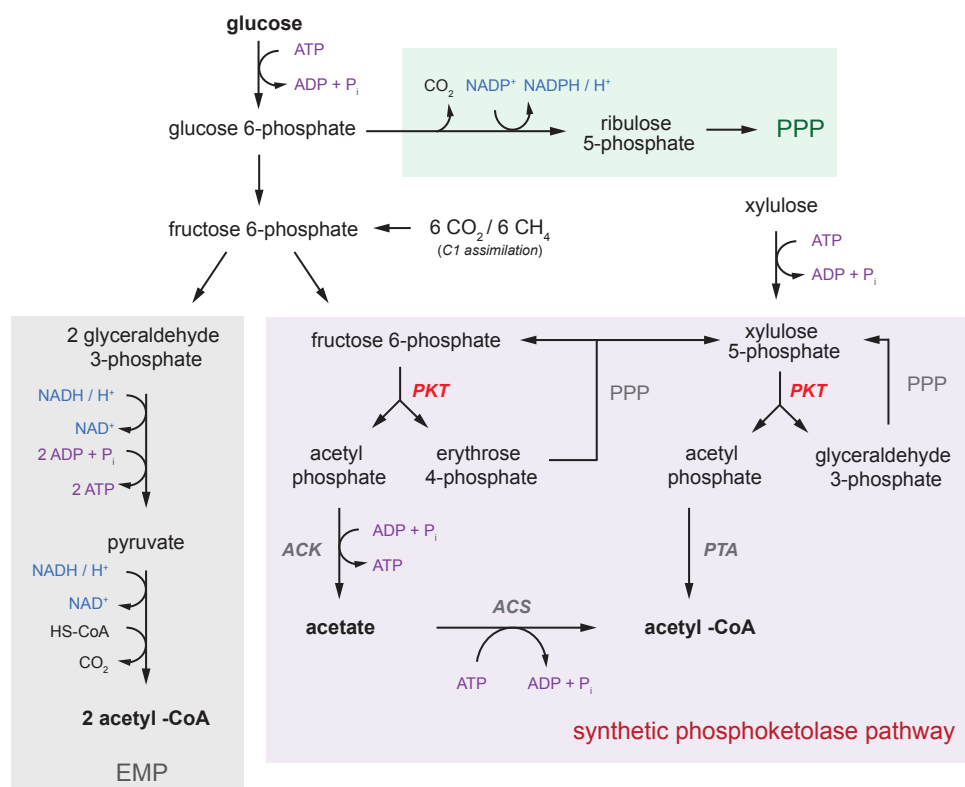


**Figure 3: Phosphoketolase based metabolic engineering strategy.** Synthetic pathways involving the catalytic action of phosphoketolase (*PKT*) allow carbon-efficient generation of the building block acetyl-CoA. Acetyl-CoA is generated from acetyl phosphate through phosphotransacetylase (*PTA*) or acetate kinase (*ACK*) and acetyl-CoA synthase (*ACS*). Erythrose 4-phosphate and glyceraldehyde 3-phosphate side products are converted by enzymes of the pentose phosphate pathway (*PPP*) and fed back into the synthetic phosphoketolase pathway. Provision of ATP and redox equivalents comes from the EMDENHOF-MEYER-PARNAS pathway (*EMP*, gray) and pentose phosphate pathway (*PPP*, green). Engineered phosphoketolase pathways might also be used in conjunction with C1 assimilation strategies, using methane or carbon dioxide as feed stock. Figure adapted from HENARD *et al.*, 2015<sup>11</sup>.

Based on structural and phylogenetic properties, phosphoketolase has been assigned to the transketolase family of ThDP-dependent enzymes<sup>20,21</sup>. Phosphoketolases are classified into two different types according to their substrate specificity. While xylulose 5-phosphate phosphoketolase (EC 4.1.2.9) prefers X5P as substrate, xylulose 5-phosphate/fructose 6-phosphate phosphoketolases (EC 4.1.2.22) exhibit dual substrate specificity for both ketose sugars. Hence, the second type is mainly found in *bifidobacteria* where it is involved in two different catalytic steps of the bifid shunt. This work will focus on xylulose 5-phosphate/fructose 6-phosphate phosphoketolase (XFPK) from *Bifidobacterium breve*, which belongs to the dual substrate specific type.

## 1.2 Phosphoketolase - A thiamine diphosphate-dependent enzyme

Early on in phosphoketolase research, the requirement of ThDP for its enzymatic activity was discovered<sup>1,22</sup>. Around the same time RONALD BRESLOW succeeded to identify the catalytic center of ThDP after a 20 year debate, revealing the molecular mechanism of thiamine diphosphate's catalytic function<sup>23,24</sup>.

### 1.2.1 Catalytic properties of thiamine diphosphate

Thiamine diphosphate is the biologically active form of vitamin B<sub>1</sub> that is required as essential cofactor for many ThDP-dependent enzymes of the anabolic and catabolic metabolism in all domains of life<sup>25</sup>. ThDP catalyzes the chemically challenging formation and breaking of carbon-carbon bonds. Figure 4 shows the chemical structure of ThDP, consisting of a 6-membered aminopyrimidine ring and a 5-membered thiazolium ring, connected via a methylene bridge, and the diphosphate moiety. Although this structure was known since the 1930s, as was the catalytic role of ThDP in the decarboxylation of pyruvate<sup>26,27</sup>, it took twenty years to reveal its mode of action.

By analyzing the proton-exchange rate at the C2 atom of thiazolium salts, BRESLOW identified the C2 carbon of the ThDP thiazolium moiety as reactive site of the cofactor<sup>23</sup>. Thus, he could confirm his hypothesis that deprotonation of the C2 carbon leads to the formation of a ThDP-carbanion/-ylide that acts as nucleophile in analogy to the cyanide anion<sup>24</sup>. Those findings established the common principle of ThDP-mediated reactions. The nucleophilic ThDP-carbanion, resulting from dissociation of the C2 proton, attacks the carbonyl group of a substrate, inverting its polarity as known from cyanide catalyzed umpolung reactions. Cleavage of the

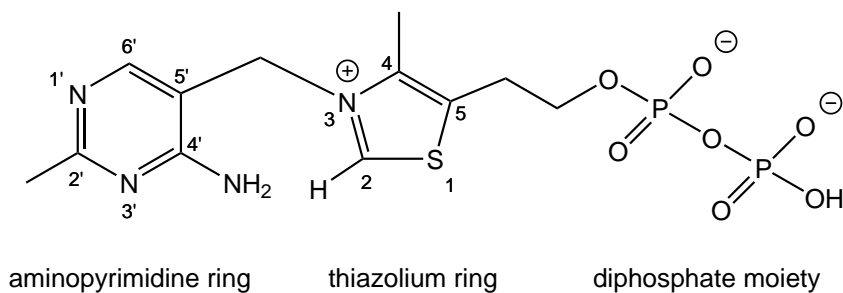


**Figure 4: Chemical structure of thiamine diphosphate.** ThDP consists of a 6-membered aminopyrimidine ring, a 5-membered thiazolium ring and the diphosphate moiety. Aminopyrimidine and thiazolium rings are connected via a methylene bridge.

adjacent carbon-carbon or carbon-hydrogen bond is promoted by stabilizing the resulting aldehyde derived carbanion/acyl carbanion equivalent through delocalization of the negative charge over the thiazolium ring<sup>28</sup>. Prominent examples for ThDP-catalyzed reactions are the decarboxylation of pyruvate and benzoin condensations.

The essential first step in every ThDP-catalyzed reaction is the activation of ThDP by abstraction of the C2 proton. However, the C2-H acidity of ThDP is very low with a  $pK_a$  of around 18 in aqueous solution<sup>29,30</sup> and a rate constant for proton exchange of only  $3 \times 10^{-3} \text{ s}^{-1}$  at pH 7 and  $4 \text{ }^\circ\text{C}$ <sup>31</sup>. Consequently, free ThDP is a poor catalyst under those conditions as only low amounts of the active nucleophilic form are present. To match the reaction rates observed in ThDP-dependent enzymes, C2-H dissociation must be significantly accelerated by the protein environment. Using a NMR-based method, KERN *et al.* were able to directly determine rate constants for C2 deprotonation of enzyme bound ThDP, showing that ThDP activation is accelerated by a factor of up to  $10^5$  in ThDP-dependent enzymes<sup>31</sup>. Basis for the significant rate enhancement is the particular conformation ThDP adopts upon binding to an enzyme. In this so called V-conformation, in contrast to the energetically more favorable F-conformation that is observed for ThDP in solution, the N4'-amino group is brought into close proximity to the C2 atom of the thiazolium ring and can act as BRØNSTED acid/base catalyst for C2 proton abstraction<sup>32</sup>. Earlier studies had postulated a co-catalytic function of not only the N4'H<sub>2</sub> group but also of the N1' atom of the aminopyrimidine moiety<sup>33</sup>. Emerging structural data on a number of ThDP-dependent enzymes also suggested a crucial role for a conserved glutamate residue in H-bonding distance of the ThDP N1' atom<sup>34</sup>. Investigations on different ThDP analogs and enzyme variants that lack the conserved glutamate finally led to the formulation of a generally-accepted mechanism for the activation of enzyme-bound ThDP that is displayed in Figure 5. Proton transfer from the conserved glutamate to the N1' of the aminopyrimidine ring initiates tautomerization

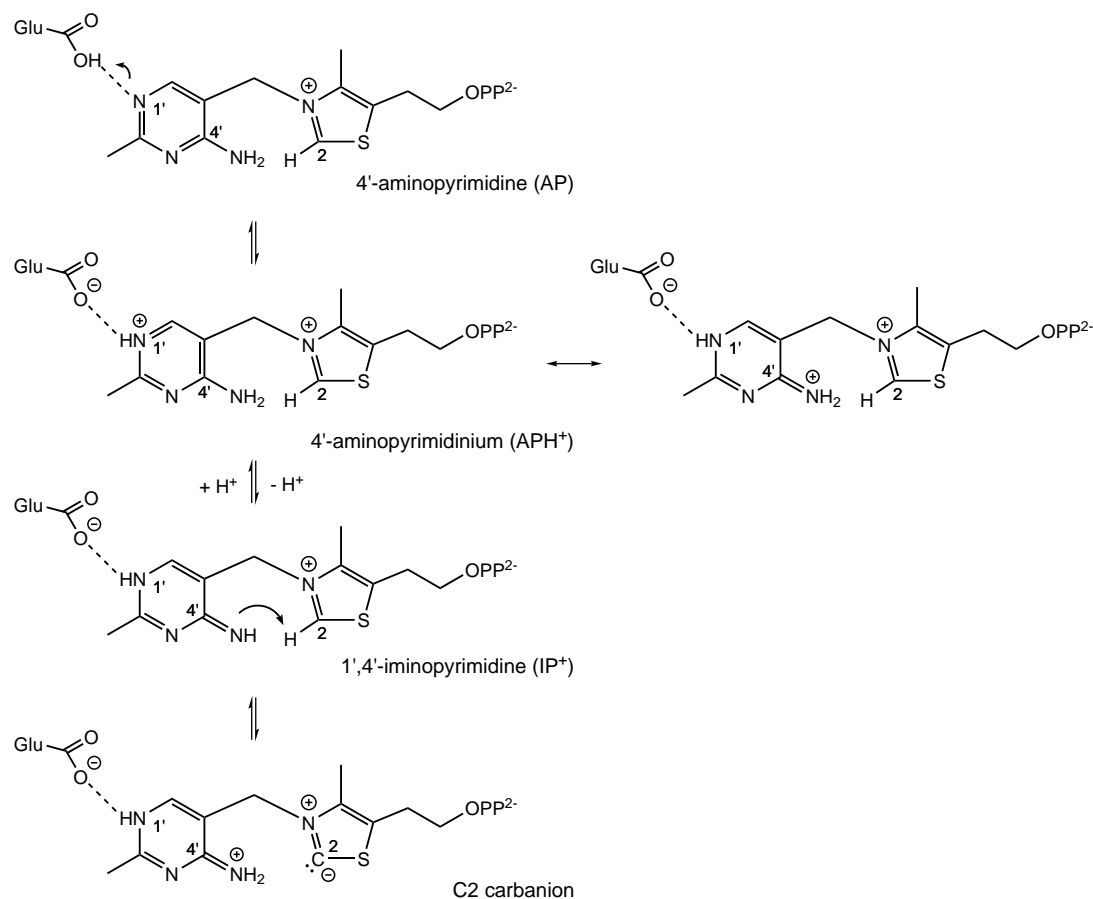


**Figure 5: Activation mechanism of thiamine diphosphate.** A proton relay initiated by a conserved glutamate residue induces formation of the reactive C2 carbanion. The different tautomeric states of the aminopyrimidine ring are indicated. Figure adapted from KLUGER AND TITTMANN, 2008<sup>28</sup>.

of ThDP from its 4'-aminopyrimidine form (AP) to the 1',4'-aminopyrimidine species (IP) via formation of the 4'-aminopyrimidinium (APH<sup>+</sup>). The resulting N4'-imino group subsequently acts as base to abstract the C2 proton and produces the activated C2 carbanion/yilde after an internal proton transfer<sup>31,35</sup>. Hence, an interplay of both aromatic ring systems contributes to the catalytic activity of ThDP<sup>36</sup>. The C2-N1'-N4'-Glu proton relay that leads to cofactor activation is regarded as a hallmark of ThDP-dependent enzymes. However, there is one exception. In the enzyme glyoxylate-carboligase, the otherwise strictly conserved Glu is replaced by valine, implying a different activation mechanism<sup>37</sup>. Experimental data suggests that enzyme-bound ThDP is protonated in the resting state and cofactor activation is triggered by substrate binding, although the mechanism behind the substrate-triggered activation is still unknown<sup>31,38</sup>.



### 1.2.2 Thiamine diphosphate-dependent enzymes - Catalytic principles and structural features

Until today more than 20 different ThDP-dependent enzymes have been described and although they all differ in their catalytic specificity, their reaction mechanisms follow a common principle via the formation of ThDP-derived covalent intermediates<sup>28</sup> (Figure 6). Over the last 60 years many of those covalent ThDP adducts were characterized by high-resolution X-ray crystallography, NMR or UV-Vis spectroscopic based methods, providing valuable information about the catalytic principles of ThDP-dependent enzymes.

The reaction sequence typically starts with the nucleophilic attack of the activated cofactor at the substrate carbonyl-group, resulting in the formation of a tetrahedral ( $sp^3$ -hybridized) covalent substrate-ThDP adduct. According to the principle of maximum overlap, the scissile substrate bond is positioned perpendicular to the thiazolium ring. In this orientation the electron pair of the post-cleavage carbanion conjugates with the thiazolium  $\pi$ -system, facilitating bond cleavage by stabilizing the developing negative charge<sup>39-41</sup>. Stabilization of the substrate-ThDP adduct in a strained conformation, manifested through out-of-plane distortion of the C2-C2 $\alpha$  bond and increased bond length of the scissile C-C bond, has been discussed as further driving force for bond cleavage by ThDP-dependent enzymes<sup>42</sup>.

C-C bond cleavage and liberation of the first product, commonly CO<sub>2</sub> or a phosphate sugar, yields a C2 $\alpha$ -carbanion/enamine which forms the central intermediate and branching point of all reactions catalyzed by ThDP dependent enzymes. However, the fate of the reactive C2 $\alpha$ -carbanion/enamine substantially varies and is determined by enzyme specific routes. Those enzyme specific pathways can broadly be clustered into protonation, oxidation and carbonylation reactions<sup>28</sup> (Figure 6). In ThDP-dependent decarboxylases like pyruvate decarboxylase or benzoylformate decarboxylase, protonation of the carbanion leads to release of an aldehyde product. Alternatively, the nucleophilic C2 $\alpha$ -carbanion/enamine attacks a carbonyl acceptor substrate, forming a new C-C bond (e.g. in transketolase or acetohydroxyacid synthase). Furthermore, a number of ThDP-dependent enzymes such as pyruvate oxidase or pyruvate dehydrogenase catalyze oxidative conversion of substrates, often employing additional cofactors like flavine adenine dinucleotide, lipoamide or iron sulfur clusters. Phosphoketolases catalyze a dehydration of the carbanion/enamine intermediate DHEThDP, a reaction step that seems unique among the ThDP enzyme family. These very different reaction outcomes are the result of individual cofactor environments provided by the

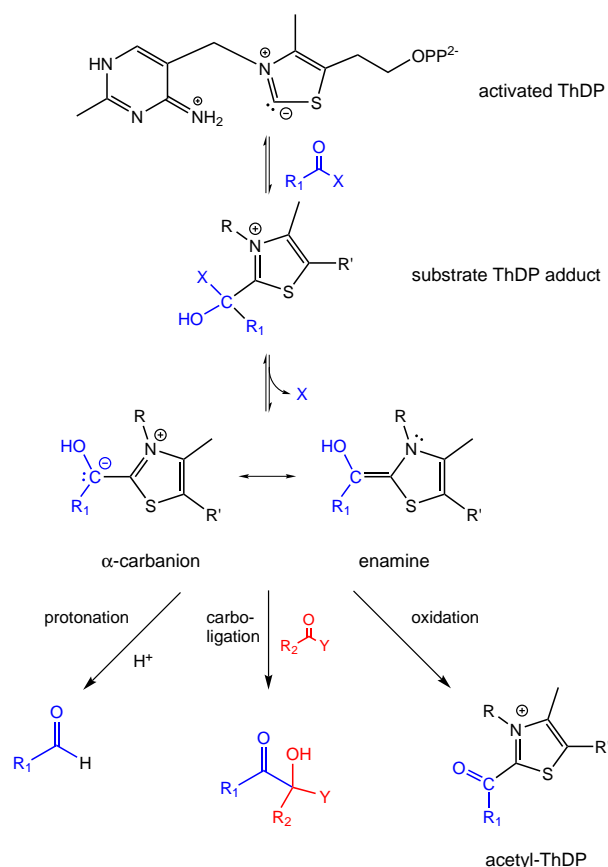


**Figure 6: General reaction mechanism of ThDP-dependent enzymes.** ThDP-catalyzed reactions proceed via the formation of covalent ThDP adduct intermediates. Enzyme specific routes determine the fate of the central C2 $\alpha$ -carbanion/enamine intermediate. Figure adapted from LÜDTKE 2013<sup>42</sup>. (R=aminopyrimidine moiety, R'=ethylidiphosphate)

respective enzymes, that allow a specific conversion of the C2 $\alpha$ -carbanion/enamine and efficient catalysis of the subsequent reaction steps. Recent studies suggest that the enzyme might do so by modulating the chemical state of the C2 $\alpha$ -carbanion, challenging the paradigm that the C2 $\alpha$ -carbanion is generally stabilized in resonance with the  $sp^2$ -hybridized enamine species<sup>43,44</sup>.

Insights into the mechanisms of ThDP-dependent enzymes were made possible by different analytical techniques enabling detection and identification of covalent ThDP intermediates. Next to high resolution X-ray crystal structures of enzymes in complex with covalent cofactor adducts, NMR and UV-Vis spectroscopic techniques were established that allow direct detection of ThDP intermediates in solution. Using a chemical-quench/<sup>1</sup>H-NMR method TITTMAN AND HÜBNER were able to observe and quantify the distribution of covalent ThDP intermediates at defined time points during the enzymatic reaction, making it possible to determine rate constants for individual reaction steps<sup>45</sup>. Additionally, specific UV-Vis and circular dichroism (CD) signals have successfully been assigned to the different tautomerization states of ThDP (AP- and IP

form), as well as to many covalent ThDP adducts, enabling direct observation of ThDP's chemical states and intermediates in the course of the reaction<sup>46,47</sup>.

Not only do ThDP-dependent enzymes share common reaction patterns, they also share certain structural features. Although showing a very low overall sequence similarity, all structurally characterized ThDP enzymes exhibit conserved tertiary structures in form of two catalytic domains, the pyrimidine- (PYR) and the phosphate (PP) binding domain<sup>20,21,48</sup>. Both domains show high structural similarity, folding into an  $\alpha$ - $\beta$  ThDP-binding fold and participate in binding of the cofactor<sup>34</sup>. The PP domain contains the strictly conserved ThDP-binding motif GDGX<sub>24-27</sub>NN that anchors the pyrophosphate moiety to the enzyme<sup>49</sup>. The conserved aspartate and asparagine residues are part of the metal binding site, coordinating the second cofactor, a divalent metal ion (usually Mg<sup>2+</sup> or Ca<sup>2+</sup>) which is crucial for ThDP binding. The PYR domain interacts with the aminopyrimidine ring and contains the conserved glutamate essential for cofactor activation<sup>34</sup>. Some enzymes also contain a third domain with specific function for the individual subfamily. The minimum functional unit of ThDP-dependent enzymes consists of two monomers, forming a dimer of active sites. ThDP is bound between the interfaces of the two subunits, either of the same monomer or between the interfaces of PP and PYR domain from different monomers. Furthermore, arrangement of the subunits differs among the nine superfamilies<sup>2</sup>. Despite the difference in quaternary structure, all enzymes form conserved ThDP binding pockets that force the cofactor to adopt the active V-conformation. Apart from the conserved binding mode, the active sites of ThDP-enzymes exhibit high variability, representing the diverse substrate and reaction range of the enzyme family<sup>48</sup>.

Overall, the protein component in ThDP enzymes provides an activating environment for the cofactor, amplifying its reactivity and guiding the individual reactions towards efficient product formation.

### 1.2.3 Thiamine diphosphate-dependent enzymes in biocatalysis

Enzymatic catalysis is characterized by remarkable rate acceleration and strict stereo-, regio- and chemoselectivity. Furthermore, enzymatic reactions are usually carried out in neutral aqueous solution without the requirement of extreme temperatures or pressure, harsh chemical conditions, heavy metals or protective groups. Hence, enzyme-catalyzed chemical transformations have been established as a practical and environmental friendly alternatives to conventional synthesis of

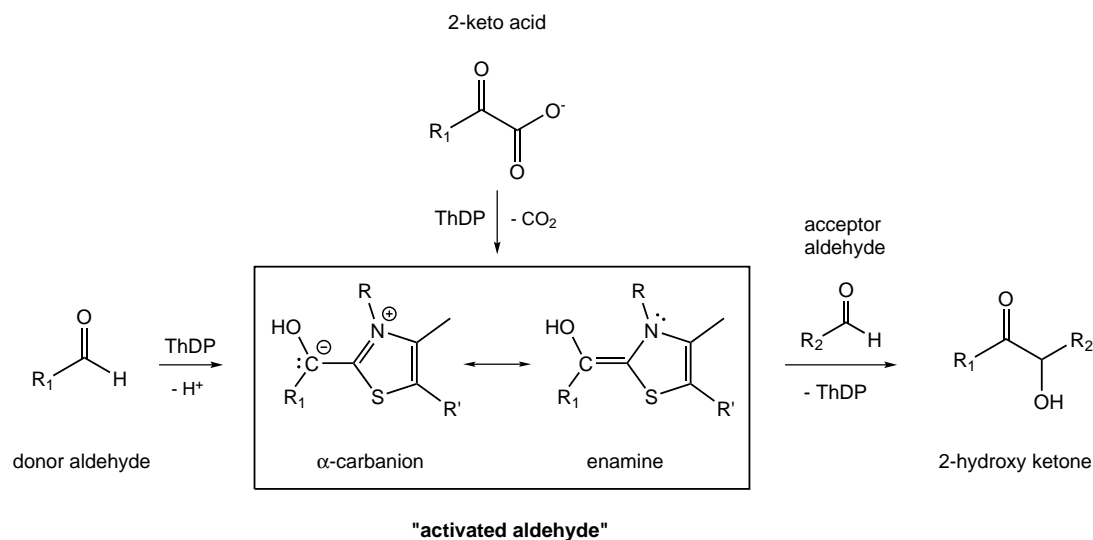


**Figure 7: Formation of 2-hydroxyketones by ThDP-dependent enzymes.** The "activated aldehyde intermediate" is formed after decarboxylation of a ThDP-bound 2-ketoacid or deprotonation of a donor-aldehyde. Reaction with an acceptor-aldehyde yields the 2-hydroxy ketone. (R=aminopyrimidine moiety, R'=ethylidiphosphate, R1/R2=phe or aryl)

organic compounds that are needed to supply the ever-growing demand of pharmaceutical and chemical industries<sup>50,51</sup>.

With their particular catalytic mechanism that enables the stereoselective formation of new carbon-carbon bonds, ThDP-dependent enzymes have been subject of intense research towards their utilization as biocatalysts<sup>52-54</sup>. Although ThDP enzymes provide high substrate- and catalytic-specificity in a physiological context, several members of the enzyme family catalyze off-pathway carbonylation reactions with non-natural acceptor substrates. Key to this intrinsic catalytic promiscuity is the formation of the reactive C2 $\alpha$ -carbanion/enamine intermediate, also referred to as "activated aldehyde intermediate". Formation of this acyl-anion equivalent alters the carbonyl group, usually exhibiting electrophilic character, nucleophilic allowing novel C-C bond formations with suitable carbon electrophiles<sup>55</sup>. Additionally, many ThDP-dependent enzymes accept a broad spectrum of non-natural donor- and acceptor substrates making them excellent candidates for chemoenzymatic synthesis.

Prominent examples are ThDP-dependent decarboxylases such as pyruvate decarboxylase (PDC) and benzoylformate decarboxylase (BFD), whose natural reactivity is the decarboxylation of 2-keto acids yielding the respective aldehyde products. However, in the presence of an aldehyde acceptor, they catalyze acetalin/benzoin type condensation reactions by transferring the activated aldehyde intermediate onto the acceptor substrate yielding chiral 2-hydroxy ketones (Figure 7). Next to 2-keto acids, aldehydes can be used as donor substrates. In this case decarboxylation is

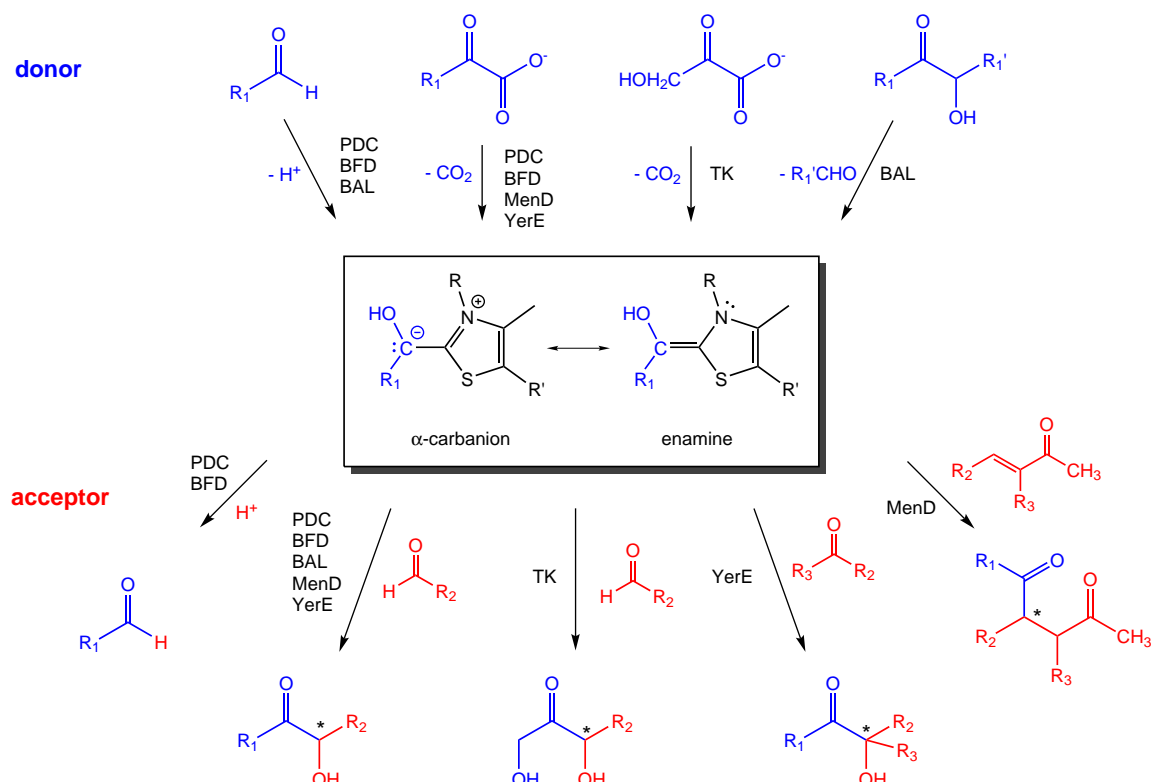


**Figure 8: Carboligation reactions catalyzed by ThDP-dependent enzymes.** Natural or non-natural donor compounds add to the activated cofactor. Deprotonation, decarboxylation or substrate cleavage produce the carbanion/enamine (activated aldehyde) intermediate that reacts with an acceptor-substrate to form the respective carboligation product. Enzymes accepting the individual donor and acceptor product are indicated next to the reaction arrow. New stereo-centers are indicated by asterisk. Figure adapted from HAILES *et al.*, 2013<sup>60</sup>. (R=aminopyrimidine moiety, R'=ethylidiphosphate)

skipped and formation of the activated aldehyde intermediate results from direct addition of the aldehyde substrate to the cofactor, allowing the production of  $\alpha$ -hydroxy ketones as important building blocks for asymmetric synthesis from cheap starting material<sup>56</sup>. The catalytic promiscuity of ThDP-decarboxylases has been exploited for the industrial production of (*R*)-phenyl-acetyl carbinol, a precursor of the pharmaceutically relevant (-)ephedrine, from acetaldehyde and benzaldehyde catalyzed by pyruvate decarboxylase<sup>57,58</sup>.

Another enzyme commonly used for biosynthesis of chiral  $\alpha$ -hydroxy ketones is benzaldehyde lyase (BAL). The ThDP-dependent enzyme catalyzes the reversible cleavage of (*R*)-benzoin and was shown to catalyze enantioselective 1,2-carboligation with a broad range of donor- and acceptor aldehydes as well as the racemic resolution of 2-hydroxy ketones (reviewed in BROVETTO *et al.* 2011<sup>54</sup>). Owing to their substrate- and stereo-specificity, those enzymes allow coupling between aromatic and/or aliphatic aldehydes with remarkable enantio- and chemoselectivity<sup>59</sup>.

Next to non-physiological 1,2-carboligation reactions with a wide variety of aromatic and aliphatic aldehyde substrates, ThDP-dependent enzymes have successfully been used for asymmetric cross-

benzoin-condensations (BAL, BFD<sub>H218A</sub>)<sup>61</sup>, asymmetric crossed aldehyde-ketone carboligations (YerE)<sup>62</sup>, 1,4-additions to  $\alpha,\beta$ -unsaturated carbonyl compounds also known as Stetter reaction (PigD, MenD)<sup>63,64</sup> and many other (reviewed in [Mueller2009a](#), 59,60,65). Some examples are depicted in Figure 8. The ThDP-dependent transferase transketolase (TK) is also widely used for synthetic applications. Enzyme-engineering approaches using site-directed mutagenesis or directed-evolution techniques have further expanded the substrate range and increased yield, chemo- and enantioselectivity of ThDP-dependent enzymes used in biotransformations<sup>54</sup>. Future research on the molecular mechanisms of established and new ThDP enzymes together with advances in enzyme engineering might further increase the scope for biocatalytic applications.

### 1.3 Structure and reaction mechanism of phosphoketolase

The enzymatic activity of phosphoketolase is known for over 50 years, but only in the last 10 years functional and structural studies on the ThDP-dependent enzyme started to emerge, revealing phosphoketolase's catalytic mechanism including a dehydration step that seems unique among the well-studied family of ThDP-dependent enzymes.

In the late 1950s, two independent groups described an enzyme from *Lactobacillus pentosum* and *Acetobacter xylinum* respectively, which catalyzes the cleavage of F6P and/or X5P under the generation of acetyl phosphate dependent on ThDP and Mg<sup>2+</sup>, that was later named phosphoketolase<sup>1,66,67</sup>. Shortly after, it was suggested that the phosphoketolase reaction proceeds via the formation of an activated aldehyde intermediate, namely DHEThDP. Also the presence of AcThDP as intermediate emerging from DHEThDP dehydration was discussed<sup>22,68-70</sup>.

This basic understanding of the phosphoketolase reaction mechanism was later supported and expanded by a kinetic study from the group of PERRY A. FREY, who suggested a catalytic mechanism for phosphoketolase (Figure 9). In a first step, nucleophilic attack of the activated cofactor at the carbonyl group of the substrate, either X5P or F6P, leads to the formation of the covalent substrate-ThDP adduct. Deprotonation of the 3-OH group and subsequent cleavage of the scissile C2-C3 bond results in liberation of the aldose-phosphate product G3P or E4P and formation of DHEThDP, the central  $\alpha$ -carbanion/enamine intermediate. The DHEThDP intermediate is protonated at the O1-hydroxy group, followed by water elimination. Dehydration of the  $\alpha$ -carbanion/enamine results in the formation of an enol-intermediate which tautomerizes to its corresponding keto form 2-acetyl-ThDP. Nucleophilic attack of the second substrate phosphate

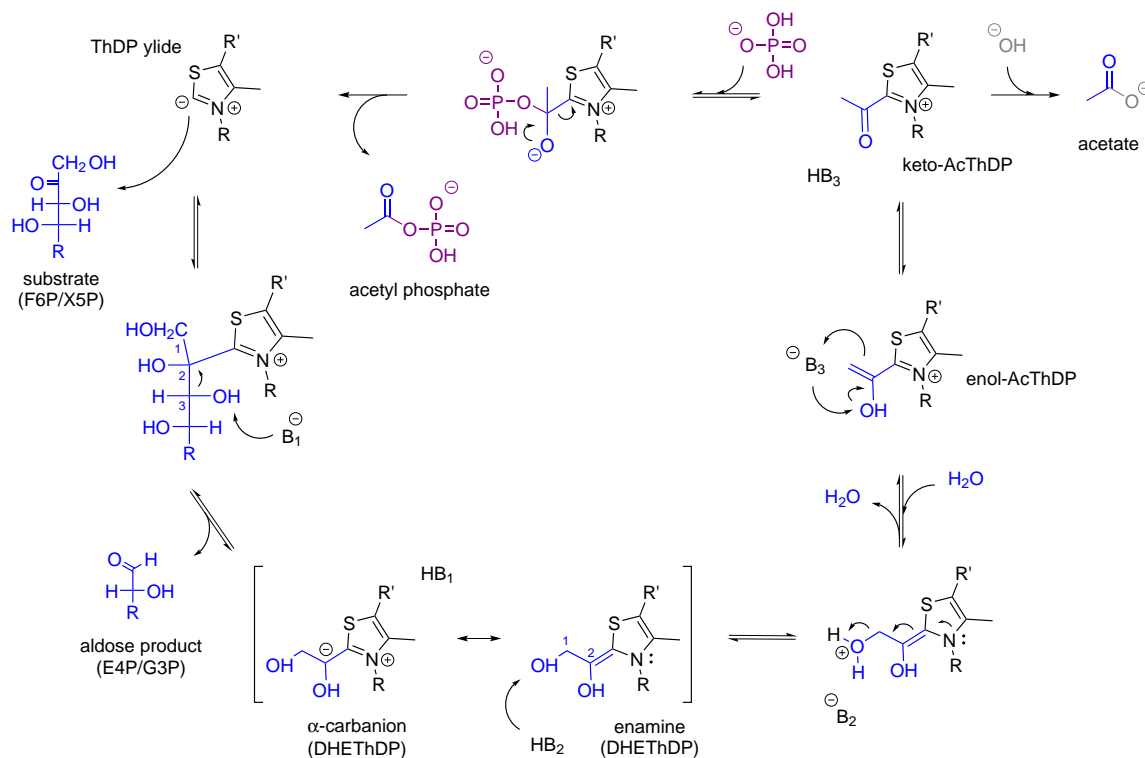


**Figure 9: Reaction mechanism of phosphoketolase.** Nucleophilic attack followed by elimination of the aldose product from the substrate-ThDP adduct leads to formation of the central carbanion/enamine intermediate DHEThDP. Protonation of DHEThDP and subsequent dehydration produces enol-AcThDP that undergoes tautomerization to its corresponding keto-form 2-AcThDP. Phosphorolytic cleavage of 2-AcThDP releases the final product acetyl phosphate and regenerates the cofactor. In absence of the acceptor substrate phosphate, AcThDP is hydrolyzed to acetate. Figure adapted from SUZUKI *et al.*, 2010<sup>73</sup> and TITTMANN, 2014<sup>4</sup>. (R=aminopyrimidine moiety, R'=ethylidiphosphate)

at the 2-acetyl-ThDP keto group yields the final product acetyl phosphate and regenerates the cofactor<sup>71</sup>.

Kinetic analysis of the phosphoketolase reaction indicates a ping-pong mechanism, in which C2-C3 bond cleavage and liberation of the aldose-phosphate product occurs independently of the presence of phosphate<sup>71</sup>. Furthermore, the data suggests dehydration of DHEThDP to proceed irreversibly, in accordance with an earlier study that proposed irreversibility of the phosphoketolase reaction<sup>66</sup>. The crystal structures of phosphoketolase from two different *bifidobacteria* strains in its resting state and with bound intermediates were determined in 2010, confirming the putative reaction mechanism and providing essential molecular details on the individual steps of the catalytic cycle<sup>72,73</sup>.

Phosphoketolase displays the common structural features of a ThDP-dependent enzyme. The 816 residues of *Bifidobacterium breve* (*B. breve*) xylulose 5-phosphate/fructose 6-phosphate phosphoketolase fold into three domains, an N-terminal PP domain, a middle PYR domain and a C-terminal domain that exhibits the characteristic  $\alpha/\beta$  ThDP-binding fold (Figure 10A). The

cofactor is bound in the V-conformation at the interface between two monomers by hydrophobic residues of PP and PYR domain of the different monomers. Besides interacting with the pyrophosphate moiety of ThDP, the PP domain harbors the second cofactor, a divalent magnesium ion, sixfold coordinated by two hydroxy-groups of the pyrophosphate, several residues of the N-terminal domain and a water molecule. The conserved glutamate residue Glu479, crucial for cofactor activation, is located in the PYR domain 2.7 Å from the aminopyrimidine N1' atom<sup>73</sup>. Residues of both monomers contribute to the active site that contains a network of conserved histidine residues (Figure 10B). Although the crystal structure suggests a dimer as functional unit, analysis by size exclusion chromatography and native polyacrylamid gel electrophoresis suggests presence of tetrameric and hexameric phosphoketolase complexes next to the dimer<sup>73,74</sup>.

The overall domain structure as well as the active site architecture of phosphoketolase closely resembles that of the related ThDP-dependent enzyme transketolase. Transketolase catalyzes the transfer of a dihydroxyethyl-unit from F6P or X5P onto an aldose acceptor as part of the non-oxidative pentose phosphate pathway. Structural resemblance of the two enzymes was hardly surprising, regarding that both enzymes utilize the same set of cofactors, act on the same substrates and partly catalyze the same reaction.

In crystal soaking experiments with the ketose-phosphate substrate F6P in the absence of the second substrate phosphate, SUZUKI *et al.* succeeded to trap the covalent intermediates DHEThDP and AcThDP in crystallo. The resulting structures are shown in Figure 11B and C. Analysis of the active site with bound intermediates revealed an array of histidine residues

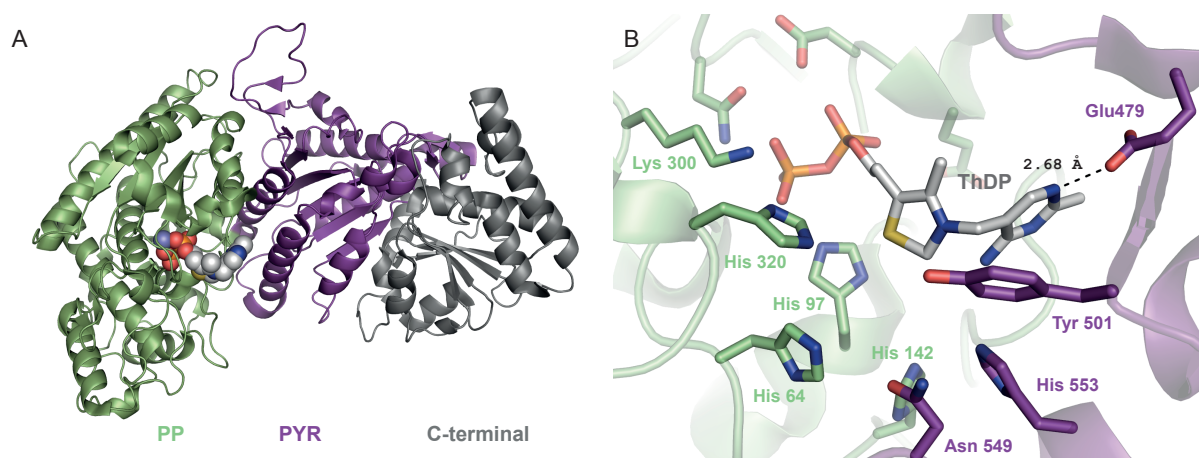


**Figure 10: Structure of *B. breve* phosphoketolase monomer and active site.** (A) The phosphoketolase monomer consists of phosphate binding (PP, green), pyrimidine binding (PYR, purple) and C-terminal domain (gray). The cofactors ThDP and  $Mg^{2+}$  are shown as spheres. (B) The active site harbors the cofactor ThDP (light gray) and consists of amino acid side chains of both PP (green) and PYR domain (purple). The conserved Glu479 and other catalytically important residues are labeled. Figure was prepared based on pdb file 3AHC (SUZUKI *et al.*, 2010<sup>73</sup>).



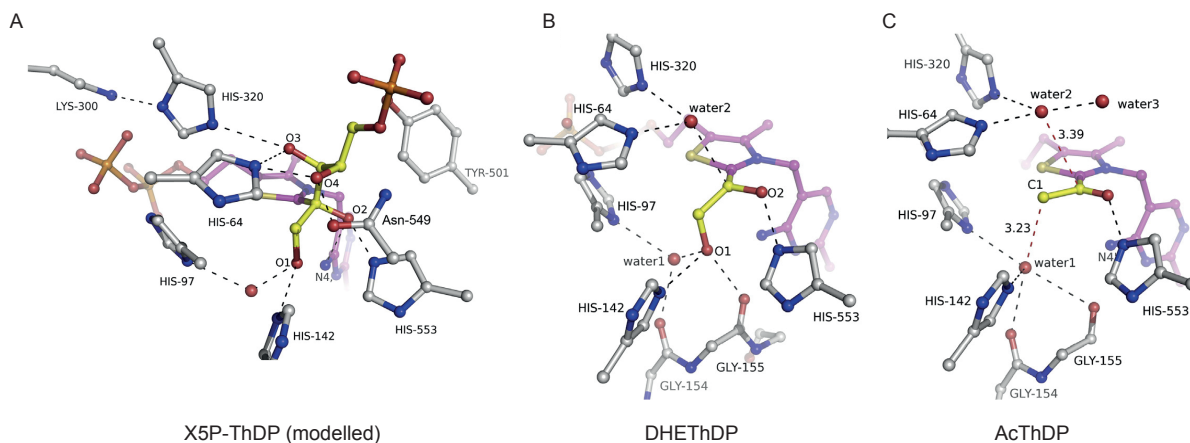


**Figure 11: Phosphoketolase active site with bound reaction intermediates.** (A) Structure of the covalent X5P-ThDP adduct from *E. coli* transketolase modelled in the active site of *B. breve* phosphoketolase. Model suggests hydrogen-bonding interactions of the intermediates O1, O2 and O3 hydroxy groups with a conserved network of histidine residues. (B) Structure of DHETHDP trapped by cryo-crystallography identifies the active site residues His97 or His142 as potential catalysts for protonation of the O1 hydroxy group prior to water elimination. (C) Structure of the post-dehydration intermediate AcThDP trapped at the phosphoketolase active site. His553 in hydrogen bonding distance to the carbonyl/hydroxy group was suggested to be involved in tautomerization of enol- to keto AcThDP. All hydrogen bonding interactions are depicted by dotted lines. Figure taken from TITTMANN, 2014<sup>4</sup>.

engaged in hydrogen bonding with intermediate hydroxy-groups, potentially acting as acid/base catalysts in the phosphoketolase reaction pathway<sup>4,73</sup>.

No structural data of the substrate ThDP adduct could be derived by cryo-crystallography, but docking models of F6P-ThDP and X5P-ThDP from transketolase into the phosphoketolase active side provide information about substrate binding and reaction of the covalent substrate adduct<sup>4,72</sup> (Figure 11A). Those models suggest His64 or His320 as base catalyst B1 for deprotonation of the substrate 3-OH group (see Figure 9). A proton relay through a His320-Lys300 dyad as suggested for transketolase seems a likely option<sup>4</sup>, although results from a computational study favor His64 as base catalyst<sup>75</sup>. The  $\alpha$ -carbanion/enamine intermediate DHETHDP resulting from C2-C3 bond cleavage and elimination of the first product needs to be protonated at the O1-hydroxy group as prerequisite for water elimination. The most obvious candidate to catalyze this step is His142 in hydrogen-bonding distance to the O1-hydroxy group, but mutational and computational studies suggest a proton relay from His97 via a neighboring water molecule (water 1, Figure 11)<sup>73,75</sup>.

Dehydration of DHETHDP leaves enol-AcThDP as covalent intermediate that is believed to undergo tautomerization to keto-AcThDP. The post-dehydration intermediate showed as trigonal-planar electron density after soaking phosphoketolase crystals with F6P in the absence of the nucleophilic acceptor substrate phosphate. This observation indicates that AcThDP accumulates in the absence of an acceptor substrate. However, at a resolution of 1.9 Å it was not possible to

determine the chemical state of the AcThDP species stabilized at the enzymes active site<sup>73</sup>. Both keto-AcThDP and the preceding enol-species seem reasonable in terms of reaction mechanism and structural data. Density functional theory studies based on structural data from *B. longum* phosphoketolase predict tautomerization via an enolate-AcThDP and propose the keto-species as stable intermediate<sup>75</sup>. All studies agree that nucleophilic attack of the second substrate phosphate occurs on the keto-form 2-AcThDP<sup>71,73,75</sup>. 2-AcThDP as intermediate of enzymatic reactions was subject of several scientific publications over the last decades and is discussed in the following chapter. Furthermore, the mechanism of enol-keto conversion is not clear. The computational studies by ZHANG AND LIU suggest tautomerization from enol-AcThDP to keto-AcThDP via the formation of an enolate species with His553 acting as acid/base catalyst, but experimental proof is missing<sup>75</sup>.

The structure of *B. breve* phosphoketolase in complex with the acceptor substrate phosphate in conjunction with mutation experiments identified the active side residues His64, His320, Gln321, Tyr501 and Asn549 important for phosphate binding or for the reaction between phosphate and AcThDP<sup>73</sup>.

#### 1.4 Acetyl-thiamine diphosphate as critical intermediate of enzymatic reactions

Early research on phosphoketolase identified acetyl-thiamine diphosphate as possible intermediate on its catalytic pathway<sup>22,69</sup>. Since, a number of enzymes were found whose reaction mechanisms potentially proceed via the formation of the covalent ThDP adduct, for example pyruvate oxidase from *lactobacillus plantarum* (*LpPOX*), pyruvate:ferredoxin oxidoreductase (PFOR) or the E1 component of the pyruvate dehydrogenase complex, that all catalyze oxidative decarboxylation of pyruvate and acyl transfer to an acceptor substrate<sup>76</sup>. However, studies on acetyl-thiazolium salts and chemically synthesized AcThDP, initiated by the proposal of AcThDP as intermediate of enzymatic reactions, revealed characteristics of the ThDP derivative that seemed critical for its role as reaction intermediate in enzymes. BRESLOW and others reported kinetic and thermodynamic instability of the examined thiazolium salt model compounds that were found to deacylate quickly in aqueous solution<sup>77-79</sup>. Next to fast hydrolysis, LIENHARD observed adduct formation of 2-acetyl-3,4-dimethylthiazolium and phosphate to some extent but no formation of acetyl phosphate<sup>80</sup>. Similar behavior was reported for chemically synthesized AcThDP. In aqueous solution, it underwent base catalyzed hydrolytic cleavage to acetate and failed to transfer the acetyl group to phosphate<sup>81,82</sup>.

Besides in phosphoketolase, enzyme-bound AcThDP was detected in *Lp*POX in absence of the second substrate phosphate<sup>41,83</sup> and in the E1 component of the pyruvate dehydrogenase complex after reaction with the non-natural substrate fluoropyruvate<sup>84</sup>. In both cases the authors reported slow hydrolysis of the intermediate in absence of the respective acyl acceptor substrates<sup>83,85,86</sup>. Most likely, the AcThDP intermediate in phosphoketolase is also subject of hydrolysis to acetate if acyl-transfer is prevented due to absence of an acceptor substrate. Considering those observations on chemically synthesized and enzyme bound AcThDP, it is remarkable how enzymes like phosphoketolase and *Lp*POX achieve acyl-transfer from the AcThDP onto the relatively weak nucleophilic acceptor phosphate while avoiding uncoupling of the reaction by an off-pathway hydrolytic cleavage of the intermediate.

In a comprehensive study including detailed kinetic characterization, <sup>1</sup>H-NMR-intermediate analysis and determination of high resolution X-ray crystal structures of the enzyme in complex with several covalent intermediates, TITTMANN and coworkers demonstrated that in *Lp*POX formation of the hydrolysis susceptible keto-AcThDP is circumvented by a coupling mechanism that links AcThDP phosphorolysis to an radical electron transfer step of the reaction<sup>41,83,86</sup>. A similar mechanism was suggested for the acyl transfer to coenzyme A in the pyruvate:ferredoxin oxidoreductase<sup>87,88</sup>. How efficient acyl-transfer from AcThDP to the respective acceptor substrates is achieved over the hydrolytic side reaction in other ThDP dependent enzymes, such as phosphoketolase or E1, is unclear yet.

## 1.5 Phosphoketolase and Transketolase - Similarities and differences

Despite their low sequence identity (only 17 % between *B. breve* phosphoketolase and *E. coli* transketolase<sup>72</sup>), the ThDP-dependent enzymes phosphoketolase and transketolase show striking structural similarity. Not only do they display the same overall domain structure consisting of similarly folded and arranged PP, PYR and C-terminal domains, the architecture of their active sites that harbors the ThDP cofactor is almost identical. Additionally, both enzymes have the same substrate specificity for F6P and X5P, catalyzing the cleavage of the C2-C3 bond of the covalent substrate-ThDP adduct under formation of the DHETHDP intermediate and E4P or G3P as products. It is assumed that the catalytic steps, cofactor activation, substrate binding and C-C bond cleavage, resulting in formation of DHETHDP, proceed in the same manner in phosphoketolase and transketolase<sup>4</sup>. The fate of the central  $\alpha$ -carbanion/enamine intermediate however differs drastically. While transketolase catalyzes the reversible transfer

of the ThDP-bound dihydroxyethyl-unit onto an aldose acceptor substrate, commonly ribose 5-phosphate (R5P) or E4P, phosphoketolase catalyzes dehydration of DHEThDP as described in the previous section (Figure 12). Crucial acid/base catalysis for the individual steps of phosphoketolase and transketolase reaction is provided by an almost identical network of conserved histidine residues (His64, His97, His142, His320 and His553 in PK; His26, His66, His100, His261 and His473 in TK, Figure 13). Overall, the active sites show distinct difference only in three positions. Asp469, strictly conserved in transketolase, is replaced by Asn549 in phosphoketolase. Tyr501 in phosphoketolase replaces the Phe434 side chain found in transketolase and the phosphoketolase Glu437 residue is located at the position of Leu382 in transketolase (Figure 13). Replacement of the conserved aspartic acid residue by the uncharged asparagine side chain is assumed to facilitate binding of the second phosphoketolase substrate phosphate, avoiding repulsion of the additional negative charge<sup>72</sup>. Tyr501 too, is part of the phosphate bind site and its replacement by the transketolase equivalent drastically increases the  $K_M$  for phosphate<sup>73</sup>. Experimental results from a phosphoketolase Glu437Gln variant indicate that Glu437 indirectly supports phosphate binding through coordination of Tyr501<sup>89</sup>.

Although high resolution X-ray structures exist of phosphoketolase and transketolase with bound DHEThDP, the critical factor responsible for the different catalytic outcome after formation of

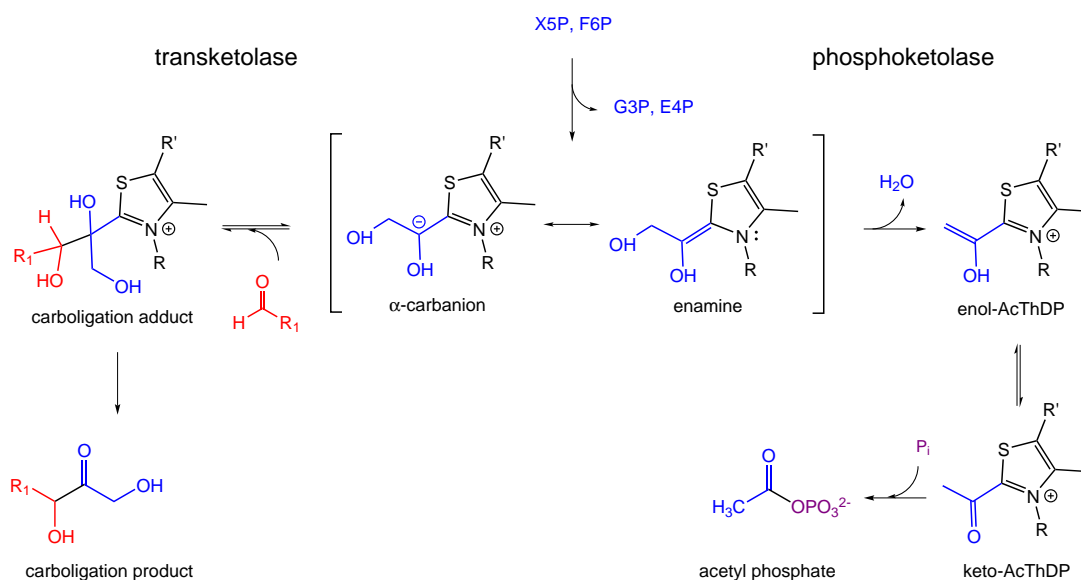


**Figure 12: Different fates of the  $\alpha$ -carbanion/enamine intermediate in phosphoketolase and transketolase.** Up to the formation of DHEThDP the reactions of phosphoketolase and transketolase proceed in the same way. Phosphoketolase catalyzes dehydration of the carbanion/enamine intermediate to AcThDP that reacts to acetyl phosphate with phosphate as second substrate. Transketolase on the other hand catalyzes the reversible carbon-carbon ligation of DHEThDP with an acceptor sugar substrate. (R=aminopyrimidine moiety, R'=ethylidiphosphate)

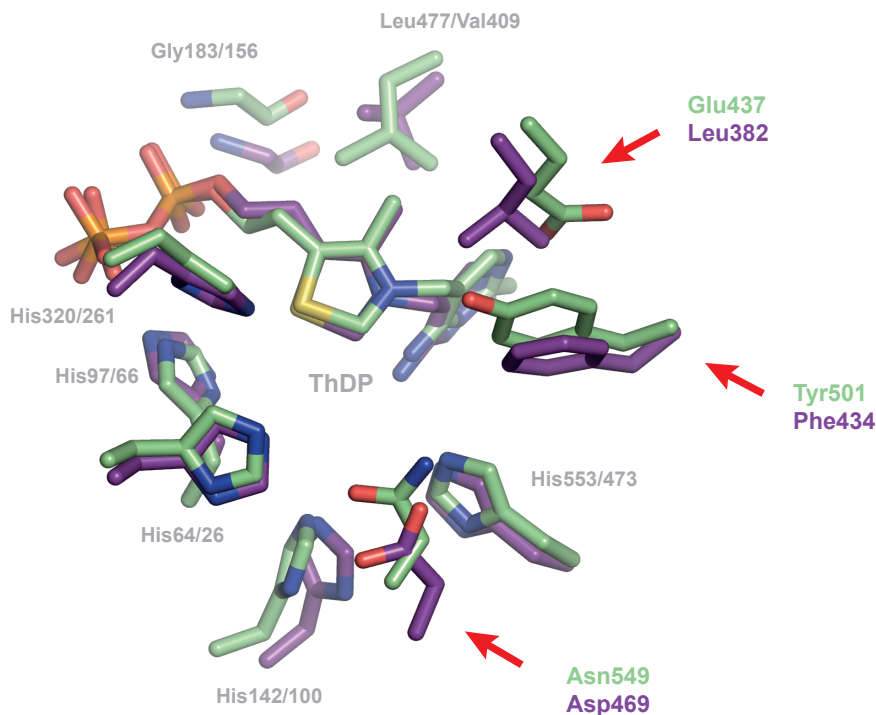


**Figure 13: Structure alignment of phosphoketolase and transketolase active sites.** Superposition of *B. breve* phosphoketolase (green) and *E. coli* transketolase (purple) reveals high similarity of their active site architecture including a network of catalytically important histidine residues. Apparent differences between the active sites of phosphoketolase (XFPK) and transketolase (TK) are the exchanges of Asn549 in XFPK to Asp469 in TK, Tyr501 that replaces a Phe residue in TK and Glu437 in XFPK instead of Leu382 in TK. Superposition prepared based on pdb files 3AHC (SUZUKI *et al.*, 2010<sup>73</sup>) and 1QGD (ISUPOV *et al.*, unpublished).

the carbanion/enamine intermediate remains unclear. Likely candidates to catalyze protonation of the DHEThDP O1-hydroxy group required for water elimination are His97 and His142<sup>73,75</sup>. Both residues likewise exist in transketolase, thus it is surprising that the dehydration occurs in phosphoketolase but not in transketolase. TITTMANN suggested that subtle differences in the orientation of His142 and the adjacent water could favor the protonation reaction, also differences in the  $pK_a$  values of the histidine side chains between the two enzymes might play a role<sup>4</sup>. However, a phosphoketolase His142Ala variant still shows residual catalytic activity and seems capable to form the post-dehydration intermediate AcThDP<sup>73</sup>. Apparently, the different activities of phosphoketolase and transketolase cannot be explained solely based on the current structural data.

Another difference between phosphoketolase and transketolase reaction lies in their reversibility. While the phosphoketolase reaction is strictly irreversible, as necessary for efficient provision of the high-energy metabolite acetyl phosphate, transketolase catalyzes forward and reverse reaction. Electron density accounting for the DHEThDP adduct in phosphoketolase indicates

that the intermediate is not stabilized as planar  $sp^2$ -hybridized enamine, but rather adopts a tetrahedral conformation, suggesting protonation at the C2 position<sup>73</sup>. Transient protonation of the pre-dehydration intermediate could contribute to the irreversibility of the phosphoketolase reaction and prevent re-ligation of carbanion/enamin intermediate and aldose phosphate product<sup>4</sup>. DHET<sub>h</sub>DP in transketolase on the other hand adopts a planar carbanion/enamine configuration and is characterized by the reversibility of the cleavage reaction<sup>90</sup>.

Taken together, our understanding of the phosphoketolase reaction is still limited compared to the extensive work that has contributed to the characterization of transketolases mode of action. Further analysis of the phosphoketolase reaction using a combination of different spectroscopic, kinetic and structural techniques will be required to provide detailed insight into its catalytic mechanism including the unique dehydration of the carbanion/enamine intermediate.

## 1.6 Objective

Within the last decade, huge progress was made towards the understanding of the phosphoketolase reaction mechanism. Especially the determination of its crystal structure in complex with the covalent pre- and post-dehydration intermediates DHEThDP and AcThDP by SUZUKI *et al.* in 2010 revealed valuable molecular details on the mode of action of this, until then, little studied member of the family of ThDP-dependent enzymes. However, several elementary steps of the phosphoketolase mechanism, such as the unique dehydration of the  $\alpha$ -carbanion/enamine intermediate or the enol- to keto-tautomerization of AcThDP, are not fully understood yet. Besides, no attention was paid to what might be one of the most critical steps in the phosphoketolase reaction: The proposed post-dehydration intermediate 2-acetyl-AcThDP (keto-AcThDP) that serves as acyl-donor for the formation of the product acetyl phosphate is very prone to hydrolysis, which raises the question how phosphoketolase achieves efficient acyl-transfer from AcThDP to phosphate while avoiding hydrolysis of the intermediate. This thesis is aiming to address the question by further elucidation of the phosphoketolase reaction mechanism with a special focus on the chemical state of the post-dehydration intermediate and its tautomerization reaction.

Furthermore, phosphoketolase will be examined for potential carboligase side reactivity, as it is described for several members of the ThDP enzyme family. With AcThDP in its enol- or enolate-form another intermediate was proposed on the phosphoketolase catalytic cycle next to the nucleophilic  $\alpha$ -carbanion/enamine intermediate DHEThDP that bears potential as substrate in C-C bond forming reactions with electrophilic acceptor substrates. A reaction emerging from the enol(ate)-azolium intermediate would represent a new type of ThDP-catalyzed carboligation. Structural characterization of phosphoketolase also revealed astonishing structural similarity to the related ThDP-dependent enzyme transketolase. Apart from three evident amino acid exchanges, the active sites of phosphoketolase and transketolase are almost identical. But whereas phosphoketolase catalyzes cleavage of F6P or X5P under generation of the high energy metabolite acetyl phosphate, transketolase mediates the transfer of a C2-fragment derived by cleavage of X5P or F6P to an acceptor sugar-substrate. Branching point in the catalytic mechanisms of phosphoketolase and transketolase is the  $\alpha$ -carbanion/enamine intermediate DHEThDP. In phosphoketolase the ThDP adduct undergoes dehydration to AcThDP, in transketolase on the other hand the intermediate acts as nucleophile for the carboligation with an acceptor phosphate sugar. No mechanistic explanation for this fundamental catalytic difference has been found yet.

By creating a "transketolase-like" phosphoketolase variant in which the differing active site residues Glu437, Tyr 501 and Asn549 are exchanged for their transketolase equivalents, the function of the side chains in the phosphoketolase reaction mechanism as well as their role in the catalytic differences between phosphoketolase and transketolase will be evaluated.



## 2 Material and Methods

### 2.1 Materials

#### Chemicals

<b>Substance</b>	<b>Supplier</b>
Acetaldehyde	Sigma-Aldrich
Acetic acid	Carl Roth GmbH & Co. KG
Acrylamide	Carl Roth GmbH & Co. KG
Agar	AppliChem GmbH
Agarose (Low EEO)	AppliChem GmbH
2-Amino-2-(hydroxymethyl)propane-1,3-diol (TRIS)	AppliChem GmbH
Bromphenol blue, sodium salt	AppliChem GmbH
Calcium chloride, hexahydrate	Carl Roth GmbH & Co. KG
Coomassie Brilliant Blue G250	AppliChem GmbH
Deuterium oxide	Sigma-Aldrich
Dimethylsulfoxide (DMSO)	Sigma-Aldrich
D-erythrose 4-phosphate sodium salt	Sigma-Aldrich
Ethanol (denatured)	Apotheke Frau Magerkuth (Göttingen)
Ethidium bromide	Carl Roth GmbH & Co. KG
Ethylenediaminetetraacetic acid (EDTA)	AppliChem GmbH
Formaldehyde solution 36.5-38 % in H <sub>2</sub> O	Sigma-Aldrich
Formaldehyde- <sup>13</sup> C solution	Sigma-Aldrich
D-Fructose 6-phosphate, disodium salt hydrate	Sigma-Aldrich
D-( <sup>13</sup> C <sub>6</sub> )Fructose 6-phosphate, disodium salt hydrate	Omicron Biochemicals, Inc
D-Glucose	AppliChem GmbH
Glycerol (anhydrous)	AppliChem GmbH
Glycine	Carl Roth GmbH & Co. KG
Glycolaldehyde dimer	Sigma-Aldrich
Guanidinium chloride	AppliChem GmbH
Hydrochloric acid (37 %)	Carl Roth GmbH & Co. KG
3-Hydroxybutyric acid	Sigma-Aldrich
4-(2-Hydroxyethyl)piperazine-1-ethanesulfonic acid (HEPES)	AppliChem GmbH

---

3-Hydroxypropionic acid	TCI Deutschland GmbH
allo-Inositol	Sigma-Aldrich
Imidazole	AppliChem GmbH
isopropyl- $\beta$ -D-thiogalactopyranoside (IPTG)	Sigma-Aldrich
Kanamycin sulfate	AppliChem GmbH
Lithium $\beta$ -hydroxypyruvate hydrate	Sigma-Aldrich
Magnesium chloride, hexahydrate	Carl Roth GmbH & Co. KG
Manganese(II) chloride, tetrahydrate	AppliChem GmbH
$\beta$ -Mercaptoethanol	Carl Roth GmbH & Co. KG
Methoxamine hydrochloride (MOX)	Sigma-Aldrich
N-methyl-N-(trimethylsilyl)trifluoroacetamide (MSTFA)	Sigma-Aldrich
Nicotinamide adenine dinucleotide (NADH)	AppliChem GmbH
Potassium chloride	Carl Roth GmbH & Co. KG
Piperazine-N,N'-bis(2-ethanesulfonic acid) (PIPES)	AppliChem GmbH
Phenylmethanesulfonyl fluoride (PMSF)	AppliChem GmbH
D-Ribose 5-phosphate, disodium salt dihydrate	Sigma-Aldrich
Pyridine anhydrous	Sigma-Aldrich
di-Sodium hydrogen arsenate, heptahydrate	Sigma-Aldrich
Sodium chloride	AppliChem GmbH
Sodium dodecyl sulfate (SDS)	AppliChem GmbH
di-Sodium hydrogen phosphate anhydrous	AppliChem GmbH
di-Sodium hydrogen phosphite pentahydrate	Sigma-Aldrich
Sodium hydroxide	AppliChem GmbH
Sodium sulfate anhydrous	Carl Roth GmbH & Co. KG
Sodium orthovanadate	Merck KGaA
Trifluoroacetaldehyde monohydrate	Sigma-Aldrich
N,N,N',N'-Tetramethylethylenediamine (TEMED)	Carl Roth GmbH & Co. KG
Thiamine diphosphate	Sigma-Aldrich
tris(hydroxymethyl)aminomethane (TRIS)	AppliChem GmbH
Tryptone	Carl Roth GmbH & Co. KG
D-Xylulose 5-phosphate, sodium salt	Sigma-Aldrich
Yeast extract	Carl Roth GmbH & Co. KG

**Enzymes, Standards and Kits**

<b>Item</b>	<b>Supplier</b>
DNaseI (bovine pancreas)	AppliChem GmbH
<i>DpnI</i>	Thermo Fisher Scientific
$\alpha$ -Glycerophosphate dehydrogenase (rabbit muscle)	Sigma-Aldrich
Lysozyme (chicken egg white)	AppliChem GmbH
Phusion polymerase	Thermo Fisher Scientific
Triosephosphate isomerase (rabbit muscle)	Sigma-Aldrich
Bradford reagent, 5x	SERVA Electrophoresis GmbH
DNA Gel Loading Dye (6x)	Thermo Fisher Scientific
GeneRuler 1 kb DNA Ladder	Thermo Fisher Scientific
Pierce <sup>TM</sup> Unstained Protein MW Marker	Thermo Fisher Scientific
dNTP mix (10 mM each)	Thermo Fisher Scientific
GC-buffer	Thermo Fisher Scientific
HF-buffer	Thermo Fisher Scientific
NucleoSpin <sup>TM</sup> Plasmid Kit	Macherey-Nagel
NucleoSpin <sup>TM</sup> Gel & PCR Clean-Up Kit	Macherey-Nagel

**Bacterial strains**

<b>Strain</b>	<b>Genotype</b>	<b>Supplier</b>
<i>E. coli</i> BL21 Star (DE3)	F <sup>-</sup> <i>ompT dcm hsdS</i> (r <sub>B</sub> <sup>-</sup> m <sub>B</sub> <sup>-</sup> ) <i>gal dcm rne131</i> (DE3)	Invitrogen
<i>E. coli</i> DH5 $\alpha$	F <sup>-</sup> $\Phi$ 80 <i>lacZ</i> $\Delta$ M15 $\Delta$ ( <i>lacZYA-argF</i> )U169 <i>recA1 endA1 hsdR17</i> (r <sub>K</sub> <sup>-</sup> m <sub>K</sub> <sup>+</sup> ) <i>phoA supE44 thi-1 gyrA96 relA1 tonA</i>	Invitrogen
<i>E. coli</i> XL1-blue	<i>recA1 endA1 gyrA96 thi-1 hsdR17 supE44 relA1 lac</i> [F' <i>proAB lacI</i> <sup>q</sup> Z $\Delta$ M15 Tn10 ( <i>Tet</i> <sup>R</sup> )]	Stratagen

**Plasmids**

<b>Plasmid</b>	<b>Properties</b>	<b>Supplier</b>
pET28b(+)	T7-promoter, N-terminal His <sub>6</sub> -tag, thromin cleavage site, T7-tag, kanamycin resistance, optional C-terminal His <sub>6</sub> -tag	Novagene

**Oligonucleotides**

<b>Name</b>	<b>Sequence (5'-3')</b>
<b>Mutagenesis</b>	
<i>BbXFPK<sub>H64S</sub></i> fwd	GGGTGGTGCCCCAG <b>CT</b> GCCGACCAGACGG
<i>BbXFPK<sub>H64S</sub></i> rev	CGTCTGGTCGGC <b>AGCT</b> GGGGCACCACCC
<i>BbXFPK<sub>E156Q</sub></i> fwd	GCGCGTAGCCAAG <b>CT</b> TGGCCACCTTCGTGG
<i>BbXFPK<sub>E156Q</sub></i> rev	CCACGAAGGTGG <b>CCAGCT</b> TGGCTACGCGC
<i>BbXFPK<sub>E437L</sub></i> fwd	CTTCGGACCGGAC <b>CT</b> GACCGCTTCCAAC
<i>BbXFPK<sub>E437L</sub></i> rev	GTTGGAAGCGGT <b>CAGGT</b> CCGGTCCGAAG
<i>BbXFPK<sub>Y501F</sub></i> fwd	CATCTGGAGCTC <b>CTT</b> CGAGTCCTTCGTC
<i>BbXFPK<sub>Y501F</sub></i> rev	GACGAAGGACT <b>CGA</b> AGGAGCTCCAGATG
<i>BbXFPK<sub>N549D</sub></i> fwd	GGTGCGAGAAGCC <b>AT</b> CGTGATCCTGACGCC
<i>BbXFPK<sub>N549D</sub></i> rev	GGCGTCAGGATC <b>ACGAT</b> GGCTTCTCGCACC
<b>Sequencing</b>	
T7 fwd	TAATACGACTCACTATAGGG
<i>BbXFPK_581</i> fwd	GCAGTCCAACAAGCTCGTCAACC
<i>BbXFPK_1313</i> fwd	CCGCTTCCAACCGCCTGAACGC
<i>BbXFPK_1939</i> fwd	GCTGGCGATGTGCCGACCCAGG

All oligonucleotides were purchased from Sigma-Aldrich. In the oligonucleotide sequences used for mutagenesis, the targeted codon is highlighted.

**Buffers and Media****Assay buffer**

20 mM	HEPES pH 7.2
1 mM	MgCl <sub>2</sub>
0.2 mM	ThDP

**Loading buffer**

20 mM	HEPES pH 7.2
300 mM	NaCl
1 mM	MgCl <sub>2</sub>
0.2 mM	ThDP

**Elution buffer**

20 mM	HEPES pH 7.2
300 mM	NaCl
1 mM	MgCl <sub>2</sub>
0.2 mM	ThDP
250 mM	Imidazole

**SEC buffer**

20 mM	HEPES pH 7.2
100 mM	NaCl
1 mM	MgCl <sub>2</sub>
0.2 mM	ThDP

**SDS running buffer**

25 mM	Tris
20 mM	Glycine
0.1 % (w/v)	SDS

**SDS sample buffer**

25 mM	Tris-HCl pH 6.6
25 % (v/v)	Glycerol
0.1 % (w/v)	SDS
0.02 % (w/v)	Bromophenolblue

**Transformation buffer**

10 mM	PIPES pH 6.7
55 mM	MnCl <sub>2</sub>
15 mM	CaCl <sub>2</sub>
15 mM	KCl

**Tris-Acetate-EDTA (TAE) buffer**

40 mM	Tris
20 mM	Acetic acid
50 mM	EDTA

**LB medium**

10 g/L	Trypton
5 g/L	Yeast extract
5 g/L	NaCl

**LB Agar**

10 g/L	Trypton
5 g/L	Yeast extract
5 g/L	NaCl
1.5 % (w/v)	Agar

**SOC medium**

20 g/L	Trypton
5 g/L	Yeast extract
10 mM	NaCl
2.5 mM	KCl
10 mM	MgCl <sub>2</sub>
20 mM	Glucose

### Equipment and Consumables

<b>Item</b>	<b>Supplier</b>
ÄKTAPrime Plus FPLC System	GE Healthcare
ÄKTAPurifier FPLC System	GE Healthcare
Agilent 5973 Network mass selective detector/ Agilent 6890 gas chromatograph	Agilent Technologies
Agilent J&W HP-5ms capillary column (30m x 0.25 mm, 0.25 $\mu$ m coating thickness)	Agilent Technologies
Arium <sup>®</sup> pro VF	Sartorius AG
AV401 NMR spectrometer	Bruker
Avanti HP-30 I centrifuge (Rotor JA-30.50)	Beckmann Coulter
Avanti JXN 26 centrifuge (Rotor JLA-8.1000)	Beckmann Coulter
Chirascan plus CD spectrometer	Applied Photophysics Ltd.
Eppendorf 5810R centrifuge (Rotor A-4-81)	Eppendorf AG
FiveEasy <sup>™</sup> pH meter	Mettler Toledo
HiPrep 26/10 desalting FPLC column	GE Healthcare
HisTrap FF 5 mL FPLC column	GE Healthcare
HisTrap desalting 5 mL FPLC column	GE Healthcare
Microfluidizer 110S	Microfluidics
Multitron Standard incubation shaker	Infors AG
NanoDrop2000	Thermo Scientific
Precision cuvettes, suprasil	Hellma GmbH
RQF 3 quench-flow instrument	KinTech Corporations
Spin-X <sup>®</sup> UF concentrator 6, 20 mL (50 kDa MWCO)	Corning GmbH
Stopped-flow system SX-20	Applied Photophysics Ltd.
Superdex <sup>™</sup> 200 HiLoad <sup>™</sup> 16/60 FPLC column	GE Healthcare
Thermocycler TProfessional	Biometra
Universal 320R centrifuge (Rotor 1420 A)	Hettich GmbH
UV-Vis Spectrometer V-650	Jasco GmbH
UV-Vis Spectrometer V-670	Jasco GmbH

## 2.2 Molecular biology methods

### 2.2.1 Preparation of chemical competent *E. coli* strains

Preparation, transformation and storage of chemical competent *E. coli* strains was performed according to INOUE *et al.*<sup>91</sup> with minor modifications.

To prepare chemical competent *E. coli* cells, frozen cultures of the respective strain (XL1blue, DH5 $\alpha$ , BL21 Star (DE3)) were streaked on a LB agar plate and incubated for 16 h at 37 °C. A single colony was used to inoculate 200 mL of LB medium. Cells were grown at 37 °C in a shaking flask to an OD<sub>600</sub> of 0.6. The culture was cooled on ice for 10 min before cells were sedimented by centrifugation with 5000 rpm for 10 min at 4 °C. The obtained pellet was resuspended in 15 mL cold transformation buffer and incubated on ice for 10 min. Cells were pelleted again as described before and resuspended in 4 mL transformation buffer. DMSO was added dropwise to a final concentration of 7 %. After incubation on ice for 10 min, aliquots of the cells were flash frozen in liquid N<sub>2</sub> and stored at -80 °C.

### 2.2.2 Transformation of plasmid DNA into *E. coli*

For the transformation of plasmid DNA into chemical competent *E. coli* strains, 10 ng plasmid DNA were added to 50  $\mu$ L of chemical competent *E. coli* cells and incubated on ice for 30 min. The bacteria were heat-shocked for 45 s at 42 °C and afterwards cooled on ice for 2 min. 1 mL of pre-warmed SOC medium was added and bacteria were grown shaking at 37 °C for 1 h. For the selection of positive transformants, cells were plated on LB agar plates containing a final concentration of 50  $\mu$ g/mL kanamycin.

### 2.2.3 Preparation of frozen storage cultures

*E. coli* cells were stored as glycerol cultures at -80 °C. For preparation of the storage cultures, cells were grown to an OD<sub>600</sub> of 0.6 to 0.8 in LB medium. 750  $\mu$ L of this culture were mixed with 250  $\mu$ L of sterile glycerol and flash frozen in liquid N<sub>2</sub>.

### 2.2.4 Isolation of plasmid DNA

In order to isolate plasmid DNA from *E. coli*, 10 mL LB medium were inoculated with a single colony of the respective strain and cells were grown overnight at 37 °C. Cells were sedimented by

centrifugation at 4000 rpm for 10 min. Plasmid DNA was isolated from the cell pellet using the NucleoSpin<sup>TM</sup> Plasmid Kit (Macherey Nagel) according to the manufacturer's manual.

### 2.2.5 Site-directed mutagenesis

Introduction of single amino acid exchanges to generate active site mutants of XFPK were performed using the QuickChange<sup>TM</sup> site-directed mutagenesis protocol (Stratagene) adapted for Phusion DNA-polymerase. In brief, mutations were introduced into the native XFPK sequence using polymerase chain reaction (PCR) with oligonucleotides coding for the respective nucleotide exchanges. The XFPK<sub>WT</sub>-pET28b(+) plasmid was used as template for all PCR reactions. The utilized oligonucleotides are listed in section 2.1. PCR was carried out according to the Phusion DNA-polymerase instruction manual (Thermo Scientific). The restriction endonuclease *DpnI* was added to the PCR product mix to digest parental DNA. The XFPK<sub>WT</sub>-pET28b(+) and XFPK<sub>H553A</sub>-pET28b(+) plasmids were a kind gift of PROF. DR. SHINYA FUSHINNOBU (University of Tokyo, Japan).

### 2.2.6 Agarose gel electrophoresis

Analysis of PCR products was carried out using agarose gel electrophoresis. DNA samples were mixed with DNA Gel Loading Dye (6x) (Thermo Fisher Scientific) in a 1:6 ratio and applied to a 1 % agarose gel. Separation of DNA fragments was conducted at 100 V for 45 min using TAE running buffer. The gel was stained in ethidiumbromide (2 mg/mL) for 10 min, allowing visualization of DNA under UV light. Size of the DNA fragments was determined using GeneRuler 1 kb DNA Ladder (Thermo Fisher Scientific) as size standard.

### 2.2.7 Determination of DNA concentration

DNA concentration was measured spectroscopically via absorbance at 260 nm using a NanoDrop 2000 device. Concentration was calculated using the LAMBERT-BEER law (Eq. 1) with an extinction coefficient of  $\epsilon = 20 \text{ mL/ng}\cdot\text{cm}$ .

$$A_{260nm} = c \cdot \epsilon \cdot d \tag{1}$$



### 2.2.8 Sequencing of plasmid DNA

Plasmid DNA was checked for the correct nucleotide sequence using the SANGER sequencing service of the commercial provider GATC Biotech AG. Utilized oligonucleotide primers are listed in section 2.1.

## 2.3 Protein production, purification and analysis

Production and isolation of recombinant XFPK proteins was carried according to SUZUKI *et al.*<sup>92</sup> with modifications.

### 2.3.1 Production of recombinant *B. breve* XFPK in *E. coli*

For heterologous production of N-terminal His<sub>6</sub>-tagged XFPK<sub>WT</sub> and active site variants, *E. coli* BL21 Star (DE3) were transformed with the XFPK<sub>WT</sub>-pET28b(+) vector or the expression plasmid coding for the respective active site variant. The expression plasmid XFPK<sub>WT</sub>-pET28b(+) was provided by PROF. DR. SHINYA FUSHINNOBU (University of Tokyo, Japan), it contains the nucleotide sequence coding for the *B. breve* phosphoketolase enzyme including an N-terminal His<sub>6</sub>-tag under the control of the T7-promoter<sup>92</sup>. A pre-culture of 200 mL LB medium was inoculated with five to ten colonies and cultivated overnight at 30 °C. Cultivation of *E. coli* was performed in 0.5 to 2 L culture flasks under constant shaking (200 rpm) at the indicated temperature. The pre-culture was used for inoculation of 6 L LB medium supplemented with 50 µg/mL kanamycin. Cells were grown at 37 °C to an OD<sub>600</sub> of 0.6 and then cooled down to 25 °C. Expression of the recombinant *xfp* gene was induced by the addition of 1 mM isopropyl-β-D-thiogalactopyranoside (IPTG). Afterwards, cells were cultivated for 16 h at 25 °C. Cells were harvested by centrifugation (4800 rpm, 20 min, 4 °C). Obtained pellets were washed with loading buffer, flash frozen and stored at -20 °C.

### 2.3.2 Purification of recombinant XFPK

Isolation of recombinant His<sub>6</sub>-tagged XFPK from the *E. coli* BL21 Star (DE3) expression cells was achieved by immobilized metal ion chromatography. Cells were resuspended in loading buffer (20 mM HEPES pH 7.2, 300 mM NaCl, 1 mM MgCl<sub>2</sub>, 0.2 mM ThDP) supplemented with 0.5 mg/mL lysozyme, 0.2 mM PMSF and 5 µg/mL DNase. Cells were lysed using a microfluidizer

(Microfluidics) at 15000 psi for five cycles. The lysate was centrifuged with 75000 x g for 40 min at 4 °C to remove cell debris. The soluble fraction was then applied to a NiNTA column (HisTrap<sup>TM</sup> FF, GE Healthcare) equilibrated with loading buffer. After washing with 100 - 200 mL loading buffer, the His<sub>6</sub>-tagged protein was eluted from the affinity column with elution buffer (20 mM HEPES pH 7.2, 300 mM NaCl, 1 mM MgCl<sub>2</sub>, 0.2 mM ThDP, 250 mM imidazole). Before applying the isolated protein to size exclusion chromatography (SEC) for further purification, buffer was exchanged to SEC buffer (20 mM HEPES pH 7.2, 100 mM NaCl, 1 mM MgCl<sub>2</sub>, 0.2 mM ThDP) using a HiPrep 26/10 desalting column (GE Healthcare). Size exclusion chromatography was carried out on HiLoad 16/600 Superdex 200 column (GE Healthcare) in SEC buffer. Fractions containing hexameric XFPK were collected and concentrated by ultrafiltration (Corning SpinX 50 kDA MWCO). If not indicated differently, for all further experiments the isolated enzyme was transferred to assay buffer (20 mM HEPES pH 7.2, 1 mM MgCl<sub>2</sub>, 0.2 mM ThDP) via a HiTrap 5 mL desalting column (GE Healthcare). Homogeneity of the final protein was evaluated by SDS-PAGE (section 2.3.4). The results of SDS-PAGE analysis are shown in the appendix.

### 2.3.3 Determination of protein concentration

Concentration of the isolated XFPK protein was determined according to BRADFORD<sup>93</sup>, using 5x Bradford Reagent (Serva) as described in the manufacturer's instruction manual.

### 2.3.4 Sodium dodecyl sulfate polyacrylamide gel electrophoresis (SDS-PAGE)

Progress of purification and homogeneity of the final protein sample were evaluated by sodium dodecyl sulfate polyacrylamide gel electrophoresis (SDS-PAGE) according to the protocol of LAEMMLI<sup>94</sup>. Protein samples were mixed with SDS sample buffer, heated to 96 °C for 5 min and applied to the SDS polyacrylamide gel (stacking gel: 5% acrylamide, pH 6.8; resolving gel: 12% acrylamide, pH 8.8). Gels were run at 35 mA in SDS running buffer. For visualization of separated proteins, gels were stained with Coomassie Brilliant Blue staining solution (0.2 % (w/v) Coomassie Brilliant Blue G250, 40 % (v/v) ethanol, 6 % (v/v) acetic acid). Pierce<sup>TM</sup> Unstained Protein MW Marker (Thermo Fisher Scientific) was used as size standard to estimate molecular weight of the proteins.

## 2.4 Biophysical methods

### 2.4.1 UV-Vis spectroscopy

All UV-Vis spectra were recorded between 300 and 600 nm in a Jasco V-650 or V-670 spectrophotometer using quartz cuvettes with a pathlength of 1 cm. Detection speed was set to 100 nm/s with a data pitch of 1 nm. A standard approach for the detection of phosphoketolase-bound AcThDP intermediate contained 2.3 mg/mL XFPK in assay buffer, substrate concentrations are indicated for the individual experiments. pH-dependent spectra were recorded in assay buffer with an increased HEPES concentration (50 mM HEPES pH 6-8.5, 1 mM MgCl<sub>2</sub>, 0.2 mM ThDP) to ensure pH stability. If not indicated otherwise, spectra were recorded in triplicate measurements and averaged. All spectra were normalized against buffer and overlaid at  $A_{600nm} = 0$ .

### 2.4.2 Secondary structure analysis by circular dichroism spectroscopy

To confirm structural integrity of the generated XFPK variants, they were analyzed by far-UV CD spectroscopy. CD spectra of the different enzyme variants were recorded between 180 - 260 nm and compared to the XFPK<sub>WT</sub> spectrum to exclude differences in secondary structure elements induced by the introduced mutations. Measurements were performed at a protein concentration of 0.1 mg/mL in 10 mM phosphate buffer pH 7.2 at 25 °C in a quartz cuvette with 1 mm pathlength. Data acquisition was carried out at a Chirascan plus CD spectrometer (Applied Photophysics) with a data interval and band width of 1 nm and a response time of 5 s.

### 2.4.3 Analysis of covalent reaction intermediates by <sup>1</sup>H-NMR spectroscopy

An acid quench/<sup>1</sup>H-NMR spectroscopy method, developed by TITTMANN *et al.*<sup>45</sup>, was applied to detect potential covalent ThDP-intermediates in the phosphoketolase reaction cycle. The experiments were carried out according to the protocol described in the aforementioned publication. XFPK was transferred into ThDP-free buffer (20 mM HEPES pH 7.2, 1 mM MgCl<sub>2</sub>) and 15 mg/mL enzyme were mixed with 100 mM F6P or 100 mM F6P plus 100 mM Na<sub>2</sub>HPO<sub>4</sub> in a 1+1 mixing ratio. The reaction was stopped in the pre-steady-state (after 60 ms) or in the steady-state (after 180 s) by the addition of quenching solution (1 M DCl, 12.5 % (w/v) trichloroacetic acid in D<sub>2</sub>O). In case of the pre-steady-state time point, the mixing steps for reaction initiation and stopping were carried out in a RQF 3 quench-flow mixing device (KinTech Corporations). Acid quenching

denatures the protein component while the acid-stable covalent ThDP reaction intermediates are released into solution. Precipitated protein was removed from the reaction mix by centrifugation (15000 rpm, 15 min, 4 °C). The supernatant containing free cofactor and ThDP adducts was filtered and applied to  $^1\text{H-NMR}$  spectroscopy. All NMR data collection and evaluation was carried out by PROF. DR. KAI TITTMANN.

## 2.5 Kinetic Methods

### 2.5.1 Steady-state kinetic analysis

The enzymatic activity of phosphoketolase was determined in a direct circular dichroism spectroscopy-based assay, detecting the formation of the product E4P that shows a negative CD signal at 300 nm. The assay mix contained 20 mM HEPES pH 7.2, 1 mM  $\text{MgCl}_2$ , 0.2 mM ThDP, 4.9 - 105  $\mu\text{M}$  XFPK and varying concentrations of F6P or  $\text{Na}_2\text{HPO}_4$ . In order to determine  $K_M$  for either F6P or phosphate, concentration of the other substrate was kept constant at 50 mM  $\text{Na}_2\text{HPO}_4$  or 150 mM F6P respectively. Measurements were initiated by addition of the enzyme to the reaction mix. Measurements were carried out at 25 °C on a Chirascan plus CD spectrometer (Applied Photophysics) recording signal at 300 nm with a band width of 1 nm and a scanning speed of 2 points/s.

The initial rates of E4P formation were determined from the initial change in CD signal  $\Delta\Theta_{300\text{nm}}$  over time. Initial changes in the CD signal in mdeg/min were converted into the initial reaction rates in mM/min using a calibration curve. For preparation of the calibration curve, the CD signal at 300 nm for different E4P concentrations was measured and plotted against the corresponding E4P concentration. Linear regression of the calibration curve yielded a conversion factor of 6.01 mdeg/mM (Figure 56). Hence, the initial reaction rate  $v$  could be calculated using Equation 2. Dependency of  $v$  on the substrate concentration  $[\text{S}]$  was analyzed using the MICHAELIS-MENTEN-equation (Eq. 3). Data from the phosphate dependent assay was fitted with Equation 4.  $k_{\text{cat}}$  and  $A_{\text{spec}}$  were calculated considering the applied protein concentration. If not indicated otherwise, data points were determined in triplicate measurements, error bars indicate standard deviation from the mean value. Margin of error of the macroscopic constants represents standard deviation of the fitted parameters.

$$v = \frac{\Delta\Theta_{300\text{nm}}/\text{min}}{6.01 \frac{\text{mdeg}}{\text{mM}}} \quad (2)$$

$v$  : initial reaction rate  
 $\Delta\Theta_{300\text{nm}}$  : initial change in CD signal at 300 nm

$$v = \frac{V_{\text{max}} \cdot [\text{S}]}{K_{\text{M}} + [\text{S}]} \quad (3)$$

$V_{\text{max}}$  : maximum activity at substrate saturation  
 $K_{\text{M}}$  : Michaelis constant

$$v = y_0 + \frac{V_{\text{max}} \cdot [\text{S}]}{K_{\text{M}}^{\text{app}} + [\text{S}]} \quad (4)$$

$V_{\text{max}}$  : maximum activity at substrate saturation  
 $K_{\text{M}}^{\text{app}}$  : apparent Michaelis constant  
 $y_0$  : offset

### 2.5.2 Transient kinetic analysis using stopped-flow absorbance spectroscopy

Transient kinetics of formation and depletion of phosphoketolase-bound AcThDP were analyzed in rapid mixing experiments via its distinct absorbance signal at 420 nm. All measurements were carried out on a SX20 stopped-flow spectrophotometer (Applied Photophysics) at 25 °C in assay buffer. General experimental setup of the transient kinetic measurements was adapted with modifications from the work of S. SCHNEIDER<sup>89</sup>.

#### Time-resolved absorbance spectra

To examine the phosphoketolase reaction for the occurrence of covalent ThDP-reaction intermediates, time resolved absorbance spectra were recorded. 48.5  $\mu\text{M}$  XFPK were mixed with 100 mM F6P or 100 mM F6P plus 100 mM  $\text{Na}_2\text{HPO}_4$  in a 1+1 mixing ration. UV-Vis spectra between 300 - 600 nm were recorded in logarithmic time intervals using photo diode array detection. All spectra were normalized against the buffer spectrum.

#### Single mixing experiments

To follow the formation of phosphoketolase bound AcThDP, 48.5  $\mu\text{M}$  XFPK were fast-mixed with varying concentrations of F6P (0 - 400 mM) in a 1+1 mixing ratio. Progress of absorbance at

420 nm was recorded over time until the steady-state was reached. To determine the apparent rate constants  $k_{\text{obs}_1}$  and  $k_{\text{obs}_2}$ , progress curves were fitted with a two-term exponential equation (Eq. 5).  $k_{\text{obs}_1}$  and  $k_{\text{obs}_2}$  were plotted against the respective substrate concentration  $[S]$ . Data of  $k_{\text{obs}_1}$  was fitted according to Equation 6 or 7 to analyze substrate dependency and determine  $k_{\text{obs}_1}^{\text{max}}$  and  $K_S^{\text{app}}$ . If not indicated otherwise, data points were determined in triplicate measurements, error bars indicate standard deviation from the mean value. Margin of error of the macroscopic constants represents standard deviation of the fitted parameters.

$$A_{420}(t) = a_1 \cdot e^{(-k_{\text{obs}_1} \cdot t)} + a_2 \cdot e^{(-k_{\text{obs}_2} \cdot t)} + c \quad (5)$$

$k_{\text{obs}_1}, k_{\text{obs}_2}$  : first order rate constants  
 $a_1, a_2$  : amplitudes  
 $t$  : time  
 $c$  : off-set

$$k_{\text{obs}} = \frac{k_{\text{obs}}^{\text{max}} \cdot [S]^n}{K_S^{\text{appn}} + [S]^n} \quad (6)$$

$k_{\text{obs}}^{\text{max}}$  : first order rate constant at substrate saturation  
 $K_S^{\text{app}}$  : substrate concentration at half  $k_{\text{obs}}^{\text{max}}$   
 $n$  : HILL-coefficient

$$k_{\text{obs}} = \frac{k_{\text{obs}}^{\text{max}} \cdot [S]}{K_S^{\text{app}} + [S]} \quad (7)$$

$k_{\text{obs}}^{\text{max}}$  : first order rate constant at substrate saturation  
 $K_S^{\text{app}}$  : substrate concentration at half  $k_{\text{obs}}^{\text{max}}$

### Sequential mixing experiments

Kinetics of the reaction between the covalent AcThDP intermediate and different acceptor substrates were investigated in double-jump stopped-flow experiments. 97  $\mu\text{M}$  XFPK were mixed with 80 mM F6P in a 1+1 mixing ratio in a stopped-flow device configured to sequential mode, followed by fast mixing with varying concentrations of the acceptor substrate as indicated for the individual experiments. Decrease of AcThDP absorbance at 420 nm was recorded over time. The aging time between the mixing steps was set to 5 s to ensure that the steady-state of the reaction was reached and AcThDP concentration remained constant. Next to the native acceptor

substrate phosphate ( $\text{Na}_2\text{HPO}_4$ ) the phosphate analogous  $\text{Na}_2\text{HAsO}_4$ ,  $\text{Na}_2\text{SO}_4$ ,  $\text{Na}_2\text{HPO}_3$  and  $\text{Na}_3\text{VO}_4$  were used as alternative nucleophilic acceptors.

For preparation of the vanadate solution, 200 mM  $\text{Na}_3\text{VO}_4$  were dissolved in assay buffer and pH adjusted to 7.2 with HCl. Solution was boiled to destroy vanadate polymers until orange color disappeared and pH was readjusted to 7.2. The procedure was repeated until a colorless solution of  $\text{Na}_3\text{VO}_4$  at pH 7.2 was obtained.

Progress curves of absorbance at 420 nm were fitted with an exponential equation (Eq. 8). The resulting apparent rate constants  $k_{\text{obs}}$  were plotted against the respective substrate concentration and data was fitted according to Equation 9 to determine  $k_{\text{obs}}^{\text{max}}$  and  $K_{\text{S}}^{\text{app}}$ . If not indicated otherwise, data points were determined in triplicate measurements, error bars indicate standard deviation from the mean value. Margin of error of the macroscopic constants represents standard deviation of the fitted parameters.

$$A_{420}(t) = a \cdot e^{(-k_{\text{obs}} \cdot t)} + c \quad (8)$$

$k_{\text{obs}}$  : first order rate constant  
 $a$  : amplitude  
 $t$  : time  
 $c$  : off-set

$$k_{\text{obs}} = y_0 + \frac{k_{\text{obs}}^{\text{max}} \cdot [\text{S}]}{K_{\text{S}}^{\text{app}} + [\text{S}]} \quad (9)$$

$k_{\text{obs}}^{\text{max}}$  : first order rate constant at substrate saturation  
 $K_{\text{S}}^{\text{app}}$  : substrate concentration at half  $k_{\text{obs}}^{\text{max}}$   
 $y_0$  : off-set

### 2.5.3 Steady-state analysis of the hydrolysis side reaction

As alternative method to determine the turnover of the phosphoketolase hydrolytic side reaction, a technique described in TITTMANN *et al.* 2005 was adapted<sup>83</sup>. Therefore, progress of AcThDP absorbance at 420 nm was recorded in a stopped-flow spectrophotometer as described in section 2.5.2 after mixing of 24  $\mu\text{M}$  with different F6P concentrations between 0.5 - 4 mM. Absorbance was recorded until total consumption of F6P. According to GIBSON *et al.*<sup>95</sup> the area underneath

the kinetic trace can be assumed to be proportional to the concentration of F6P in solution, hence the F6P concentration can be described by the following term:

$$[\text{F6P}]_{\text{total}} = \alpha \left[ \int_{t_0}^{t_{\text{end}}} A_{420\text{nm}}(t) dt - A_{420\text{nm}}(t_{\text{end}}) \cdot (t_{\text{end}} - t_0) \right] \quad (10)$$

As  $A_{420\text{nm}}(t_{\text{end}}) = 0$ , the term can be written:

$$[\text{F6P}]_{\text{total}} = \alpha \left[ \int_{t_0}^{t_{\text{end}}} A_{420\text{nm}}(t) dt \right] \quad (11)$$

This relationship allows determination of the F6P concentration at any point of the reaction by simple proportionality:

$$\frac{\int_{t_0}^{t_{\text{end}}} A_{420\text{nm}}(t) dt}{[\text{F6P}]_{\text{total}}} = \frac{\int_{t_1}^{t_2} A_{420\text{nm}}(t) dt}{[\text{F6P}]_{t_2-t_1}} \quad (12)$$

Consequently the reaction rate  $v = d[\text{F6P}]/dt$  in the steady-state can be calculated from:

$$v = \frac{\int_{t_1}^{t_2} A_{420\text{nm}}(t) dt}{\int_{t_0}^{t_{\text{end}}} A_{420\text{nm}}(t) dt} \cdot \frac{[\text{F6P}]_{\text{total}}}{(t_2 - t_1)} \quad (13)$$

- $A_{420\text{nm}}$  : absorbance of AcThDP at 420 nm
- $t_0$  : starting point of the reaction
- $t_{\text{end}}$  : end point of the reaction
- $t_1$  : starting point of steady-state phase
- $t_2$  : end point of steady-state phase
- $\alpha$  : proportionality factor

The integrals were determined in approximation from the sum of the areas below each data point.

The time points  $t_1$  and  $t_2$  mark the start and the end of the steady-state phase as depicted in



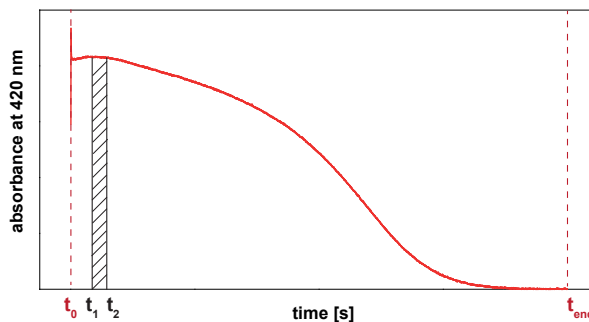


**Figure 14: Exemplary progress curve of AcThDP absorbance.** The area below the progress curve is proportional to the applied F6P concentration and can be used to determine the substrate concentration at every point of the reaction. The time points  $t_0$  and  $t_{end}$  mark the start and end point of the reaction. The time points  $t_1$  and  $t_2$  mark start and end of the steady-state phase. The area underneath the progress curve that represents the steady-state phase is shaded.

Figure 14. In order to determine  $k_{cat}$ , the obtained reaction rates were plotted against the applied F6P and data was fitted with the MICHELIS-MENTEN equation (Eq. 3).

## 2.6 Analysis of carboligation products by gas chromatography-mass spectrometry

Products of phosphoketolase carboligation side reactions were identified and quantified using gas chromatography coupled to mass spectrometry (GC-MS). For a standard reaction,  $24 \mu\text{M}$  XFPK were incubated with  $20 \text{ mM}$  F6P and  $100 \text{ mM}$  of an aldehyde acceptor (formaldehyde, acetaldehyde, trifluoroacetaldehyde, glycolaldehyde) in assay buffer at  $23 \text{ }^\circ\text{C}$  for 1 - 16 h. For extraction of products and remaining substrate sugars, extraction solution ( $32.25 \%$  (v/v) methanol,  $12.5 \%$  (v/v) chloroform in  $\text{H}_2\text{O}$ ) was added in a 2:1 ratio. To convert the analytes into their methoxyimino- and trimethylsilyl-derivatives,  $20 - 40 \mu\text{L}$  of the polar phase were evaporated under nitrogen, redissolved in  $30 \mu\text{L}$   $30 \text{ mg/mL}$  methoxamine hydrochloride in pyridine and incubated for at  $23 \text{ }^\circ\text{C}$  16 h, followed by addition of  $15 \mu\text{L}$  of the second derivatization agent N-Methyl-N(trimethylsilyl)trifluoroacetamide (MSTFA). GC-MS measurements were performed on a Agilent 5973 Network mass selective detector connected to a Agilent 6890 gas chromatograph equipped with a capillary HP5-ms column (Agilent) with the following dimensions:  $30 \text{ m} \times 0.25 \text{ mm}$ ;  $0.25 \mu\text{m}$  coating thickness. Helium was used as carrier gas with a flow of  $1 \text{ mL/min}$ . The temperature gradient was set as follows:  $70 \text{ }^\circ\text{C}$  for 2 min,  $70\text{-}220 \text{ }^\circ\text{C}$  at  $8 \text{ k/min}$ ,  $220\text{-}330 \text{ }^\circ\text{C}$  at  $8 \text{ k/min}$ ,  $330 \text{ }^\circ\text{C}$  for 2 min, with an inlet temperature of  $250 \text{ }^\circ\text{C}$ . Electron energy of  $70 \text{ eV}$ , ion source temperature of  $230 \text{ }^\circ\text{C}$  and a transfer line temperature of  $330 \text{ }^\circ\text{C}$  was used, mass spectra were recorded between

70 and 600  $m/z$ . Products were identified based on retention time and mass spectrum by library search with the NIST mass spectrometry database and in comparison to pure reference substance.

Quantification of the reaction products 3-hydroxypropionic acid and dihydroxyacetone was carried out with an internal standard (allo-inositol). Absolute quantities of reaction products were calculated using a calibration curve that relates defined quantities of pure target substance to signal ratio of target substance and internal standard. The masses used for quantification were 219 for 3-hydroxypropionic acid, 248 for dihydroxyacetone and 318 for allo-inositol. For integration of the corresponding signal peaks, the Agilent ChemStation software was used.

The GC-MS analysis was carried out in close cooperation with DR. TILL ISCHEBECK (Department of Plant Biochemistry). DR. TILL ISCHEBECK developed the protocol for sample preparation and GC-MS analysis, assisted in data acquisition and performed data analysis for quantification of the reaction products.

## 2.7 Detection of transketolase activity

In order to detect potential transketolase activity of XFPK<sub>Y501F/N549D</sub> and XFPK<sub>E437L/Y501F/N549D</sub>, the phosphoketolase variants were incubated with transketolase substrates and analyzed for the formation of transketolase products by GC-MS. The reaction mix contained 105  $\mu$ M of XFPK<sub>Y501F/N549D</sub> or XFPK<sub>E437L/Y501F/N549D</sub>, 20 mM F6P and 20 mM R5P in assay buffer. Samples were incubated at 23 °C for 16 h and analyzed by GC-MS for presence of the transketolase product sedoheptulose 7-phosphate as described in section 2.6.

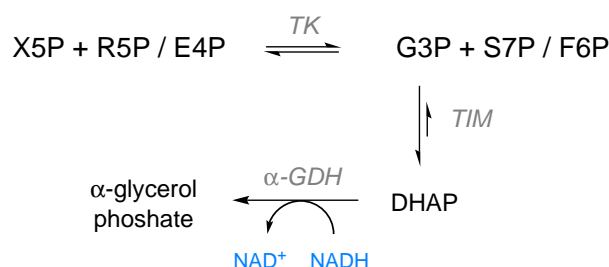


**Figure 15: Schematic representation of the coupled transketolase activity assay.** By coupling the transketolase (TK) reaction to the reactions of triosephosphate isomerase (TIM) and  $\alpha$ -glycerolphosphate dehydrogenase ( $\alpha$ -GDH), the transketolase product is removed and the equilibrium of the reversible reaction shifted towards product formation. Transketolase converts xylulose 5-phosphate (X5P) and ribose 5-phosphate (R5P) or erythrose 4-phosphate (E4P) to glyceraldehyde 3-phosphate (G3P) and sedoheptulose 7-phosphate (S7P) or fructose 6-phosphate (F6P). TIM catalyzes conversion of G3P to dihydroxyacetone phosphate (DHAP) that is converted in an irreversible reaction to  $\alpha$ -glycerol phosphate by  $\alpha$ -GDH.

In an alternative experimental approach, adapting a protocol designed for spectroscopic detection of transketolase activity<sup>96</sup>, the transketolase reaction was coupled to two further enzymatic reactions to shift the equilibrium towards product formation as depicted in Figure 15. 105  $\mu$ M of XFPK<sub>Y501F/N549D</sub> or XFPK<sub>E437L/Y501F/N549D</sub> were incubated with 10 mM X5P, 10 mM R5P or E4P, 1.5 U  $\alpha$ -glycerolphosphate dehydrogenase, 15 U triosephosphate isomerase and 1 mM NADH at 23 °C for 2 h. The reaction mix was analyzed by GC-MS for presence of the potential transketolase products sedoheptulose 7-phosphate or fructose 6-phosphate. Product extraction, derivatization and GC-MS measurement was carried out as described in section 2.6.

## 3 Results

### 3.1 Spectroscopic analysis of reaction intermediates in the phosphoketolase reaction cycle

DHEThDP and AcThDP were predicted as intermediates on the phosphoketolase reaction pathway early after discovery of its enzymatic activity<sup>70</sup>. Trapping of both ThDP adducts in cryo-crystallographic studies on *B. breve* phosphoketolase could finally confirm their role as covalent reaction intermediates<sup>73</sup>. Many covalent and non-covalent intermediates of ThDP-dependent enzymes exhibit spectral signatures in the UV-Vis range<sup>47</sup>. In a preliminary study, a UV-Vis absorbance band was observed when phosphoketolase reacted with F6P. The band was assumed to be derived from the post-dehydration intermediate AcThDP<sup>89</sup>.

In order to verify and specify assignment of the reported signal, the phosphoketolase reaction was investigated for absorbance bands that might be assigned to covalent ThDP-adducts arising on the reaction pathway. UV-Vis spectra between 300 and 600 nm were recorded of phosphoketolase in its ground state and after addition of both substrates F6P and phosphate, or of F6P alone (Figure 16). No changes in absorbance were detectable between the ground state spectrum and that recorded after the addition of both substrates F6P and phosphate. However, when F6P alone was added to the enzyme, we observed an absorbance band with  $\lambda_{max}$  at 420 nm as reported before. This band was also detectable when  $\beta$ -hydroxypyruvate or glycolaldehyde were used as alternative substrates instead of F6P, although higher substrate concentrations were required to obtain a signal with comparable strength (Figure 55, Appendix). In all cases the signal disappeared when phosphate was added to the reaction mix, indicating accumulation of one or both intermediates in absence of the acceptor substrate, leading to the observed spectral signal.

Time-resolved absorbance spectra were recorded using a stopped-flow spectrophotometer with photodiode array detection in order to observe potential transient intermediates and to record the evolution of the absorbance band at 420 nm. Still, no signal was observed after rapid mixing of phosphoketolase with both substrates (Figure 17B). Time-resolved monitoring of the absorbance band at 420 nm after rapid-mixing of phosphoketolase with F6P as only substrate revealed maximum absorbance after around 60 ms in the pre-steady-state of the reaction (Figure 17A). The signal then remained stable for several minutes (Figure 58, Appendix). SUZUKI *et al.* reported accumulation of AcThDP after soaking phosphoketolase crystals with F6P in the absence of phosphate, whereas they assume the DHEThDP intermediate to be of transient character<sup>73</sup>. Due

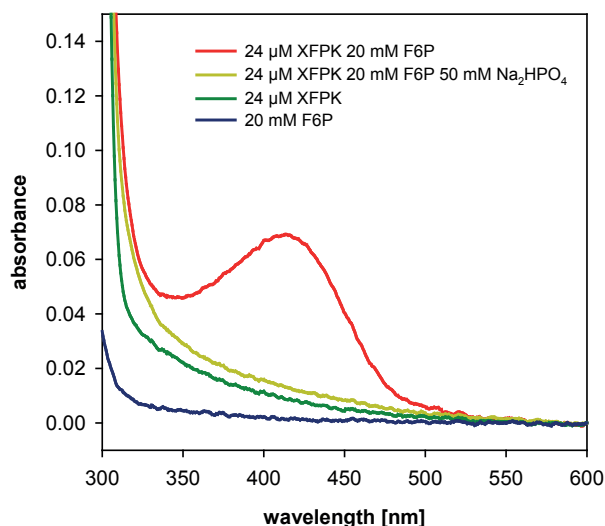


**Figure 16: UV-Vis absorbance spectrum of phosphoketolase in its resting state and after substrate addition.** No differences in absorbance were observed between phosphoketolase ( $24\ \mu\text{M}$ ) in its resting state (green) or after addition of both substrates F6P ( $20\ \text{mM}$ ) and  $\text{Na}_2\text{HPO}_4$  ( $50\ \text{mM}$ ) (light green). Addition of F6P alone leads to formation of an absorbance band with  $\lambda_{max}$  at  $420\ \text{nm}$  (red).

to the longevity of the observed signal it is likely that phosphoketolase bound AcThDP accounts for the absorbance band.

Distribution of covalent ThDP intermediates during the phosphoketolase reaction was further analyzed using an acid quench/ $^1\text{H}$ -NMR method described by TITTMAN *et al.*<sup>45</sup>. Covalent ThDP adducts are stable under acidic conditions and can be isolated from the protein compound by acid precipitation. Different substituents at the C2 atom of the thiazolium ring cause specific  $^1\text{H}$ -NMR chemical shifts of the aminopyrimidine C6'-H singlets, which can be used to distinguish the different ThDP adducts. We analyzed the distribution of covalent ThDP intermediates in the phosphoketolase reaction under steady-state conditions, as well as in the pre-steady-state 60 ms after reaction initiation where maximum absorbance at  $420\ \text{nm}$  was observed. Obtained signals were identified as free cofactor, DHEThDP and AcThDP with the help of chemically synthesized reference substances. ThDP and DHEThDP show chemical shifts of  $8.01\ \text{ppm}$  and  $7.31\ \text{ppm}$ , AcThDP yields three signals at  $7.36$ ,  $7.37$  and  $8.6\ \text{ppm}$  derived from three different conformations, keto-, hydrate- and internal carbinol form of AcThDP<sup>45,81</sup> (Figure 17C, top row). In the absence of the nucleophilic acceptor substrate phosphate, AcThDP occurred as predominant intermediate together with free cofactor and a small amount of DHEThDP under steady-state conditions (Figure 17). A similar distribution was observed in the pre-steady-state (data not shown). This distribution matches the observations from X-ray crystallographic experiments, showing accumulation of AcThDP in the absence of phosphate. It is assumed that phosphoketolase bound AcThDP undergoes hydrolysis to acetate if no phosphate molecule is present at the active site acting as acceptor for the acyl-moiety. Hydrolysis of AcThDP to acetate seems to be the rate limiting step under the applied reaction conditions. In the reaction of phosphoketolase

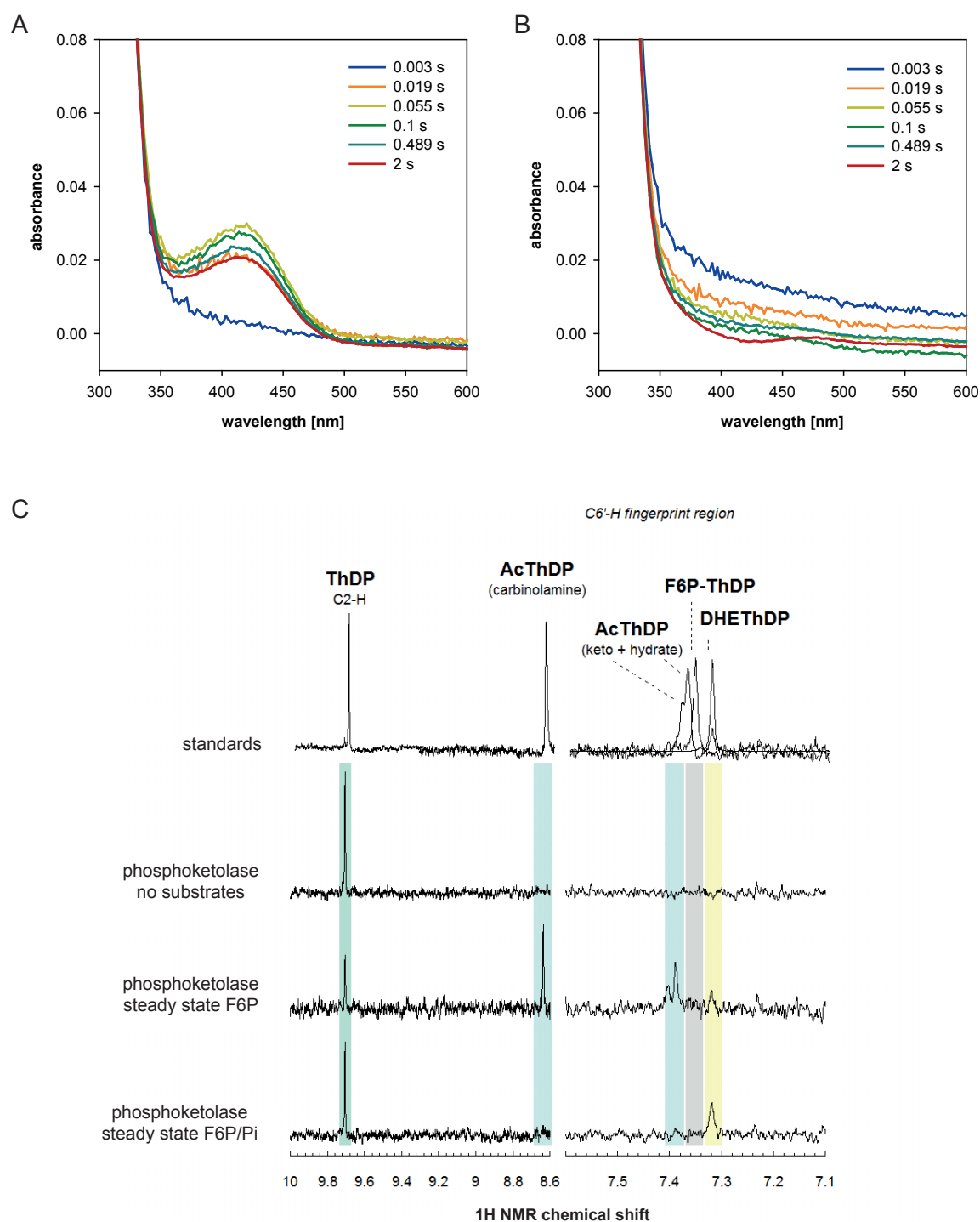


**Figure 17: Analysis of covalent ThDP-intermediates in phosphoketolase.** (A) Time-resolved absorbance spectra recorded after fast-mixing of  $24 \mu\text{M}$  XFPK with  $100 \text{ mM}$  F6P shows evolution of the absorbance band with  $\lambda_{max}$  at  $420 \text{ nm}$ . (B) Time-resolved absorbance spectra recorded after fast-mixing of  $24 \mu\text{M}$  XFPK with  $100 \text{ mM}$  F6P and  $100 \text{ mM}$   $\text{Na}_2\text{HPO}_4$  does not show a spectral signal. Depicted are the difference spectra after subtraction of the XFPK ground state spectrum. (C)  $^1\text{H}$ -NMR analysis of covalent ThDP intermediates.  $158 \mu\text{M}$  XFPK were mixed with  $100 \text{ mM}$  F6P or  $100 \text{ mM}$  F6P and  $100 \text{ mM}$   $\text{Na}_2\text{HPO}_4$ . The reactions were acid quenched after 3 seconds and isolated cofactor adducts were subjected to  $^1\text{H}$ -NMR. C6'- $^1\text{H}$ -NMR signals of ThDP and chemically synthesized ThDP intermediates expected in the phosphoketolase reaction are shown in the top panel. Signals derived from ThDP intermediates accumulated in the different reactions are depicted below. Accumulation of AcThDP was observed in the reaction of XFPK with F6P. In presence of both substrates, free ThDP, DHETHDP and AcThDP were detected.

with both substrates, DHETHDP was detected as only covalent ThDP adduct, while most of the cofactor was found in its unsubstituted state (Figure 17C, bottom row). As we did not detect any absorbance signal under the same reaction conditions, it can be excluded that DHETHDP accounts for the absorbance band. Thus, the spectral signal at 420 nm can be assigned to the presence of the covalent AcThDP intermediate.

### 3.2 Analysis of the AcThDP UV-Vis absorbance spectrum

Recognized as an important intermediate for several ThDP-dependent enzymatic reactions, FREY and colleagues characterized chemically synthesized AcThDP and found an absorbance band at 310 nm that they could assign to the keto-form of AcThDP<sup>81</sup>. In comparison, the observed signal of phosphoketolase-bound AcThDP is considerably shifted to longer wavelength. Furthermore, it has not finally been resolved if it is actually keto-AcThDP that is accumulated at the active site of phosphoketolase in the absence of a nucleophilic acceptor. Resolution of the X-ray diffraction data did not allow evaluation of the chemical state of the intermediate and the observed electron density could also present enol- or enolate-AcThDP<sup>73</sup>.

In cooperation with the group of PROF. DR. RICARDO MATA, Department of Computational Chemistry and Biochemistry, University of Göttingen, theoretical calculations were carried out in order to analyze correlation between AcThDP in its various chemical states and the observed absorbance band at 420 nm. Several covalent ThDP intermediates exhibit UV-Vis bands that result from charge transfer transitions<sup>84</sup>. Hence, MATA and colleagues performed time-dependent density functional theory and incremental equation-of-motion coupled cluster calculations on isolated AcThDP in the V-conformation to predict potential charge transfer transitions and the corresponding transition energies for the different tautomers of AcThDP. Their results suggest charged transfer transitions for enol- and keto-AcThDP from the  $\pi$ -orbital of the pyrimidine ring to the thiazolium ring delocalized towards the acyl-substituent with transition energies of 413 nm for the keto- and 340 nm for the enol-tautomer. For the enolate-tautomer, they assume a different charge transfer transition from the  $\pi$ -system of the acyl-substituent to the thiazolium ring with a corresponding transition energy of 431 nm. The computed oscillator strength was slightly higher for the enolate adduct compared to the keto-species. From those results they conclude, that the observed absorbance band at 420 nm does not originate from a single AcThDP tautomer, but most likely from coexistence of keto- and enolate-AcThDP.

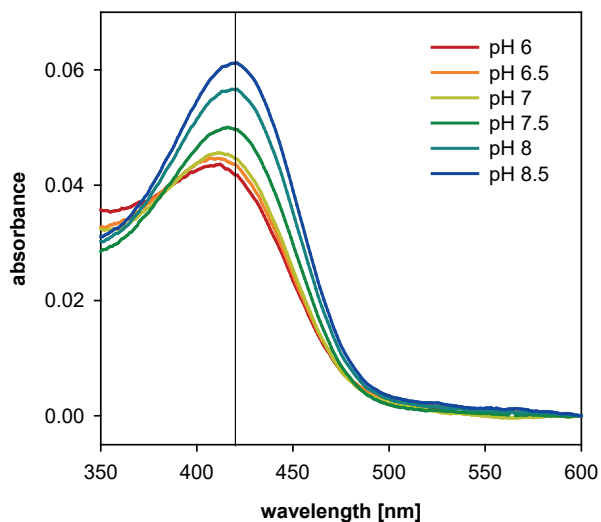


**Figure 18: pH-dependence of the AcThDP absorbance band.** Absorbance spectra of  $24\ \mu\text{M}$  XFPK with  $20\ \text{mM}$  F6P were recorded at different pH values between pH 6 and pH 8.5. Towards alkaline conditions, signal strength increases and  $\lambda_{max}$  is slightly shifted to longer wavelength.

During a pH-dependent analysis of the AcThDP absorbance band, distinct changes in the spectral signal were observed. UV-Vis absorbance spectra were recorded after mixing phosphoketolase with  $20\ \text{mM}$  F6P under different pH conditions between pH 6 and 8.5. With increasing pH, an increase of the signal strength was observed. Furthermore, the maximum of the absorbance band shifted slightly from  $411\ \text{nm}$  at pH 6 to  $421\ \text{nm}$  at pH 8.5 (Figure 18). Changes in this pH range certainly influence protonation states of active site residues, consequently altering the electrostatic environment of the AcThDP intermediate, which might account for the detected alterations of the spectral signal. Results from the computational analysis of the different AcThDP tautomers indicate presence of both enolate- and keto-form under the applied reaction conditions. Keeping that in mind, changes in the absorbance band could also point towards a change in the distribution of enolate- and keto-tautomers. Compared to keto-AcThDP, the calculated excitation energy for the enolate-form was slightly lower, yet stronger in oscillator strength. Thus, redshift of the absorbance maximum together with the enhanced signal strength could indicate an increase of the enolate fraction. However, the theoretical excitation energies of both species are too similar to distinguish them properly by UV-Vis spectroscopy. Consequently, MATA and colleagues searched for side chain mutations in the phosphoketolase active site that would further separate the calculated transition energies of the different tautomers. The suggested amino acid exchanges Glu156Gln and Asn549Asp were inserted by site directed mutagenesis and the resulting recombinant phosphoketolase variants XFPK<sub>E156Q</sub> and XFPK<sub>N549D</sub> characterized for their catalytic and spectroscopic properties. Both variants showed catalytic activity for the conversion of F6P to E4P and exhibited the absorbance band around  $420\ \text{nm}$  after addition of F6P, indicating accumulation of the post-dehydration intermediate AcThDP as observed for the



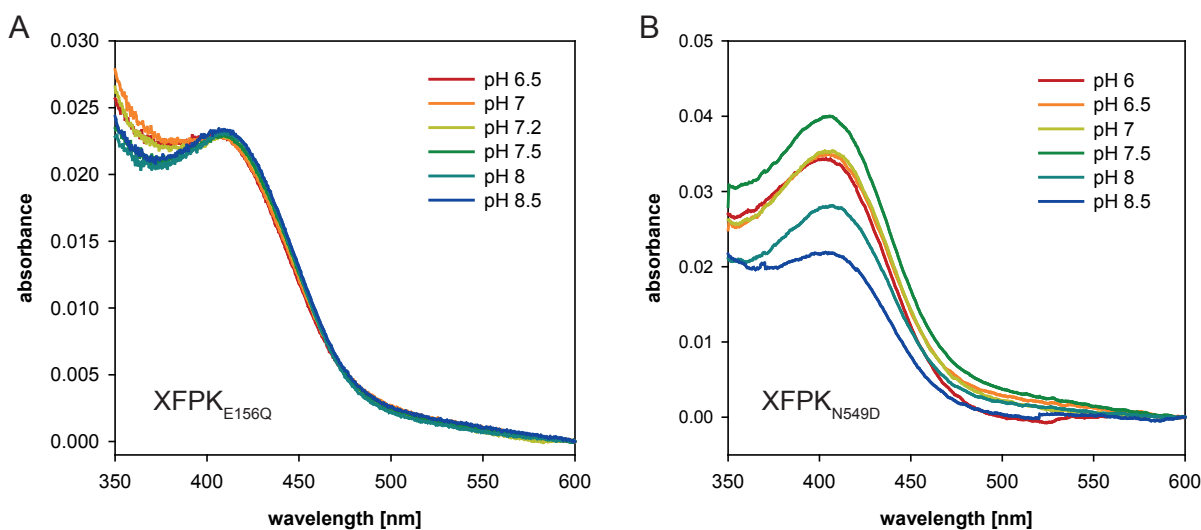


**Figure 19: pH-dependence of the AcThDP absorbance band in the phosphoketolase variants XFPK<sub>E156Q</sub> and XFPK<sub>N549D</sub>.** Absorbance spectra of (A) XFPK<sub>E156Q</sub> (24  $\mu$ M) or (B) XFPK<sub>N549D</sub> (24  $\mu$ M) with 20 mM F6P were recorded at different pH values between pH 6 and pH 8.5. The introduced mutations were supposed to lead to separation of the enolate-AcThDP and keto-AcThDP absorbance band. For both variants no signal separation was observed.

wild-type enzyme. According to MATA and colleagues, the Glu156Gln mutation should cause a blue shift of the keto-AcThDP absorbance maximum of around 0.4 eV. For the Asn549Asp mutation they predict a blue shift of the keto signal and a red shift of the enolate absorbance maximum of about 0.4 eV in both cases. Unfortunately, the pH-dependent absorbance spectra of neither phosphoketolase variant exhibited signs of signal separation. In both variants the maximum of the absorbance band showed a slight blue shift ( $\lambda_{max}$  404 - 410 nm) and reduction of the amplitude compared to the wild-type enzyme (Figure 19). Whereas the spectral signal from XFPK<sub>E156Q</sub> did not exhibit any pH-dependency (Figure 19A), a decrease in amplitude was observed for XFPK<sub>N549D</sub> at pH 8 and 8.5, showing a reverse behavior to wild-type phosphoketolase (Figure 19B).

Overall, experimental data did not match the theoretical calculations. Presumably, influence of the phosphoketolase active site environment on the absorbance signal of the post-dehydration intermediate is more complex than covered in the theoretical considerations. Consequently, it was not possible to determine experimentally whether the pH dependent effects on the absorbance signal of the AcThDP intermediate are caused by a change in the ratio of enolate- and keto AcThDP or are rather an effect of different protonation in the environment of the intermediate.

### 3.3 Kinetic analysis of the phosphoketolase reaction

#### 3.3.1 Development of a direct steady-state assay for phosphoketolase activity

Phosphoketolase activity is commonly determined by detection of acetyl phosphate formation, using a colorimetric end-point assay. Acetyl phosphate reacts with hydroxylamine to acetyl hydroxamate that forms a colored complex with  $\text{Fe}^{2+}$  ions, allowing spectroscopic detection at 505 nm<sup>97</sup>. This method and adaptations thereof have been applied successfully to demonstrate phosphoketolase activity and to determine kinetic parameters of the phosphoketolase reaction<sup>71,73</sup>, but come with the disadvantages of a discontinuous assay. Additionally, a coupled enzymatic assay was described. Generation of acetyl phosphate by phosphoketolase was linked to the formation of ATP through the action of acetate kinase. ATP formation was in turn coupled to the formation of NADPH via hexokinase and glucose-6-phosphate dehydrogenase, allowing spectroscopic detection of increasing NADPH concentrations at 340 nm<sup>18</sup>. This assay permits continuous monitoring of the reaction, but as the hydroxamate method, it only allows observation of the reaction if acetyl phosphate is formed as product, making it impossible to investigate the off-pathway hydrolysis reaction to acetate in absence of phosphate as acyl-acceptor.

In order to determine and compare kinetic parameters for both, the phosphoketolase-catalyzed conversion of F6P and phosphate to E4P and acetyl phosphate as well as the side reaction of F6P and  $\text{H}_2\text{O}$  to E4P and acetate, a direct steady-state assay was established, monitoring formation of E4P. E4P is optically active and yields a negative CD signal with an absorbance maximum at 290 nm (Figure 56A, Appendix), enabling direct observation of the phosphoketolase reaction product. The experimental procedure of the assay is described in detail in section 2.5.1. In brief, a calibration curve was prepared, correlating the CD signal to E4P concentration. The calibration curve showed linear dependency of the CD signal on the E4P concentration in the observed range (Figure 56B, Appendix). To determine initial reaction rates of the phosphoketolase reaction, the enzyme was mixed with different F6P concentrations and progression of the E4P-CD signal was recorded over time. The progress curves exhibited an initial linear phase that allowed the determination of initial reaction rates using the standard curve. The initial reaction rates displayed characteristic hyperbolic dependency on the substrate concentration (Figure 20A) and analysis according to MICHAELIS-MENTEN (Eq. 3) yielded a  $k_{\text{cat}}$  of  $14.3 \pm 0.3 \text{ s}^{-1}$  for the conversion of F6P and phosphate to E4P and acetyl phosphate with a  $K_{\text{M}}$  of  $32.1 \pm 2.3 \text{ mM}$  for F6P. This data is comparable to macroscopic kinetic constants published earlier for the

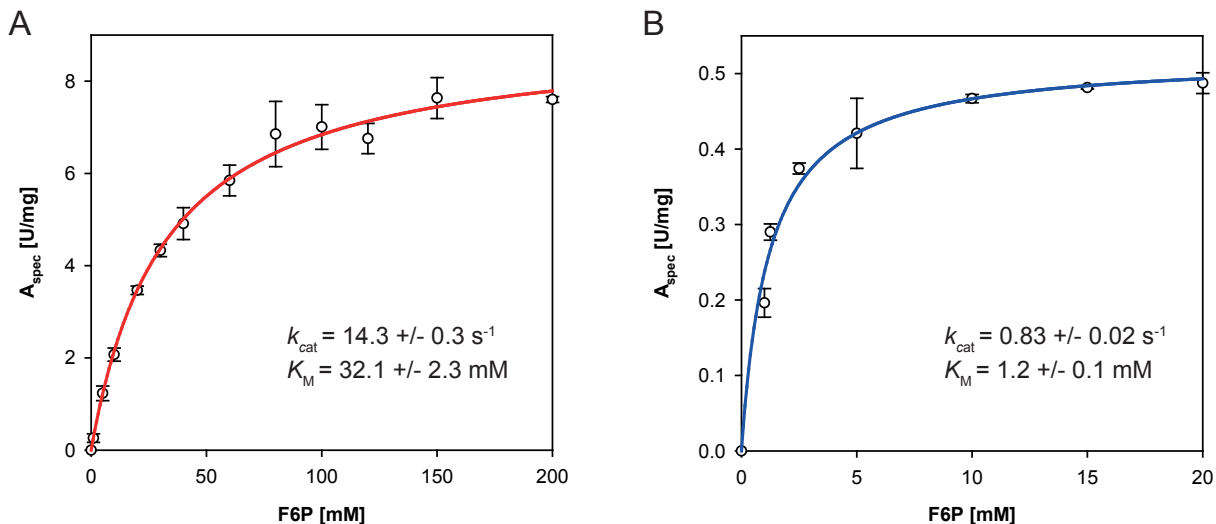


**Figure 20: Steady-state kinetic analysis of the phosphoketolase reaction.** Kinetic parameters for the phosphoketolase catalyzed conversion of (A) F6P and  $\text{Na}_2\text{HPO}_4$  to E4P and acetyl phosphate or (B) of F6P to E4P and acetate in absence of phosphate were determined using the CD spectroscopy based assay for E4P detection. Initial reaction rates were determined under steady-state conditions and plotted against the applied F6P concentration. Data was fitted using the MICHAELIS-MENTEN equation (Eq.3, red and blue line). Resulting kinetic parameters are indicated in the respective diagram.

phosphoketolase reaction<sup>71,92</sup>, indicating suitability of the developed assay for the kinetic analysis of the reaction under steady-state conditions.

The assay also enabled analysis of the hydrolytic side-reaction of phosphoketolase with F6P to E4P and acetate in the absence of phosphate. Analysis of the F6P dependent reaction rates, determined under phosphate-free conditions, using the MICHELIS-MENTEN equation (Eq. 3), revealed that the reaction occurs with a turnover of  $0.83 \pm 0.02 \text{ s}^{-1}$  (Figure 20B). Thus, the velocity of the side reaction is substantially lower compared to the reaction in presence of the acyl-acceptor substrate phosphate. Presumably, it is limited by the rate of hydrolysis of AcThDP to acetate, as indicated by accumulation of the AcThDP intermediate in the NMR-based intermediate analysis (see section 3.1).

Aiming to determine  $K_M$  for the acceptor substrate phosphate, the assay was repeated with varying concentrations of phosphate at a fixed F6P concentration of 150 mM. Plotting of the initial reaction rates against the applied phosphate concentration showed hyperbolic dependency on the substrate concentration, approaching a maximum specific activity  $A_{\text{spec}}^{\text{max}}$  of  $9.9 \text{ U/mg}$  that is comparable to the one observed in the F6P dependent assay ( $9.0 \pm 0.2 \text{ U/mg}$ ) (Figure 21). But the data set revealed an offset of  $5.2 \text{ U/mg}$  and did not follow typical MICHAELIS-MENTEN kinetics. Consequently, data was fitted with a modified equation considering the offset (Eq. 4), that yielded an apparent  $K_M$  of  $3.8 \pm 0.7 \text{ mM}$ . This is slightly higher than the  $K_M$  value of

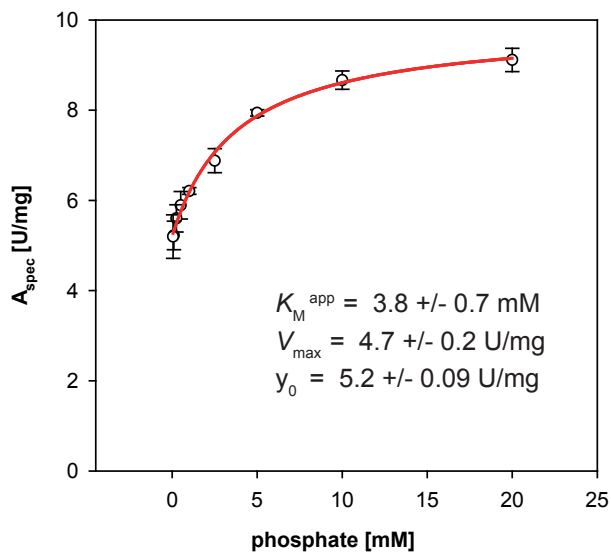


**Figure 21: Steady-state kinetic analysis of the phosphoketolase reaction depending on phosphate concentration.** Initial reaction rates were determined under steady-state conditions for different  $\text{Na}_2\text{HPO}_4$  concentrations by monitoring the increasing E4P concentration and plotted against the applied  $\text{Na}_2\text{HPO}_4$  concentration. Data did not follow MICHAELIS-MENTEN kinetics and were instead fitted with Equation 4 (red line).  $K_M^{\text{app}}$  represents phosphate concentration half-maximum velocity. The calculated maximum velocity  $V_{\text{max}}$  and the offset  $y_0$  add up to the observed maximum specific activity  $A_{\text{spec}}^{\text{max}}$ .

$1.2 \pm 0.2 \text{ mM}$  published by SUZUKI *et al.* for *B. breve* phosphoketolase. Due to the hydrolytic background activity of phosphoketolase with F6P at a rate of approximately  $0.8 \text{ s}^{-1}$ , non-linear fitting of the data was expected to give an coinciding offset. Instead a value about five times higher was obtained. The reason for this discrepancy could not finally be resolved, but the increasing inaccuracy of the applied assay towards lower substrate concentrations due to declining signal amplitudes should be considered.

Overall, this direct, CD spectroscopy-based steady-state assay provides a useful new tool to analyze the kinetics of the phosphoketolase reaction in the presence and absence of the acyl-acceptor. Limitations might occur for low substrate concentrations ( $< 0.5 \text{ mM}$ ) as applied for determination of the  $K_M$  for phosphate, due to small signal amplitudes. Still, the assay allowed direct comparison of the reaction velocities of main phosphoketolase reaction and off-pathway hydrolysis, revealing that the hydrolytic side reaction to acetate occurs at a rate 20 times lower than the main reaction.

### 3.3.2 Transient kinetic analysis of AcThDP formation

Using a combined approach of time-resolved absorbance spectroscopy and  $^1\text{H-NMR}$ -based intermediate analysis, the absorbance band at 420 nm could be assigned to the covalent intermediate AcThDP accumulating during the phosphoketolase reaction in the absence of the acceptor substrate phosphate (see section 3.1). This specific spectral signature provided the opportunity for a detailed transient-kinetic analysis of formation and depletion of the AcThDP intermediate by

stopped-flow spectroscopy, such being able to resolve individual steps of the phosphoketolase reaction mechanism.

For observation of AcThDP formation, phosphoketolase was rapidly mixed with different F6P concentrations in the absence of inorganic phosphate in a stopped-flow mixing device and progression of the absorbance at 420 nm was recorded over time. The spectral signal quickly increases in the initial stage of the reaction, then remains constant for several minutes before signal depletion sets in (Figure 22A and Figure 58, Appendix). At higher substrate concentrations (5 - 100 mM F6P) the progress curves exhibit a kinetic overshooting with maximum absorbance at 420 nm between 40 and 60 ms in the pre-steady-state of the reaction (Figure 22A). This pre-steady-state phase can be described by a two-term exponential model, followed by a steady-state phase with constant AcThDP concentration (Figure 22B). Rate constants for the two pre-steady-state phases were determined by fitting the concentration dependent progress curves with a two-term exponential equation (Eq. 5). The apparent rate constants of the first phase  $k_{\text{obs}_1}$  showed sigmoidal dependency on the F6P concentration. Fitting with the HILL-equation (Eq. 6) yielded a  $k_{\text{obs}_1}^{\text{max}}$  of  $75.2 \pm 2.5 \text{ s}^{-1}$  (Figure 22C). The rate constants of the second phase  $k_{\text{obs}_2}$  however did not display substrate dependency and showed a constant value of about  $4.7 \text{ s}^{-1}$  (Figure 22D). Such substrate-independent kinetics indicate that  $k_{\text{obs}_2}$  is associated to an internal rearrangement or decay process.

The observed progress curves exhibiting a kinetic overshooting suggest that one species is quickly build up after rapid mixing of enzyme and substrate, which then partly converts into a second species, resulting in an equilibrium of both in the steady-state. Since AcThDP appears as predominant intermediate under the applied reaction conditions, as demonstrated in the  $^1\text{H-NMR}$  intermediate analysis, these two species presumably correspond to two different forms of AcThDP rather than an additional ThDP adduct. Considering the results from the computational studies that suggest presence of keto- and enolate-AcThDP (section 3.2), these are most likely enolate- and keto-form of the intermediate. This leads to the proposal of the following scenario: After rapid mixing of phosphoketolase and F6P, an excess of enolate-AcThDP is formed, accounting for the peak in absorbance after 40 - 60 ms. The enolate-intermediate then partly tautomerizes to the corresponding keto-form, resulting in a steady-state equilibrium of enolate- and keto-AcThDP. Over time, slow hydrolysis of keto-AcThDP to acetate leads to depletion of the spectral signal. In this model,  $k_{\text{obs}_1}$  would summarize the rate constants of all steps leading to the formation of enolate-AcThDP.  $k_{\text{obs}_2}$  could be assigned to the tautomerization between enolate-AcThDP and

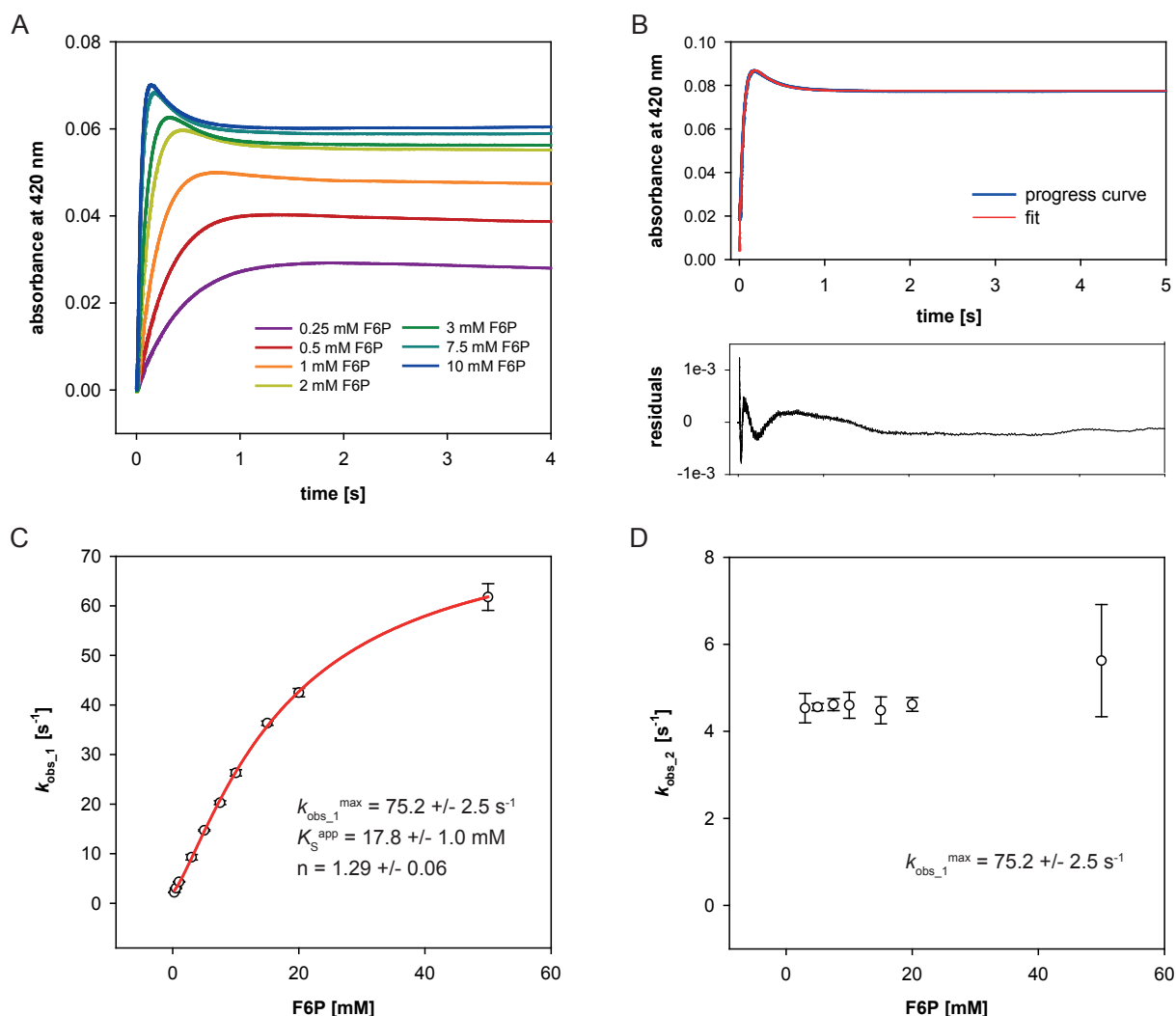


**Figure 22: Transient kinetic analysis of AcThDP formation in phosphoketolase.** (A) Progress curves of absorbance at 420 nm after rapid-mixing of  $24 \mu\text{M}$  phosphoketolase with different concentrations of F6P show a kinetic overshooting at higher substrate concentrations. (B) Progress curves (blue line) were fitted with a two-term exponential model (Eq. 5, red line) to obtain apparent rate constants of AcThDP formation. Deviation of the applied fit from the represented data is shown as residuals plot (for details see section 2.5.2). (C) Apparent rate constants of the first exponential phase of AcThDP formation  $k_{\text{obs}_1}$  were plotted against the applied substrate concentration. Kinetic parameters were determined by fitting with the HILL-equation (Eq. 6, red line). (D) Apparent rate constants of the second exponential phase of AcThDP formation  $k_{\text{obs}_2}$  were plotted against the applied substrate concentration. The apparent rate constants did not show substrate dependency.

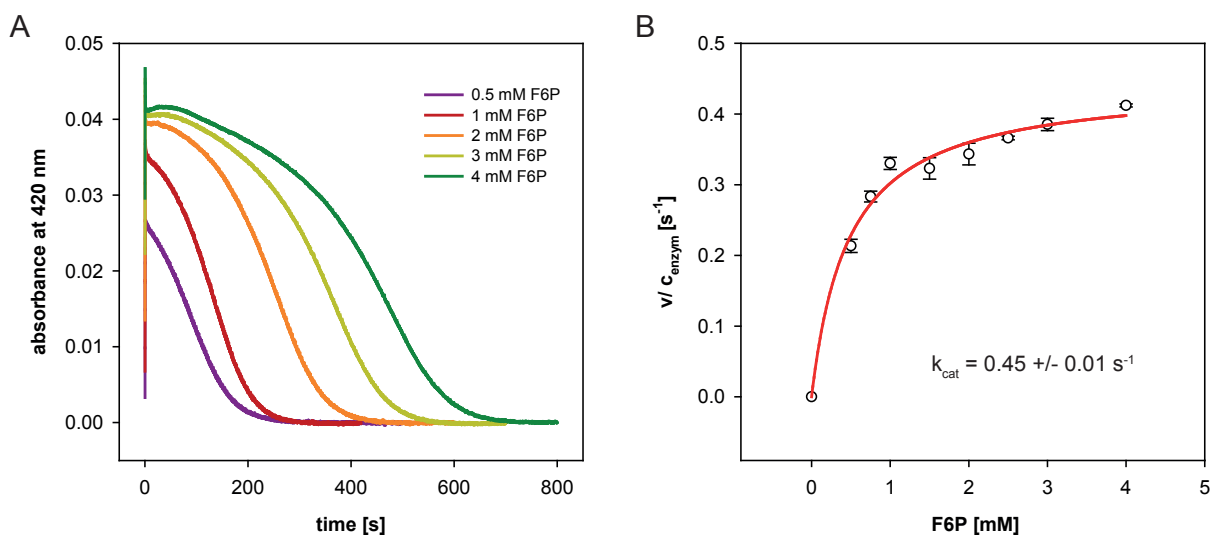


**Figure 23: Kinetic analysis of the hydrolytic side reaction.** (A) Progression of absorbance after rapid-mixing of  $24 \mu\text{M}$  XFPK with different concentrations of F6P was recorded until complete consumption of F6P. Area below the progress curves was determined and used to calculate reaction rates as described in section 2.5.3. (B) Obtained reaction rates were plotted against the applied F6P concentration and fitted according to MICHAELIS-MENTEN (Eq. 3, red line).

the corresponding keto form 2-acetyl-ThDP. Furthermore, this model implies parallel presence of enolate-and keto AcThDP in the steady-state of AcThDP formation and depletion by hydrolysis, rather than accumulation of only keto-AcThDP as proposed before.

In addition, the obtained progress curves of AcThDP absorbance were used to determine the turnover of the phosphoketolase hydrolytic side reaction. Analysis of the progress curves using the method of GIBSON *et al.*<sup>95</sup> that is described in detail in section 2.5.3 allows determination of the reaction rate from the area below the kinetic traces. Hence, progress curves at F6P concentrations between 0.5 - 4 mM were recorded until complete consumption of F6P (Figure 23A). The area below the whole progress curve as well as the area below the steady-state phase (constant AcThDP absorbance) were determined for every substrate concentration and used to calculate reaction rates according to Equation 13. The rates were plotted against the applied F6P concentration, fitting with the MICHAELIS-MENTEN equation yielded a  $k_{\text{cat}}$  of  $0.45 \pm 0.01 \text{ s}^{-1}$  (Figure 23B). This value is comparable to the turnover number determined for the reaction of phosphoketolase with F6P to E4P and acetate in the absence of phosphate by the CD spectroscopy-based steady-state assay of  $0.83 \pm 0.02 \text{ s}^{-1}$ , confirming the suitability of the newly established steady-state assay.

### 3.3.3 Transient kinetic analysis of AcThDP depletion

Accumulation of AcThDP as observed in  $^1\text{H-NMR}$  intermediate analysis as well as in stopped-flow spectroscopy lets assume that the hydrolysis of phosphoketolase bound AcThDP to acetate occurs slow compared to formation of the intermediate. Presumably, it even is the rate limiting step of the side-reaction, in which case a rate constant of about  $0.5 - 0.8 \text{ s}^{-1}$  as determined in the steady-state assays can be estimated. Reaction of AcThDP with phosphate on the other hand has to proceed at a much higher rate, as no accumulation of the post-dehydration intermediate can be observed when the acceptor substrate is present.

In order to determine the rate of depletion of phosphoketolase-bound AcThDP through reaction with phosphate, we set up a double-jump stopped-flow experiment. Phosphoketolase was premixed with 20 mM F6P in a stopped-flow mixing device set to sequential mixing mode. The reaction mix was incubated for 5 s to ensure population of the post-dehydration intermediate before fast-mixing with different concentrations of  $\text{Na}_2\text{HPO}_4$ . Depletion of AcThDP was monitored via decrease in absorbance at 420 nm. Decline of the signal appeared in an exponential manner and the apparent rate constants  $k_{\text{obs}_3}$  were determined by fitting the individual progress curves with a single-term

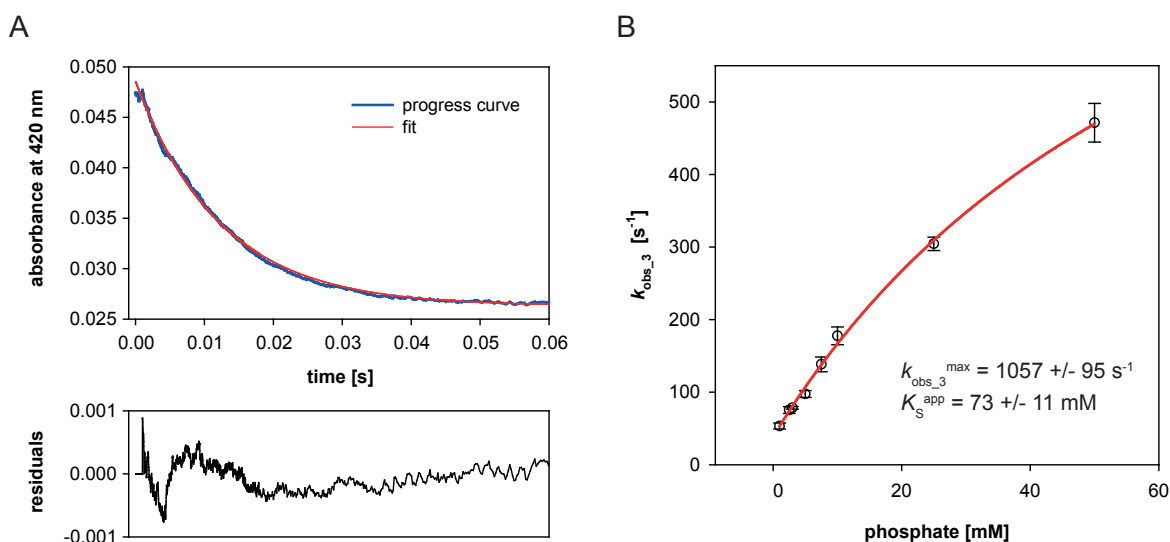


**Figure 24: Transient kinetic analysis of AcThDP depletion.** Phosphoketolase was mixed with 20 mM F6P in a stopped-flow device set to sequential mixing mode. The reaction mix was aged for 5 s to ensure population of the AcThDP intermediate. In a second mixing step the aged solution was fast-mixed with different concentrations of  $\text{Na}_2\text{HPO}_4$ , depletion of AcThDP was detected via decrease of absorbance at 420 nm over time. (A) Progress curves (blue line) were fitted with an exponential model (Eq. 8, red line) to determine apparent rate constants. Deviation of the applied fit from the represented data is shown as residuals plot. (B) Apparent rate constants were plotted against the applied phosphate concentration. Non-linear regression with an hyperbolic function (Eq. 9, red line) yielded the kinetic parameters  $k_{\text{obs}_3}^{\text{max}}$  and  $K_{\text{S}}^{\text{app}}$  as indicated in the diagram.



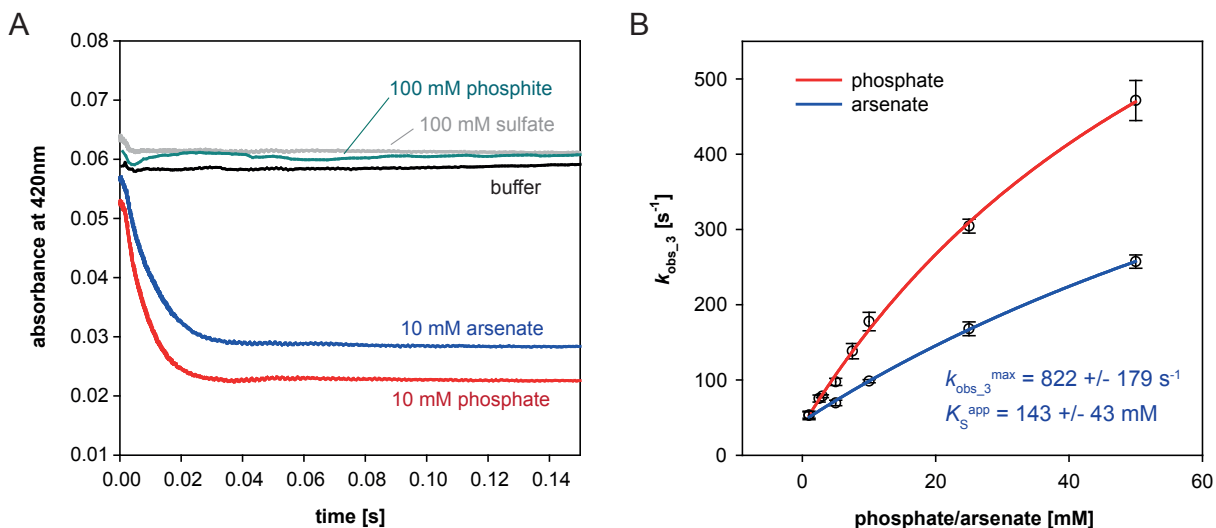


**Figure 25: Testing of alternative nucleophilic acceptor substrates.** (A) Progression of the AcThDP absorbance signal after mixing with different potential acyl-acceptors. AcThDP was populated at the phosphoketolase active site by mixing 24  $\mu\text{M}$  XFPK with 20 mM F6P in a stopped-flow device set to sequential-mixing mode. In a second rapid-mixing step different acceptor substrates were added to the reaction mix and progression of absorbance at 420 nm recorded over time. Only phosphate and arsenate caused signal depletion. (B) Dependency of the apparent rate constants on phosphate (red) or arsenate (blue) concentration. Data was fitted according to Equation 9 (solid lines), kinetic parameters  $k_{\text{obs}_3}^{\text{max}}$  and  $K_{\text{S}}^{\text{app}}$  for the reaction with arsenate as acyl-acceptor substrate are depicted in the diagram. Data for the phosphate plot was taken from Figure 24.

exponential model (Eq. 8) (Figure 24A). Apparent reaction constants were plotted against the applied phosphate concentrations. Depletion of AcThDP occurs very rapidly after addition of phosphate, at a concentration of 50 mM phosphate the reaction displays an apparent rate constant of  $> 450 \text{ s}^{-1}$ . Due to limitations in time-resolution of the experimental setup, it was not possible to determine reliable rate constants for phosphate concentrations above 50 mM, so substrate saturation could not be reached which might lower the accuracy of the apparent rate constant  $k_{\text{obs}_3}^{\text{max}}$  of  $1057 \pm 95 \text{ s}^{-1}$ , determined by fitting data with Equation 9 (Figure 24B). Nevertheless, it could be confirmed that the reaction of the covalent phosphoketolase intermediate AcThDP with phosphate occurs more than 1000 times faster than the competing hydrolysis to acetate.

Next, it was tested whether nucleophiles other than phosphate are accepted as acceptor substrates by phosphoketolase and show a reaction with AcThDP. Arsenate has physicochemical properties very similar to those of phosphate and was successfully used to replace inorganic phosphate as substrate in enzymatic reactions<sup>98</sup>. As further co-substrate alternatives sulfate, vanadate and phosphite were chosen. Reactivity of the phosphate analogues towards phosphoketolase-bound AcThDP was tested by repeating the double-jump stopped-flow experiment described above with  $\text{Na}_3\text{AsO}_4$ ,  $\text{Na}_2\text{SO}_4$ ,  $\text{Na}_3\text{VO}_4$  or  $\text{Na}_2\text{HPO}_3$  instead of inorganic phosphate. No depletion of the AcThDP signal at 420 nm was observed after rapid mixing with sulfate, vanadate or phosphite at

concentrations of up to 200 mM. However, after mixing with arsenate a fast decline in absorbance at 420 nm was monitored, comparable to signal decrease after mixing with phosphate (Figure 25A), indicating a successful reaction between arsenate and AcThDP. The progression of signal depletion was recorded for different arsenate concentrations. Apparent rate constants  $k_{\text{obs}}$  were determined by fitting the progress curves with an exponential equation and plotted against the applied substrate concentration. Data analysis performed equally as for phosphate yielded  $822 \pm 179 \text{ s}^{-1}$  for  $k_{\text{obs}}^{\text{max}}$  and  $143 \pm 43 \text{ mM}$  for the apparent  $K_{\text{S}}^{\text{app}}$  (Figure 25B). The maximum apparent reaction rate is only slightly reduced when arsenate is used as nucleophilic acceptor in the phosphoketolase reaction instead of phosphate, the apparent  $K_{\text{S}}^{\text{app}}$  is approximately doubled. These data show that arsenate is a fairly good replacement for phosphate as acyl-acceptor. The chemical properties of the other tested co-substrate alternatives are presumably too different to those of inorganic phosphate to take over its function in the phosphoketolase reaction.

Observation of formation and depletion of the covalent AcThDP intermediate via its absorbance band in different rapid mixing experiments made it was possible to determine rate constants for several individual steps of the phosphoketolase reaction, providing further insight into the reaction mechanism. The obtained kinetic parameters are summarized in Figure 45.

### 3.3.4 pH-dependence of the phosphoketolase reaction

Analysis of the absorbance band assigned to AcThDP revealed pH-dependence of the spectral signal at 420 nm (section 3.2). In order to survey whether those differences in the spectral behavior go along with changes in the reactivity of the covalent cofactor adduct, a pH-dependent kinetic analysis of the phosphoketolase reaction was carried out.

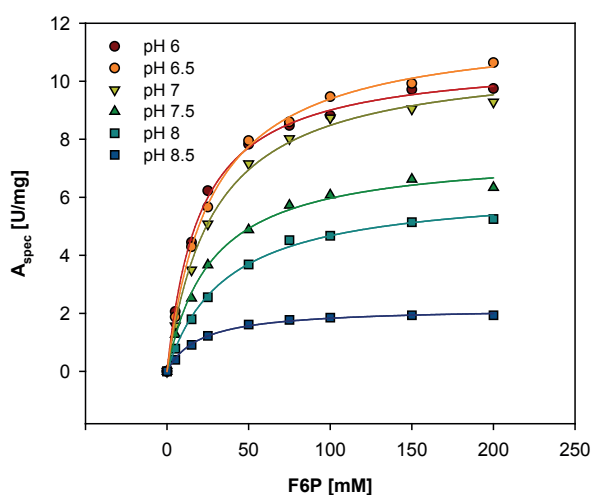


**Figure 26: pH-dependent steady-state kinetic analysis of the phosphoketolase reaction.** Enzymatic activity of XFPK at different pH conditions was determined using the CD spectroscopic steady-state assay for E4P detection. The plot shows concentration dependent initial reaction rates at the respective pH, fitted according to MICHAELIS-MENTEN (Eq.3, solid lines). The resulting kinetic parameters are depicted in Table 1. Initial reaction rates were determined in single measurements.

**Table 1: Macroscopic kinetic constants of the phosphoketolase reaction at different pH.** The error represents standard deviation of the fitted parameters.

pH	$k_{\text{cat}}$ ( $\text{s}^{-1}$ )	$K_{\text{M}}$ (mM)	$k_{\text{cat}}/K_{\text{M}}$ ( $\text{s}^{-1}\text{mM}^{-1}$ )
6	17.1 $\pm$ 0.2	20.1 $\pm$ 1.1	0.9
6.5	18.8 $\pm$ 0.2	26.8 $\pm$ 1.2	0.7
7	17.2 $\pm$ 0.3	28.3 $\pm$ 2.0	0.6
7.5	11.9 $\pm$ 0.3	26.8 $\pm$ 2.4	0.4
8	10.0 $\pm$ 0.2	35.6 $\pm$ 2.4	0.3
8.5	3.5 $\pm$ 0.1	20.0 $\pm$ 1.3	0.2

Before analyzing pH-dependent AcThDP intermediate formation and depletion by transient-kinetic methods, a pH-dependent steady-state assay was performed to evaluate the impact of changes in the proton concentration on the overall phosphoketolase reaction. Enzymatic activity of phosphoketolase was determined under different pH-conditions in the range of pH 6 to pH 8.5 using the CD spectroscopy based steady-state assay, detecting formation of the substrate E4P (for experimental details see section 2.5.1 and 3.3.1). The resulting concentration dependent initial rate constants are plotted in Figure 26. Non-linear regression using the MICHAELIS-MENTEN equation (Eq. 3) yielded  $K_{\text{M}}$  and  $k_{\text{cat}}$  for the individual pH values that are listed in Table 1. Phosphoketolase shows maximum activity at pH 6 to 7 which is close to the published pH-optimum for *B. breve* phosphoketolase of 5.5 to 6.5<sup>92</sup>. A drop in activity occurs between pH 7 and pH 7.5 with  $k_{\text{cat}}$  further decreasing towards more alkaline conditions. At pH 8.5 turnover is reduced about 80 % compared to maximum activity at pH 6.5.

The most distinct effect on the enzymatic activity as well as on the AcThDP absorbance band was observed at pH 8.5, the most alkaline pH value tested in the assay. Hence, it was decided to perform the transient-kinetic experiments at pH 8.5 and compare them to standard assay conditions (pH 7.2). Formation and depletion of the phosphoketolase reaction intermediate AcThDP was analyzed by stopped-flow spectroscopy as described in section 2.5.2, 3.3.2 and 3.3.3. The resulting data is presented in Figure 27. The apparent rate constants  $k_{\text{obs}_1}$  for AcThDP formation and  $k_{\text{obs}_3}$  for reaction of the cofactor adduct with phosphate at pH 8.5 were determined and plotted against the applied substrate concentration. Analysis of the apparent rate constants associated to AcThDP formation using equation 6 yielded a  $k_{\text{obs}_1}^{\text{max}}$  of  $34 \pm 4 \text{ s}^{-1}$  and an apparent  $K_{\text{S}}^{\text{app}}$  of  $49 \pm 9 \text{ mM}$ . The rate of AcThDP formation is reduced approximately by half compared to pH 7.2. Interestingly, the progress curves of absorbance at 420 nm, measured at pH 8.5 after fast-mixing of phosphoketolase and F6P, did not display the kinetic overshooting as observed under standard assay conditions at pH 7.2 (Figure 27C). Consequently, no kinetic

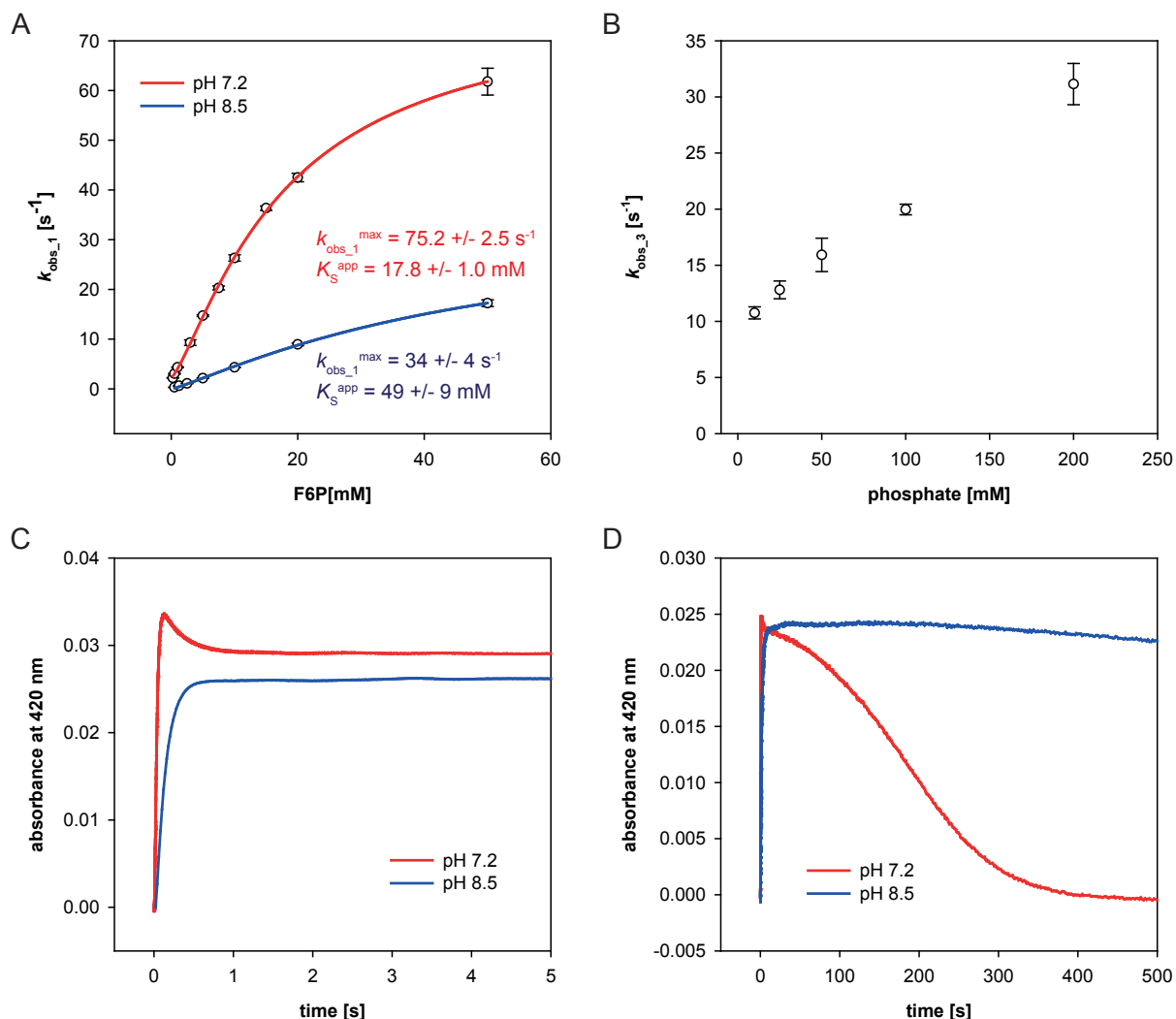


**Figure 27: pH-dependent transient kinetic analysis of AcThDP formation and depletion.** (A) Apparent rate constants of AcThDP formation  $k_{\text{obs}_1}$  at pH 7.2 and pH 8.5 plotted against the F6P concentration. Data was fitted with Equation 6 (red and blue lines). The resulting kinetic constants are depicted in the diagram. Data for the pH 7.2 plot was taken from Figure 22. (B) Apparent rate constants of AcThDP depletion by reaction with phosphate  $k_{\text{obs}_3}$  at pH 8.5 plotted against the applied  $\text{Na}_2\text{HPO}_4$  concentration. Apparent rate constants are markedly decreased compared to those determined at pH 7.2 (cf. Figure 24). (C) Progression of absorbance at 420 nm after rapid-mixing of phosphoketolase with 10 mM F6P at pH 7.2 (red) or at pH 8.5 (blue). Kinetic overshooting as it occurs at pH 7.2 can not be observed at the higher pH. (D) Progression of absorbance at 420 nm after rapid-mixing of phosphoketolase with 1 mM F6P at pH 7.2 (red) or 1.25 mM F6P at pH 8.5 (blue). Signal depletion seems to be slowed down at alkaline pH.

information could be derived for a potential tautomerization between the postulated enolate- and keto-form of AcThDP. The apparent rate constants  $k_{\text{obs}_3}$  associated to AcThDP depletion through reaction with inorganic phosphate show linear dependence on the phosphate concentration at pH 8.5 in the observed concentration range. They are assumed to follow hyperbolic kinetics, but due to the parallel presence of  $\text{Mg}^{2+}$  ions in the reaction mix, phosphate concentrations could not be increased further, preventing substrate saturation of the reaction. However, the apparent rate constant at 50 mM phosphate shows a 30 fold reduction in  $k_{\text{obs}_3}$  from  $471 \pm 27 \text{ s}^{-1}$  at pH 7.2 to  $15.9 \pm 1.5 \text{ s}^{-1}$  at pH 8.5, indicating that the reaction between phosphoketolase bound AcThDP and inorganic phosphate is distinctly slowed down under alkaline conditions. Furthermore, it was noticed that the lifespan of the absorbance signal at 420 nm was increased at pH 8.5. Even at low F6P concentrations of 1.25 mM no complete depletion of the signal was observed in the measurement time of 500 s (Figure 26D). This indicates that not only the reaction with phosphate but also hydrolysis of AcThDP to acetate seems to be impaired at a higher pH. This observation was rather surprising, as hydrolysis of free AcThDP is assumed to be  $\text{OH}^-$  catalyzed and was shown to proceed faster under alkaline conditions<sup>82</sup>.

Overall, an increase in pH leads to a decrease in phosphoketolase activity. Regarding the individual reaction steps, especially depletion of AcThDP by phosphorolytic or hydrolytic cleavage seems to be impaired at a higher pH. Based on spectral changes in the absorbance band of AcThDP during pH-titration it was speculated whether an increase in pH goes along with an increased concentration of enolate-AcThDP. A higher share of enolate-AcThDP would explain a lower rate of hydrolytic- and phosphorolytic cleavage, as the enolate species would be less prone to react with water or phosphate. However, these considerations are highly speculative and whether the mentioned effects are caused by changes in the protonation state of active site residues, of the respective acyl-acceptor substrate or by changes in the chemical state of the post-dehydration intermediate itself can not be assessed at this point.

### 3.4 Histidine 553 as catalyst for the tautomerization reaction?

All functional and structural studies on phosphoketolase agree that attack of the nucleophilic acceptor phosphate leading to product formation occurs on the keto- form of AcThDP. However, the underlying mechanism of the preceding tautomerization remains unclear and the active site residues mediating its catalysis have not been identified yet. The transient-kinetic observation of AcThDP formation in combination with the computational results from MATA and colleagues

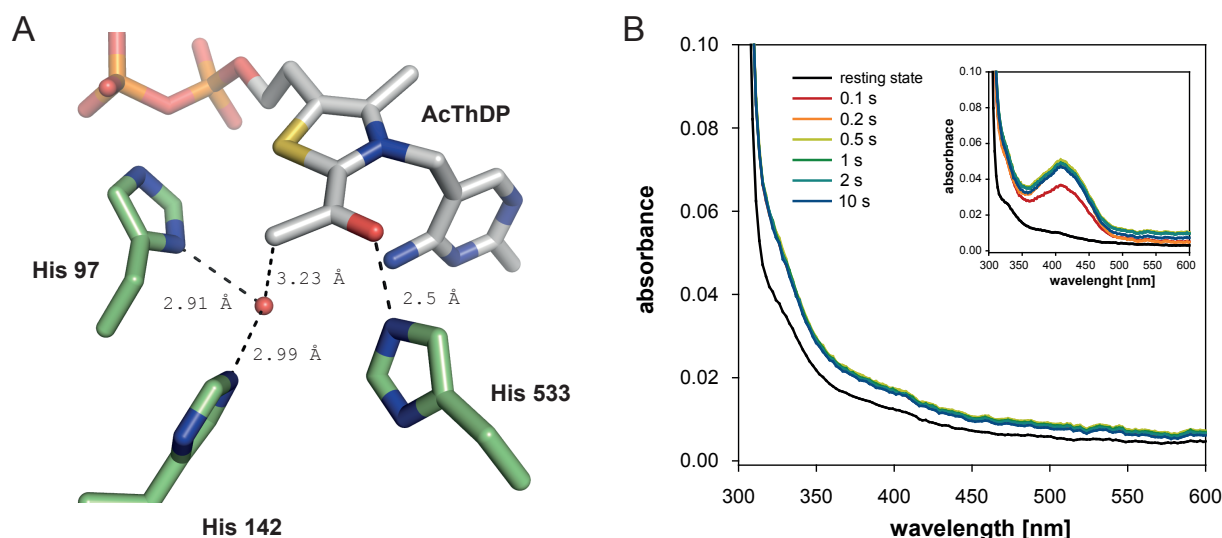


**Figure 28: Investigation on the catalytic role of His553.** (A) Active site environment of AcThDP in XFPK<sub>WT</sub> showing distances between histidine residues and the acyl-moiety of the covalent cofactor adduct. His553 is located in hydrogen bonding distance to the hydroxy/carbonyl-group of AcThDP, likely acting as acid-base catalyst for the tautomerization from enol- to keto-AcThDP in the phosphoketolase reaction. His97 and His142 contact a water molecule (red sphere) that is located in close proximity to the acyl group. The figure was prepared based on pdb file 3AHD (SUZUKI *et al.*, 2010<sup>73</sup>). (B) Time-resolved absorbance spectrum of XFPK<sub>H553A</sub> after mixing with 20 mM F6P is missing the AcThDP absorbance signal at 420 nm. Inset shows time-resolved evolution of the absorbance band in the wild-type enzyme.

indicate tautomerization of the post-dehydration enol-intermediate to keto-AcThDP to proceed via the formation of enolate-AcThDP, as has been proposed before<sup>75</sup>. The active site residue His553 lies in hydrogen-bonding distance of the AcThDP's hydroxy/carbonyl group (Figure 28A) and was proposed as likely candidate for an acid-base catalyst in the conversion of enol- to keto-AcThDP, but its involvement was not yet confirmed by experimental data<sup>4,75</sup>.

To investigate the potential role of His553 in the tautomerization step of the phosphoketolase reaction, the phosphoketolase variant XFPK<sub>H553A</sub> was recombinantly expressed, purified and examined for its ability to catalyze the phosphoketolase reaction or parts thereof. The variant was subjected to the CD spectroscopy-based steady-state assay, but did not display enzymatic activity in form of E4P release, even at high protein concentrations of up to 10 mg/mL. Also, no absorbance signal was detected after addition of F6P to XFPK<sub>H553A</sub>, as shown in a time-resolved absorbance spectrum recorded by photodiode array detection in a stopped-flow spectrophotometer (Figure 28B), indicating failure of the enzyme variant to form the AcThDP intermediate. These results are consistent with observations by SUZUKI *et al.* who reported inactivity of the XFPK<sub>H553A</sub> variant in the hydroxamate-assay and failed to trap AcThDP in crystallo after soaking XFPK<sub>H553A</sub> crystals with F6P<sup>73</sup>. Most likely, His553 is involved in catalytic steps preceding AcThDP formation. Additional to its putative role in mediation of the keto-enol-tautomerization, His553 is believed

to play a role in stabilization and/or protonation of the ThDP-F6P-adduct prior to C-C bond cleavage and release of E4P<sup>73,75</sup>. Such an involvement would explain the deficiency of the enzyme to form E4P as observed in the steady-state assay. Furthermore, His553 was proposed as potential acid-base catalyst for the dehydration of DHEThDP<sup>73</sup>. Unfortunately, inactivity of the XFPK<sub>H553A</sub> variant prevents experimental evaluation of the residue's role in the conversion from enol- to keto-AcThDP.

In their computational investigations on *B. longum* phosphoketolase, ZHANG AND LIU calculated relative energies of intermediates and transition states occurring on the enzymes reaction pathway. For the putative proton transfer from His553 to the C1 atom of enol-AcThDP their calculations yield an energy barrier of over 100 kJ/mol<sup>75</sup>. This unusually high barrier provokes to think about an additional or alternative mechanism that could play a role in the tautomerization reaction.

### 3.5 Carboligation side reactions in phosphoketolase

#### 3.5.1 Reaction of AcThDP with electrophilic acceptor substrates

ThDP-dependent enzymes are known for their ability to catalyze carbon-carbon ligation reactions, either as their main physiological activity or in form of off-pathway side reactions. This ability is based on the formation of reactive intermediates on their catalytic pathway and has been exploited for a number of biocatalytic applications. So far, all known carboligation reactions catalyzed by ThDP-dependent enzymes are emerging from the central  $\alpha$ -carbanion/enamine intermediate. Next to the  $\alpha$ -carbanion/enamine intermediate DHEThDP, the phosphoketolase reaction pathway presumably harbors a second reactive intermediate bearing potential as substrate for carboligation reactions.

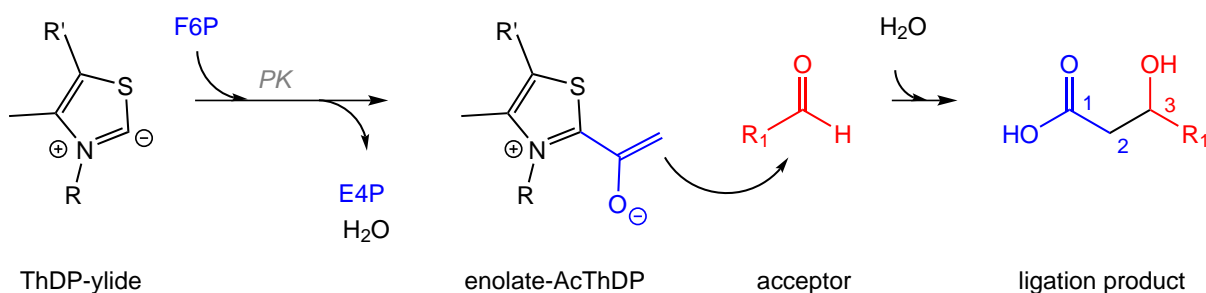


**Figure 29: Schematic representation of a potential ligation reaction between enolate-AcThDP and an aldehyde acceptor.** Addition of the ketose-substrate F6P to the activated cofactor, followed by liberation of E4P and dehydration leaves enolate-AcThDP at the phosphoketolase active site. Potential reaction of the nucleophilic intermediate with an aldehyde acceptor would yield a 3-hydroxy carbonacid as ligation product. ( $R_1 = \text{H}, \text{CH}_3$ , etc.)

From detailed spectroscopic and kinetic investigations of the phosphoketolase reaction mechanism, supported by computational calculations, evidence was collected that the necessary tautomerization from enol- to keto-AcThDP at the phosphoketolase active site proceeds via the formation of an enolate intermediate. Furthermore, our results suggest that both enolate-AcThDP and its corresponding keto-form are present when the post-dehydration intermediate accumulates in the absence of the acyl-acceptor substrate phosphate. Enolate anions are strong nucleophiles that react with carbon-electrophiles in C-C bond forming reactions. If the presumption of an enolate-intermediate on the phosphoketolase reaction pathway is correct, addition of a carbon-electrophile as acceptor substrate to the phosphoketolase reaction could potentially lead to adduct formation between enolate-AcThDP and the electrophilic acceptor under the formation of a new C-C bond (Figure 29). Suitable candidates for electrophilic acceptors would presumably be small aldehydes such as formaldehyde or acetaldehyde.

In order to test for a potential reaction between AcThDP and the aldehyde acceptors, formaldehyde or acetaldehyde were added to the reaction of phosphoketolase with F6P. UV-Vis spectra were recorded with and without the addition of an aldehyde acceptor to check for changes in the AcThDP absorbance band that might indicate a reaction between phosphoketolase intermediate and aldehyde acceptor. Whereas absorbance at 420 nm was not altered after addition of acetaldehyde, a small decrease in the spectral signal was visible when the reaction was supplemented with formaldehyde. Decrease of the absorbance band after formaldehyde addition was more distinct

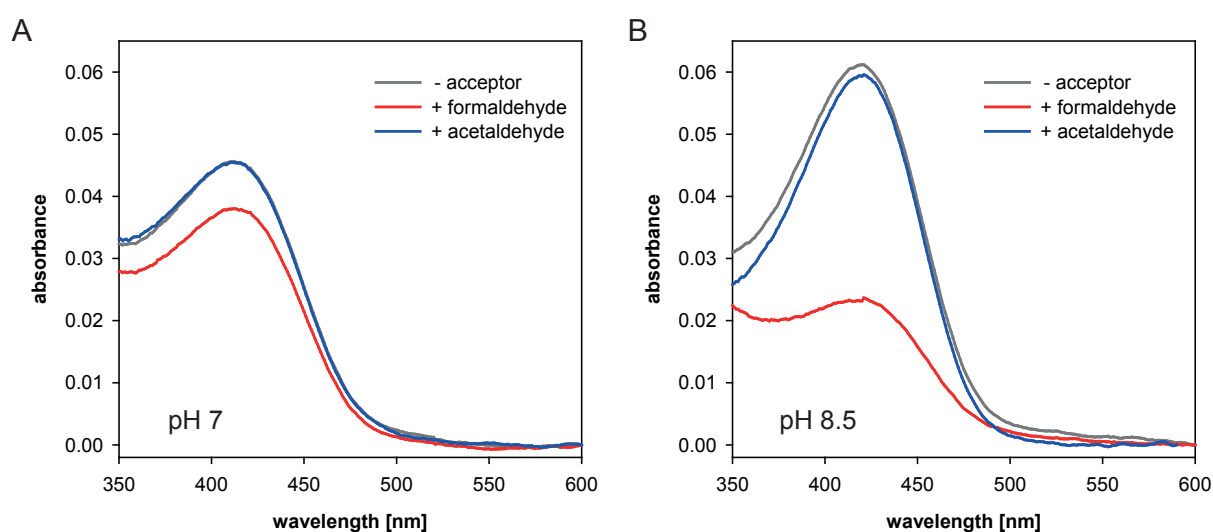


**Figure 30: Absorbance spectra of AcThDP after addition of aldehyde acceptor substrates.** UV-Vis absorbance spectra were recorded of 24  $\mu$ M XFPK with 20 mM F6P without (grey) or with addition of 100 mM formaldehyde (red) or 100 mM acetaldehyde (blue). Experiments were conducted at (A) pH 7 or (B) pH 8.5. After addition of formaldehyde, signal decrease can be observed.



at increased pH (Figure 30). The drop in absorbance might indicate a decrease in AcThDP concentration and as such a potential addition of formaldehyde to the reaction intermediate.

Depletion of the absorbance band was also monitored in a stopped-flow sequential mixing experiment. Phosphoketolase was premixed with F6P to populate AcThDP at the enzyme's active site. After an aging period of 5 s, the reaction mix was rapid-mixed with different formaldehyde concentrations, and depletion of the absorbance at 420 nm was recorded over time (Figure 59, Appendix). The signal decrease appeared concentration dependent, however recovery of the signal after depletion of the acceptor substrate could not be observed, indicating inactivation of the enzyme by formaldehyde. Whether the decrease in absorbance is simply a result of an inactivation process or whether a ligation reaction between enolate-AcThDP and formaldehyde contributes to the signal depletion could not be judged in the employed experimental setup. Hence, further analytical methods needed to be applied to test for a potential ligation product of the phosphoketolase post-dehydration intermediate and formaldehyde.

### 3.5.2 Analysis of ligation products by GC-MS

Observation of a decrease in the AcThDP absorbance band after addition of formaldehyde initiated the idea of a potential carboligation side reaction between the post-dehydration intermediate and the aldehyde. To follow up on this hypothesis, product analysis of the ligation reaction was carried out by gas chromatography-mass spectrometry. Phosphoketolase was incubated with F6P as donor-ketose and formaldehyde as acceptor for 1 - 16 h at 25 °C. Reaction products were extracted and derivatized as described in section 2.6 and subjected to GC-MS analysis.

The resulting chromatogram showed two small peaks with a retention time of 9.2 min and 12.7 min that did not appear in the control reactions without enzyme, without formaldehyde or without F6P, suggesting they represent ligation products between a product or intermediate of the phosphoketolase reaction and formaldehyde (Figure 32A and 33A, data for control without F6P not shown). Analysis of the corresponding mass spectrum by comparison against the NIST mass spectrometry database indicated that the peak at 9.2 min likely originates from 3-hydroxypropionic acid, the product of the predicted C-C ligation reaction between enolate-AcThDP and formaldehyde (Figure 31). This was confirmed by GC-MS analysis of commercially available 3-hydroxypropionic acid as reference substance, which exhibited a very similar retention time and fragmentation pattern (Figure 32C+D).

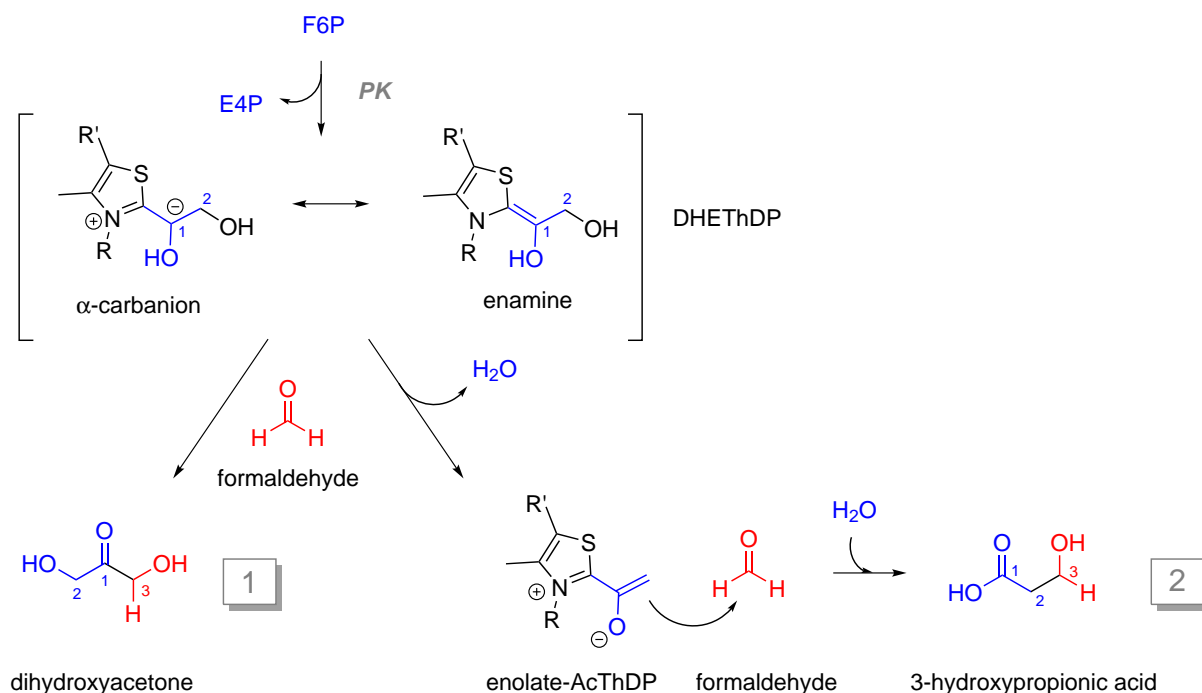


**Figure 31: Potential ligation reactions of phosphoketolase reaction intermediates with formaldehyde.** The  $\alpha$ -carbanion/enamine intermediate DHEThDP as well as the predicted enolate-AcThDP, resulting from dehydration of the latter, are potential substrates for a C-C bond forming reaction with formaldehyde. Reaction with the acceptor substrate would yield dihydroxyacetone or 3-hydroxypropionic acid as ligation products.

To verify that the detected 3-hydroxypropionic acid actually originates from a ligation reaction between the phosphoketolase enolate-intermediate and formaldehyde, the experiment was repeated with  $^{13}\text{C}$ -labeled F6P as donor-substrate and  $^{13}\text{C}$ -labeled formaldehyde as acceptor in individual experiments. Ligation between enolate-AcThDP and formaldehyde using  $^{13}\text{C}$ -F6P as donor should result in incorporation of two isotope-labeled carbon atoms, yielding  $[1,2-^{13}\text{C}]$ -3-hydroxypropionic acid. Incorporation of one  $^{13}\text{C}$ -atom to  $[3-^{13}\text{C}]$ -3-hydroxypropionic acid is expected in case labeled formaldehyde is used as acceptor (see chemical formulas in Figure 34B+C). The respective mass spectra are shown in Figure 34. The signature peak at  $m/z = 219$  detectable for the reference substance (Figure 32D) and in the reaction with unlabeled substrates (Figure 34A) is shifted to  $m/z = 221$  in the reaction with labeled F6P (Figure 34B) and to  $m/z = 220$  when isotope-labeled formaldehyde was used (Figure 34C). This indicates mass increase by two, respectively one, as would be expected after incorporation of two respectively one  $^{13}\text{C}$ -labeled carbon atom into the ligation product. Also the peak with an  $m/z = 116$  shows increase by one when using either of the labeled substrates, suggesting it is associated to a fragment containing one carbon atom of donor and acceptor each. Those results strongly suggest formation of the aforementioned  $^{13}\text{C}$ -labeled 3-hydroxypropionic acid products with  $^{13}\text{C}$ -F6P as donor as well as with labeled formaldehyde

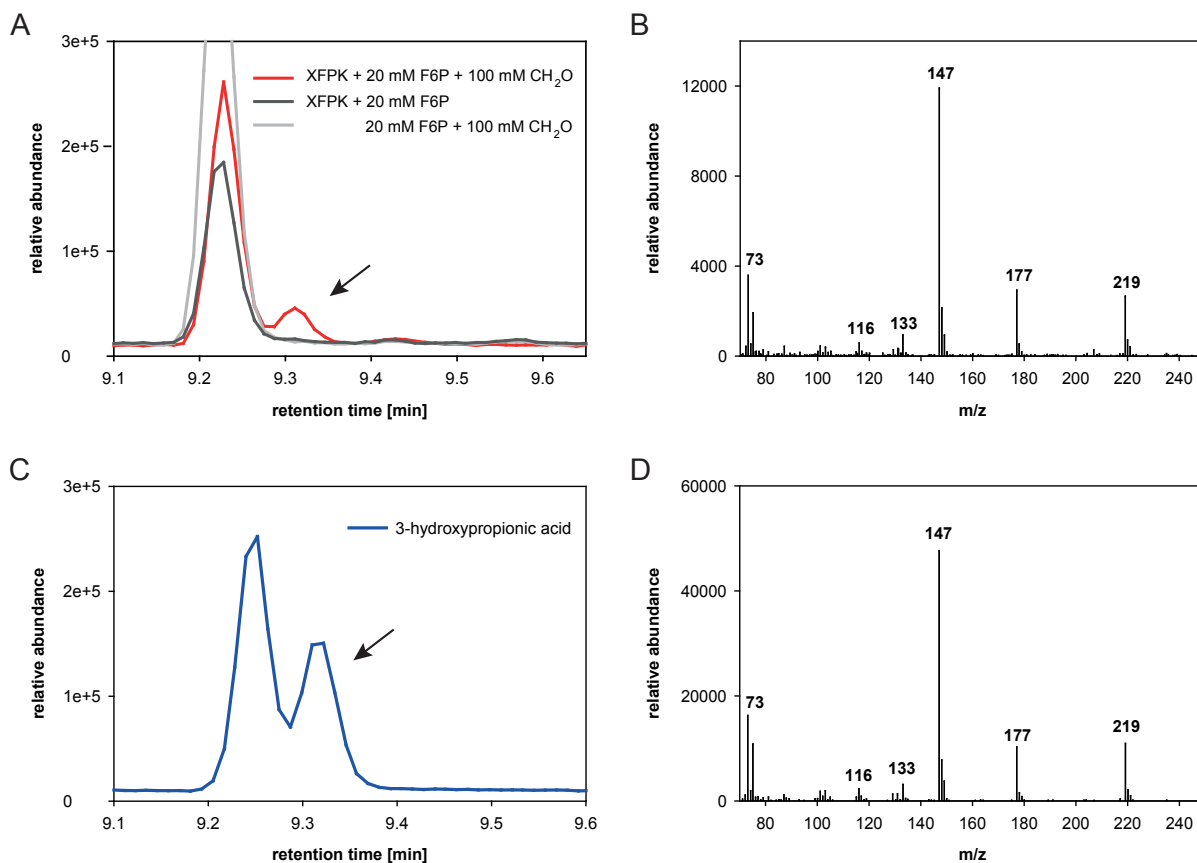


**Figure 32: Detection of 3-hydroxypropionic acid by GC-MS.** (A) Chromatogram of product analysis by GC-MS after reaction of  $24\ \mu\text{M}$  XFPK with 20 mM F6P and 100 mM formaldehyde (red) shows presence of additional product peak (indicated by arrow), compared to control reactions (dark gray = without formaldehyde, light gray = without XFPK). (B) Mass-spectrum corresponding to additional product peak shown in diagram A. Resemblance in retention time and mass-fragmentation pattern strongly suggests additional product peak to correspond to 3-hydroxypropionic acid. (C) Chromatogram and (D) mass spectrum of pure 3-hydroxypropionic acid.

as acceptor, confirming the predicted reaction between phosphoketolase-bound enolate-AcThDP intermediate and formaldehyde.

The second product with a retention time of 12.7 min was identified by library search and comparison to a reference substance as dihydroxyacetone (Figure 33). A ligation reaction between the  $\alpha$ -carbanion/enamine of the phosphoketolase reaction DHETThDP would yield dihydroxyacetone (Figure 31). Isotopic labeling with  $^{13}\text{C}$ -F6P led to a shift in the mass-charge ratio by two of several peaks in the mass spectrum (Figure 34D+E), indicating incorporation of two labeled carbon atoms into the product compound. Application of  $^{13}\text{C}$ -labeled formaldehyde resulted in a mass increase by one for the same fragments (Figure 34F). This labeling pattern would correspond to  $[1,2\text{-}^{13}\text{C}]\text{-1,3-dihydroxypropan-2-one}$  and  $[3\text{-}^{13}\text{C}]\text{-1,3-dihydroxypropan-2-one}$  (see chemical formulas in Figure 34E+F), the theoretical ligation products derived by ligation of DHETThDP with formaldehyde using  $^{13}\text{C}$ -labeled donor or acceptor substrate. The obtained

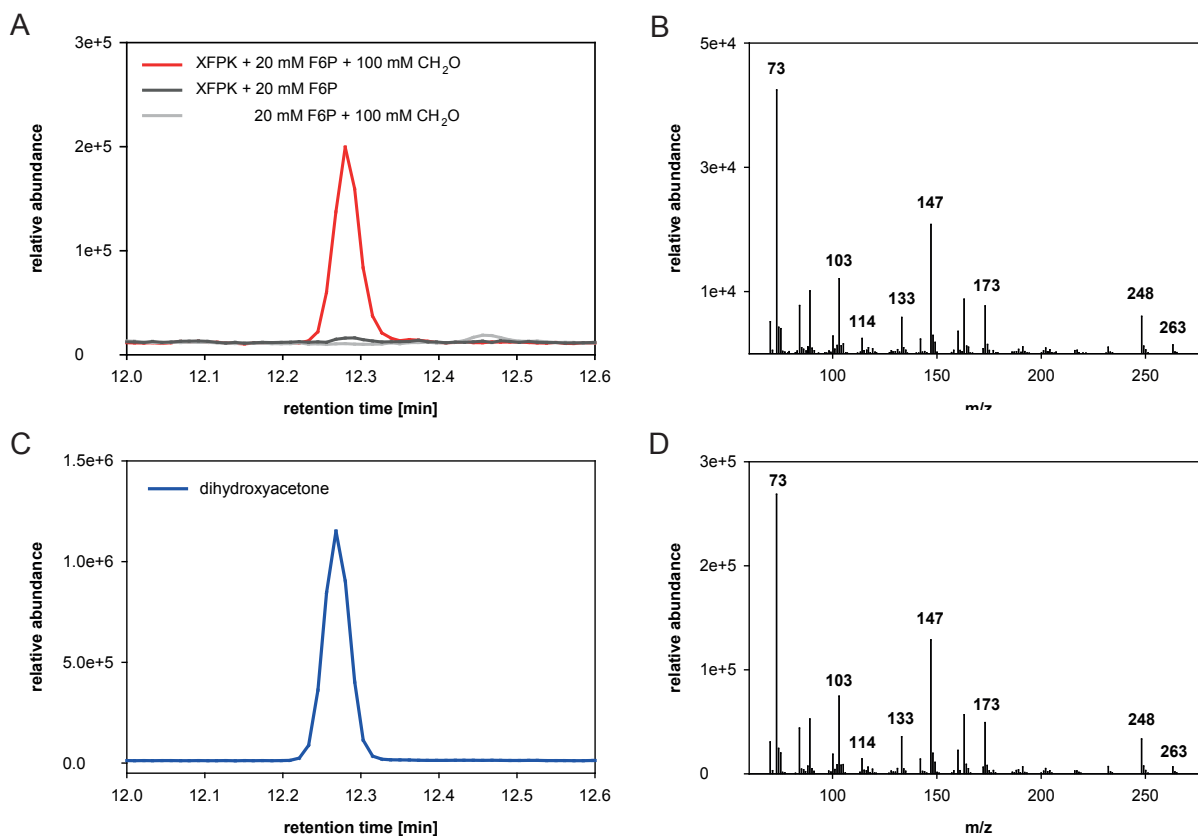


**Figure 33: Detection of dihydroxyacetone by GC-MS.** (A) Chromatogram of product analysis by GC-MS after reaction of  $24 \mu\text{M}$  XFPK with 20 mM F6P and 100 mM (red) shows presence of additional product peak, compared to control reactions (dark gray = without formaldehyde, light gray = without XFPK). (B) Mass spectrum corresponding to additional product peak shown in diagram A. Resemblance in retention time and mass-fragmentation pattern strongly suggests additional product peak to correspond to dihydroxyacetone. (C) Chromatogram and (D) mass spectrum of dihydroxyacetone.

data strongly suggest a reaction between the pre-dehydration intermediate DHET<sub>h</sub>DP and the aldehyde acceptor indeed takes place.

It seems that phosphoketolase as many other ThDP-dependent decarboxylases and transferases catalyzes a C-C ligation of the central carbanion/enamine intermediate with aldehyde acceptors yielding 2-hydroxy ketones as side reaction. Moreover, phosphoketolase exhibits a second side reactivity. The enzyme seems to catalyze a ligation between its covalent AcThDP intermediate and an aldehyde acceptor. Observation of latter reaction strongly supports the assumption that parts of AcThDP exist as stable enolate during the phosphoketolase reaction cycle.

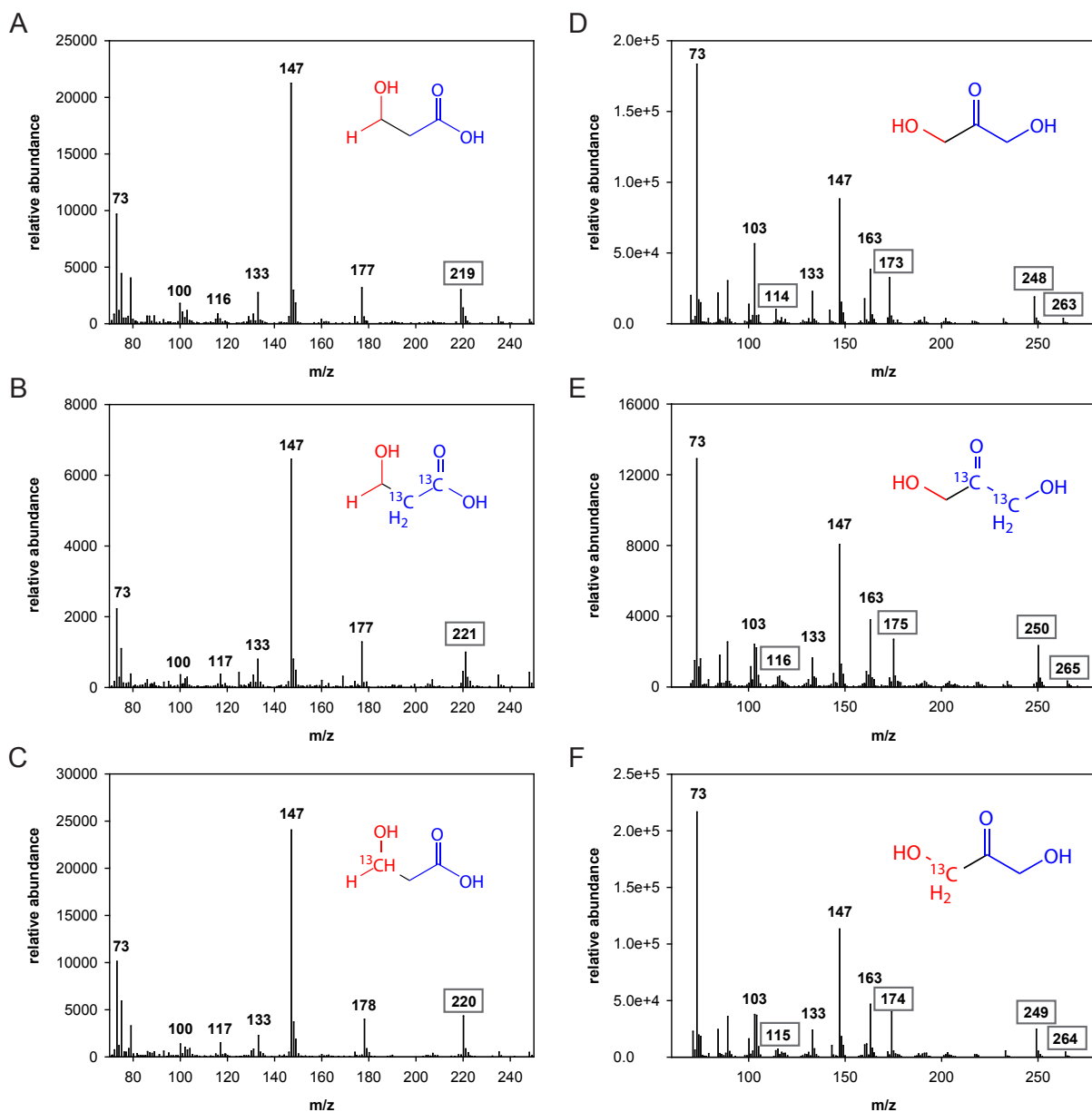


**Figure 34: GC-MS analysis of  $^{13}\text{C}$ -labeled ligation products.** Left column (A-C) shows mass spectra assigned to the ligation product of enolate-AcThDP and formaldehyde after reaction of XFPK with labeled or non-labeled F6P or formaldehyde. Chemical formulas of the predicted products are depicted in the respective diagram. Peaks indicating mass increase of the observed compound are marked in gray squares. Right column (D-F) shows mass spectra assigned to the ligation product of DHEThDP and formaldehyde after reaction of XFPK with labeled or non-labeled F6P or formaldehyde. Chemical formulas of the predicted products are depicted in the respective diagram (note that modification of functional groups from derivatisation is not shown). Peaks indicating mass increase of the observed compound are marked in gray squares. For details see text.

### 3.5.3 Quantification of ligation products by GC-MS

Both ligation products appeared in very low quantities in the GC-MS analytics. In order to determine product yields of the detected side reactions, quantification of the ligation products 3-hydroxypropionic acid and dihydroxyacetone was carried out by GC-MS. Quantification was performed in close collaboration with DR. TILL ISCHEBECK, Department of Plant Biochemistry, University of Göttingen, who was responsible for the experimental design and carried out data analysis and evaluation. Calibration curves were prepared from pure 3-hydroxypropionic acid and dihydroxyacetone, that allowed determination of absolute quantities of the ligation products in the reaction mix against an internal standard. The calibration curves of both compounds exhibit linear dependency of the signal in the considered analyte range (Figure 57, Appendix) . Control reactions of phosphoketolase with F6P without addition of the aldehyde acceptor and F6P and formaldehyde without enzyme were carried out to validate the applied quantification method.

As expected from the qualitative analysis, the total amount of ligation products detected after incubation of phosphoketolase with 20 mM F6P and 100 mM formaldehyde was rather small. Quantification yielded total amounts of  $3.8 \pm 0.3$  nmol 3-hydroxypropionic acid and  $12.8 \pm 1.3$  nmol dihydroxyacetone in the reaction mix. Related to the amount of F6P substrate of 2000 nmol, ligation of enolate-AcThDP and formaldehyde showed a product yield of only 0.2 %. Approximately 0.6 % of the substrate sugar were converted in the reaction of DHETHDP and the aldehyde acceptor to dihydroxyacetone. No ligation products were detected in the control reactions.

Analyzing the overall turnover of F6P to E4P in the presence and absence of formaldehyde, it was noticed that conversion is drastically decreased in the presence of the aldehyde acceptor. Absolute quantification of the phosphosugar substrate and product could not be achieved with satisfying accuracy yet, but comparison of GC-MS chromatograms in presence and absence of formaldehyde revealed that only a low amount of E4P is formed in the reaction containing formaldehyde, while

**Table 2: Total amounts of carboligation products.** The total amounts of 3-hydroxypropionic acid (3-HPA) and dihydroxyacetone (DHA) after reaction of 2.4 nmol XFPK with 2000 nmol F6P and 10  $\mu$ M formaldehyde (FA) were determined by quantitative GC-MS. Overall yield in percent is given in brackets.

reaction	3-HPA [nmol]		DHA [nmol]	
XFPK + F6P + FA	$3.8 \pm 0.3$	(0.2 %)	$12.8 \pm 1.3$	(0.6 %)
XFPK + F6P	0	(0 %)	0	(0 %)
F6P + FA	0	(0 %)	0	(0 %)

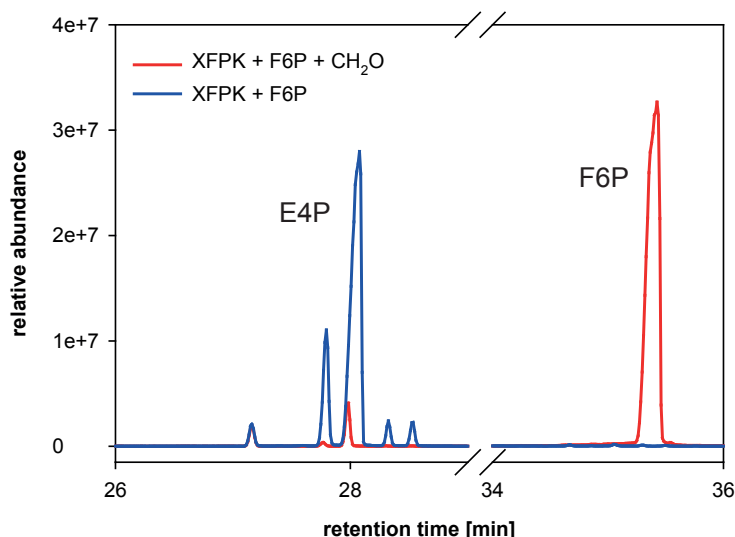


**Figure 35: Analysis of F6P conversion in presence of formaldehyde by GC-MS.** The reaction of  $24\ \mu\text{M}$  XFPK and  $20\ \text{mM}$  F6P with or without addition of  $100\ \text{mM}$  formaldehyde was analyzed by GC-MS. The excerpt shows the peaks corresponding to ketose-substrate F6P and aldose-product E4P. No F6P was detectable in the control reaction (blue), indicating complete conversion to E4P. Detection of remaining F6P together with very small E4P peak indicate impaired enzymatic activity in presence of the aldehyde acceptor (red).

there is still a lot of F6P detectable. In the control reaction of phosphoketolase with F6P alone, the F6P peak has completely vanished and E4P is detected as only product (Figure 35). From preliminary attempts to quantify F6P and E4P in the reaction mix, conversion of below 10 % in the presence of formaldehyde was estimated. The strong reduction in enzymatic activity after addition of the aldehyde acceptor is assumed to be caused by chemical modifications of phosphoketolase through formaldehyde. Formaldehyde reacts with amino- and thiol groups of several amino acid side chains, inducing different chemical modifications and cross-links that can severely impair the enzymes functionality<sup>99</sup>. Results from the spectral analysis of phosphoketolase reaction after formaldehyde addition also implied enzyme inactivation (section 3.5.1).

The very low yields observed for the carboligation side reactions are presumably a result of a decrease in enzymatic activity caused by the employed aldehyde acceptor. Replacing formaldehyde by electrophilic acceptors that do not lead to enzyme modification and subsequent rate decline should therefore significantly increase the product yield of both carboligation reactions.

### 3.5.4 Testing of alternative aldehyde acceptors

Analysis of substrates and products by GC-MS revealed that the conversion of F6P to E4P by phosphoketolase is greatly impaired after the addition of formaldehyde as electrophilic acceptor substrate, presumably due to chemical modifications of the enzyme. Thus, acetaldehyde, glycolaldehyde and trifluoroacetaldehyde were tested as alternatives acceptors in the carboligation reaction with the phosphoketolase reaction intermediates. The latter compound is significantly bigger than formaldehyde or acetaldehyde, but should exhibit an increased electrophilicity at

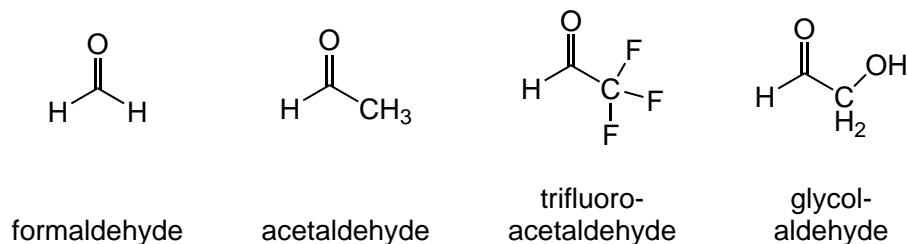


**Figure 36: Potential acceptor substrates for phosphoketolase catalyzed carboligation reactions.** Depicted compounds were tested as acceptor substrates for carboligation reactions with phosphoketolase bound DHEThDP or enolate-AcThDP.

the carbonyl-carbon atom compared to acetaldehyde due to the negative inductive effect of the substituents.

Analysis of the reaction containing 24  $\mu$ M phosphoketolase, 20 mM F6P and 100 mM of either acetaldehyde, glycolaldehyde or trifluoroacetaldehyde by GC-MS showed almost complete conversion of F6P to E4P after 1 h (Figure 60, Appendix). Enzymatic activity of phosphoketolase seems largely unaffected by the presence of the different aldehydes. However, no ligation product could be detected for the reaction of acetaldehyde with either DHEThDP or enolate-AcThDP by GC-MS product analysis. Glycolaldehyde and trifluoroacetaldehyde too, did apparently not react with any of the covalent ThDP adducts of the phosphoketolase reaction, as no ligation products were detected.

From analysis of the active site structure, we assume that a potential tetrahedral adduct of enolate-AcThDP with an aldehyde acceptor needs to be oriented similar to the substrate-cofactor adduct (see Figure 11A). In the crystal structure of the trapped AcThDP intermediate, this space is occupied by two water molecules, surrounded by several histidine and other rather bulky side chains (Figure 37, left). Those partly enclose the intermediate (Figure 37, right) and might interfere with binding or optimal orientation of larger aldehyde acceptors and thus prevent adduct formation. One of the active site residues that potentially interferes with accommodation of larger aldehyde acceptors is histidine 64. In order to increase space around the enolate-AcThDP intermediate, aiming to reduce steric confinements for adduct formation, the active site residue His64 was replaced by serine as less bulky side chain that should still be capable of hydrogen bonding interactions with hydroxy groups of the covalent cofactor adducts. The amino acid exchange was introduced into the phosphoketolase nucleotide sequence by site-directed mutagenesis. The resulting recombinant XFPK<sub>H64S</sub> variant was tested for its phosphoketolase activity using the CD spectroscopy-based steady-state assay. No formation of E4P was detected, even when enzyme concentration was increased 10 fold to 50  $\mu$ M. Nevertheless, partial conversion



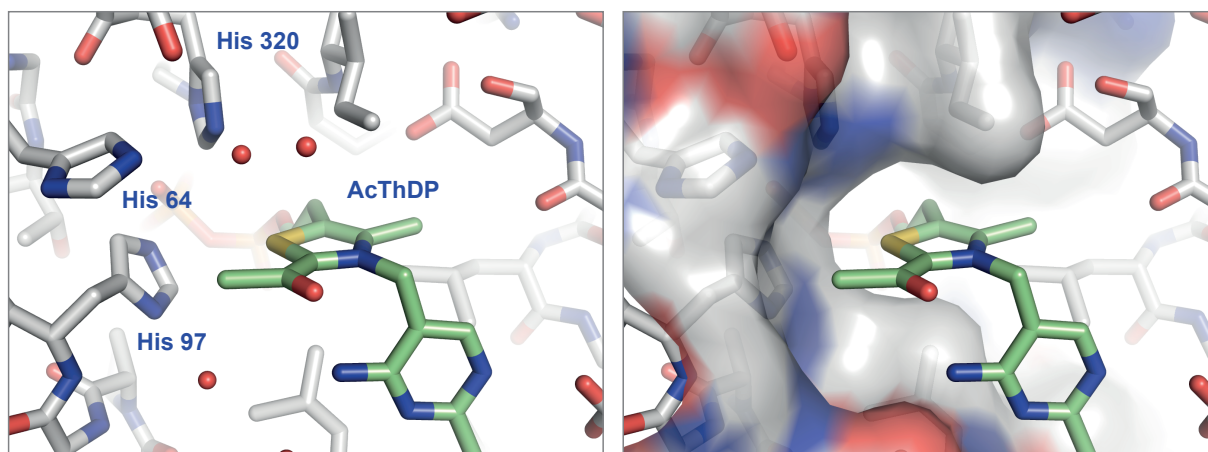


**Figure 37: Active site environment of AcThDP in phosphoketolase.** The covalent cofactor adduct is shown in green, water molecules in the immediate environment of the acyl-moiety are depicted as red spheres. Display of the solvent-accessible surface area (right) shows enclosure of the intermediate by catalytically important histidine residues.

of F6P to E4P was observed after 16 h in GC-MS (Figure 38), indicating residual activity of the phosphoketolase variant. Subsequently, the variant was analyzed for potential C-C ligation reactions with formaldehyde, acetaldehyde glycolaldehyde and trifluoroacetaldehyde as acceptors. With dihydroxyacetone, only the reaction product of DHETThDP and formaldehyde was detected. No indication was found for ligation reactions with other acceptors or with enolate-AcThDP as donor. Although no formation of AcThDP was observed by UV-Vis analysis, detection of residual phosphoketolase activity lets assume that the variant is capable of forming both the DHETThDP and the enolate-AcThDP intermediate. Absence of the ligation product 3-hydroxypropionic acid emerging from AcThDP seems therefore surprising at first sight, but due to the significantly reduced reaction rate, inactivation of the enzyme by formaldehyde presumably occurs faster than the ligation between enolate-AcThDP and the aldehyde acceptor.

Replacement of His64 by a less bulky side chain did not extend the spectrum for non-natural acceptor substrates. The drastic decrease in enzymatic activity by the exchange of His64 demonstrates the important role of the active site residue in the phosphoketolase catalytic cycle. It was assumed that His64 either acts as acid-base catalyst in the deprotonation of the 3-OH-group prior to substrate cleavage, or alternatively aids to stabilize the negative charge resulting from deprotonation<sup>4,73</sup>. In any case the function of His64 seems to be essential for the phosphoketolase reaction. Other side chains that might restrict space for proper binding and orientation of an acceptor substrate like His320, N549 and Y501 were also found to be crucial for phosphoketolase activity.

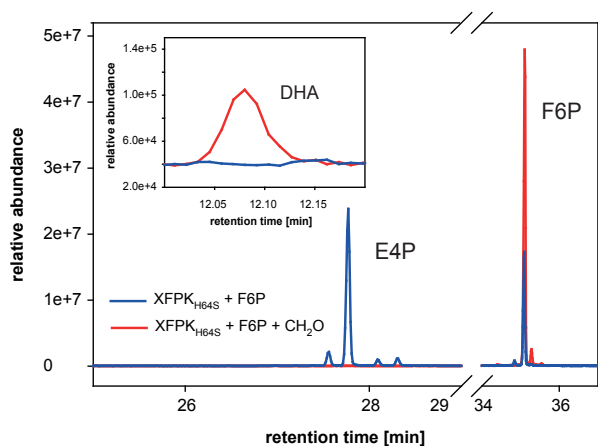


**Figure 38: GC-MS product analysis of XFPK<sub>H64S</sub>.** The reaction of 48.5  $\mu$ M XFPK<sub>H64S</sub> and 20 mM F6P with (red) or without addition of 100 mM formaldehyde (blue) was analyzed by GC-MS. Substrate F6P is still detectable after 16 h reaction time, indicating phosphoketolase activity of XFPK<sub>H64S</sub> is markedly decreased compared to the wild-type enzyme. Conversion is further reduced after addition of formaldehyde. However, detection of dihydroxyacetone (inset), the ligation product of DHETHDP and formaldehyde implies residual phosphoketolase activity.

By detection of 3-hydroxypropionic acid and dihydroxyacetone as ligation products of the phosphoketolase reaction intermediates DHETHDP and AcThDP with formaldehyde proof of principle was provided for a carboligase side activity of phosphoketolase. However, observed conversion rates are extremely low and C-C bond formation with aldehyde acceptors other than formaldehyde could not be achieved. For a potential application of phosphoketolase in biosynthesis, conversion rates would need to be greatly increased and the acceptor substrate spectrum broadened.

### 3.6 Generation and analysis of a "transketolase-like" phosphoketolase variant

The related ThDP-dependent enzymes phosphoketolase and transketolase are very similar in structure and function. Especially their active site architectures show striking similarity. Still, both enzymes achieve different catalytic outcomes at crucial points in the reaction cycle. Up to the formation of DHETHDP both reactions proceed more or less identical, but whereas phosphoketolase catalyzes the dehydration of the DHETHDP intermediate, in transketolase the 2-carbon-moiety is transferred onto a ketose-acceptor. So far, no structural differences were found that would account for such a different catalytic outcome. There are three evident amino acid exchanges between the active sites of *B. breve* phosphoketolase and *E. coli* transketolase: Glu437, Tyr501 and Asn549 in phosphoketolase are replaced by Leu382, Phe434 and Asp469 in transketolase. In order to determine the function of those side chain exchanges and to evaluate their role in the different catalytic activities of phosphoketolase and transketolase, it was aimed to replace the active site residues in phosphoketolase by their corresponding transketolase counterparts. As the phosphoketolase variants XFPK<sub>Y501F</sub> and XFPK<sub>E437Q</sub> variant were already characterized in other studies<sup>73,89</sup>, the exchange of Asn549 to aspartic acid was taken as starting point for the stepwise generation of a "transketolase-like" phosphoketolase variant.

### 3.6.1 Characterization of XFPK<sub>N549D</sub>

The active site residue asparagine 549 in phosphoketolase replaces a strictly conserved and catalytically important aspartic acid residue in transketolase<sup>100</sup>. Structural studies showed that the side chain is part of the phosphate binding site and thus it was suggested that replacement of the negatively charged aspartic acid serves to facilitate binding of the also negatively charged phosphoketolase substrate phosphate<sup>4,72</sup>. In order to evaluate the role of asparagine 549, the exchange to aspartic acid was introduced by site directed mutagenesis and the resulting recombinant enzyme variant analyzed for its catalytic abilities.

The UV-Vis spectrum of XFPK<sub>N549D</sub> with 20 mM F6P shows the specific AcThDP absorbance band at 420 nm that disappears after the addition of inorganic phosphate (Figure 39), demonstrating that XFPK<sub>N549D</sub> exhibits phosphoketolase activity and is able to form and stabilize the post-dehydration intermediate AcThDP. Consequently, the CD spectroscopy-based steady-state assay was applied to determine kinetic constants for the phosphoketolase variant. In two separate assays F6P and Na<sub>2</sub>HPO<sub>4</sub> concentrations were varied to obtain  $K_M$  values for both substrates. Initial rate constants were determined from the increase of E4P concentration over time. They showed hyperbolic dependency in both cases that was successfully analyzed using the MICHELIS-MENTEN equation (Eq. 3) (Figure 40). The two independent assays yielded  $k_{cat}$  values of  $0.69 \pm 0.05 \text{ s}^{-1}$  and  $0.36 \pm 0.06 \text{ s}^{-1}$ , showing that enzymatic turnover of the XFPK<sub>N549D</sub> variant is reduced 20-40 fold compared to the wild-type enzyme. As expected, the apparent  $K_M$  of the variant for phosphate was increased from  $3.8 \pm 0.7 \text{ mM}$  to  $7.9 \pm 0.9 \text{ mM}$ . However, elevation of

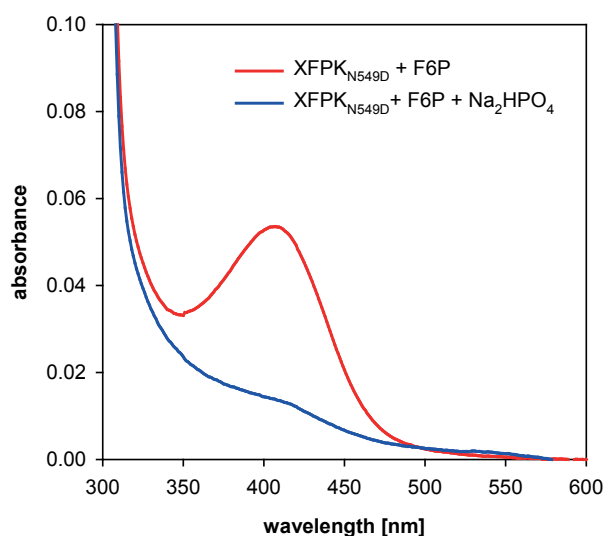


**Figure 39: UV-Vis absorbance spectrum of XFPK<sub>N549D</sub> after substrate addition.** The Absorbance spectrum of 24  $\mu\text{M}$  XFPK<sub>N549D</sub> and 20 mM F6P exhibits the AcThDP absorbance band at 420 nm. Addition of 50 mM Na<sub>2</sub>HPO<sub>4</sub> leads to depletion of the spectral signal.

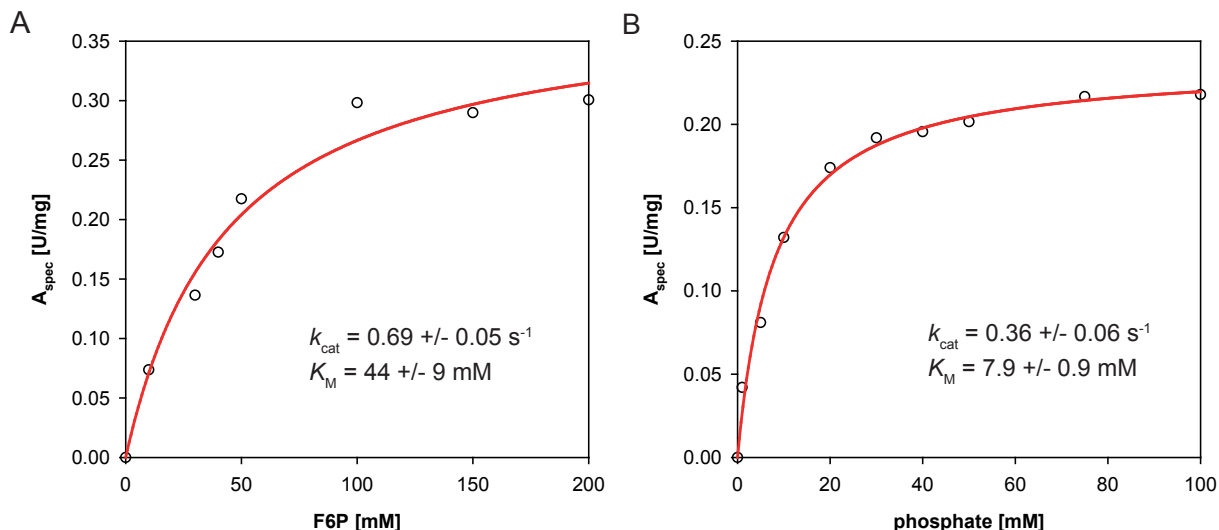


**Figure 40: Steady-state kinetic analysis of XFPK<sub>N549D</sub>.** Initial reaction rates depending on (A) F6P or (B) Na<sub>2</sub>HPO<sub>4</sub> concentration were determined under steady-state conditions by monitoring increase in E4P concentration. Initial reaction rates were plotted against the applied substrate concentration and fitted using the MICHAELIS-MENTEN equation (Eq.3, red line). Resulting kinetic parameters are indicated in the respective diagram. The assay was carried out at a XFPK<sub>N549D</sub> concentration of 105  $\mu\text{M}$ . Initial reaction rates were determined in single measurements.

$K_{\text{M}}$  was less pronounced than expected. The  $K_{\text{M}}$  for F6P of  $44.1 \pm 8.7 \text{ mM}$  is slightly increased compared to that of the wild-type enzyme ( $32.1 \pm 2.3 \text{ mM}$ ).

To complete kinetic characterization of the XFPK<sub>N549D</sub> variant, formation and depletion of the post-dehydration intermediate AcThDP was analyzed by stopped-flow spectroscopy as described for the wild-type enzyme. Analysis of AcThDP formation was performed based on progression of absorbance at 420 nm over time after rapid-mixing of XFPK<sub>N549D</sub> with different concentrations of F6P. In contrast to the wild-type enzyme, no kinetic overshooting was observed and progress curves could be described by a single term exponential model (Figure 61, Appendix). Apparent rate constants  $k_{\text{obs}_1}$ , derived by fitting of the progress curves with Equation 8, were plotted against the applied F6P concentrations. They showed hyperbolic dependency on the substrate concentration (Figure 41A).  $k_{\text{obs}_1}^{\text{max}}$  was determined by fitting data with Equation 7, yielding an apparent maximum rate constant for AcThDP formation of  $4.96 \pm 0.09 \text{ s}^{-1}$ . Hence, introduction of aspartic acid instead of asparagine at position 549 does not only seem to influence binding of the acceptor substrate phosphate, but also interferes with steps leading up to the formation of the post-dehydration intermediate, decreasing the corresponding apparent rate constant by a factor of 15.

An even more drastic impact was observed on the reaction of AcThDP and phosphate. In order to determine a rate constant for the depletion of the intermediate through nucleophilic attack

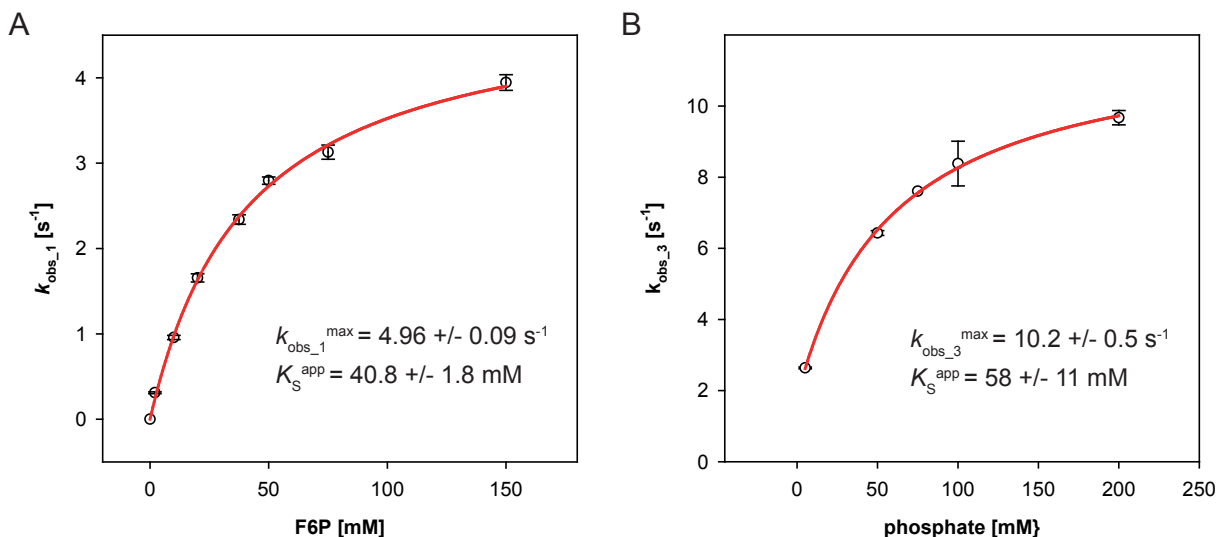


**Figure 41: Transient kinetic analysis of AcThDP formation and depletion in XFPK<sub>N549D</sub>.** (A) Apparent rate constants for AcThDP formation  $k_{\text{obs}_1}$  were determined by fitting progression of absorbance at 420 nm after fast-mixing of  $24 \mu\text{M}$  XFPK<sub>N549D</sub> with different concentrations of F6P in a stopped-flow device with a single-term exponential model (Eq.8). They were plotted against the applied F6P concentration. Fitting with Equation 7 (red line) yielded the kinetic constants depicted in the diagram. (B) Apparent rate constants for AcThDP depletion by reaction with phosphate  $k_{\text{obs}_3}$  were determined in a double-jump stopped-flow experiment as described in section 2.5.2 and plotted against the applied  $\text{Na}_2\text{HPO}_4$  concentration. Apparent rate constant  $k_{\text{obs}_3}^{\text{max}}$  and apparent  $K_S^{\text{app}}$  were determined by fitting data with Equation 9 (red line).

by phosphate, a double-jump stopped-flow experiment was carried out as described in sections 2.5.2 and 3.3.3. In brief, the post-dehydration intermediate AcThDP was accumulated in a preceding mixing step and then fast-mixed with different concentrations of  $\text{Na}_2\text{HPO}_4$ . Depletion of AcThDP was observed by recording decrease of its absorbance at 420 nm over time. Progress curves were fitted with an exponential term (Eq. 8) and the resulting apparent rate constants  $k_{\text{obs}_3}$  were plotted against the corresponding phosphate concentrations. Fitting with Equation 7 yielded an apparent rate constant  $k_{\text{obs}_3}^{\text{max}}$  of  $10.2 \pm 0.5 \text{ s}^{-1}$  and an apparent  $K_S^{\text{app}}$  of  $58 \pm 11 \text{ mM}$ . Although accuracy of those constants might be reduced by the low density of data points, they clearly indicate that the reaction between AcThDP and phosphate in the XFPK<sub>N549D</sub> variant occurs distinctly slower compared to wild-type phosphoketolase where the reaction happens with  $> 1000 \text{ s}^{-1}$ .

Altogether, the phosphoketolase variant XFPK<sub>N549D</sub> has retained its phosphoketolase function, however activity is reduced about 95%. Analysis of individual reaction steps revealed that the formation of the post-dehydration intermediate AcThDP as well as its reaction with the acceptor substrate phosphate is slowed down in the enzyme variant, indicating involvement of the residue in multiple steps of the phosphoketolase reaction mechanism. As expected, replacement of asparagine 549 by aspartic acid reduces the affinity for the acyl acceptor phosphate as suggested by its

increased  $K_M$ . Although the increase in  $K_M$  was less distinct than expected from mutagenesis studies of other residues of the phosphate binding site, it seems to have a strong effect on the reaction of AcThDP with phosphate.

### 3.6.2 Characterization of XFPK<sub>Y501F/N549D</sub> and XFPK<sub>E437L/Y501F/N549D</sub>

Exchange of asparagine 549 to its transketolase counterpart aspartic acid slightly reduced phosphoketolase activity. Yet, the phosphoketolase variant XFPK<sub>N549D</sub> still catalyzes dehydration of the carbanion/enamine intermediate DHET<sub>h</sub>DP quite efficiently. In order to evaluate whether introduction of the two remaining "transketolase-like" mutations changes the phosphoketolases catalytic characteristics, maybe even towards a possible transketolase activity, glutamic acid 437 and tyrosine 501 were replaced by their transketolase equivalents. Recombinant XFPK<sub>Y501F/N549D</sub> and XFPK<sub>E437L/Y501F/N549D</sub> were derived by heterologous production in *E. coli*, after introduction of the additional amino acid exchanges into the plasmid coding for XFPK<sub>N549D</sub> by site directed mutagenesis one at a time. Both phosphoketolase variants behaved similar to wild-type protein during purification. Structural integrity of the mutant enzymes was confirmed by secondary structure analysis using CD spectroscopy (Figure 62, Appendix).

Both enzyme variants were analyzed for their ability to catalyze the phosphoketolase reaction. In the E4P-detecting activity assay, residual enzymatic activity was observed for XFPK<sub>Y501F/N549D</sub> at very high protein and substrate concentrations of  $>100 \mu\text{M}$  enzyme and 200 mM F6P and  $\text{Na}_2\text{HPO}_4$  (Figure 63, Appendix). Activity was not sufficient to determine kinetic constants under steady-state conditions. The triple variant XFPK<sub>E437L/Y501F/N549D</sub> did not exhibit detectable phosphoketolase activity in form of conversion of F6P to E4P.

Furthermore, UV-Vis absorbance spectra of the variants were recorded to check for formation of the absorbance band at 420 nm associated to the covalent AcThDP intermediate. In accordance to the results from the activity assay, no change in absorbance was observed between XFPK<sub>E437L/Y501F/N549D</sub> in its resting state and after addition of F6P as substrate that would indicate formation of the post-dehydration intermediate (Figure 42B). Upon addition of 20 mM F6P to  $24 \mu\text{M}$  XFPK<sub>Y501F/N549D</sub> the characteristic absorbance signal was observed with an amplitude comparable to that of wild-type phosphoketolase. However, the spectral signal did not disappear after addition of  $\text{Na}_2\text{HPO}_4$ , but showed only a slight decrease (Figure 42A), suggesting an impaired reaction between AcThDP and phosphate.

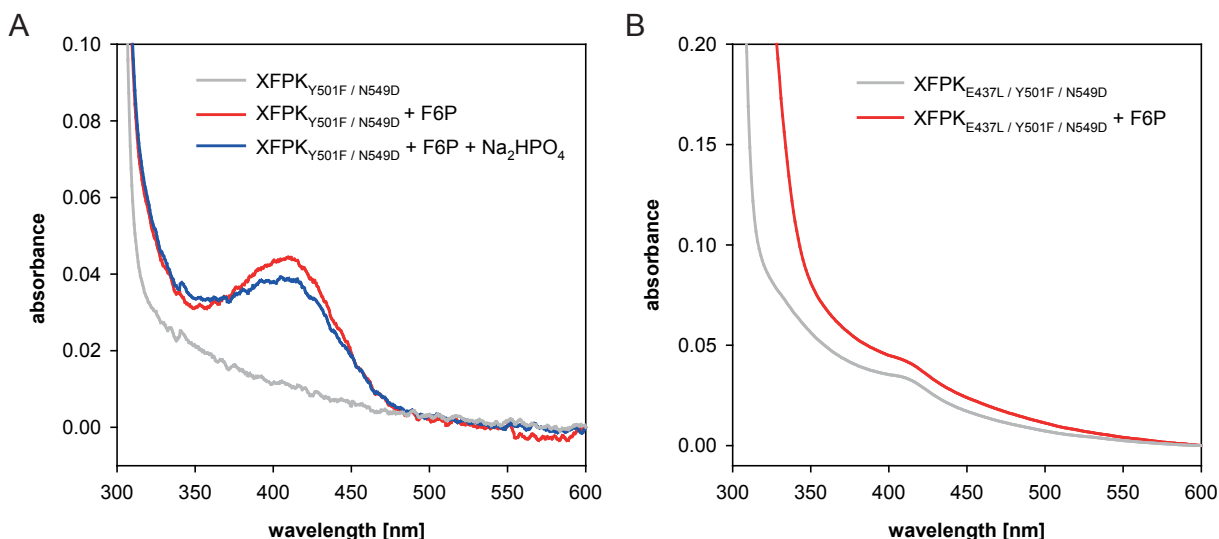


**Figure 42: UV-Vis absorbance spectra of XFPK<sub>Y501F/N549D</sub> and XFPK<sub>E437L/Y501F/N549D</sub>.** (A) UV-Vis spectrum of 24  $\mu$ M XFPK<sub>Y501F/N549D</sub> and 20 mM F6P shows the AcThDP absorbance band at 420 nm (red). Addition of 50 mM Na<sub>2</sub>HPO<sub>4</sub> leads to slight decrease in absorbance but does not deplete the signal (blue). (B) UV-Vis spectrum of 105  $\mu$ M XFPK<sub>E437L/Y501F/N549D</sub> in resting state (gray) and after addition of 100 mM F6P (red). Absence of spectral signal at 420 nm indicates inability of the variant to form the AcThDP intermediate.

To study formation and depletion of AcThDP in XFPK<sub>Y501F/N549D</sub> in more detail, the variant was subjected to stopped-flow spectroscopic analysis. In a first experiment, XFPK<sub>Y501F/N549D</sub> was fast-mixed with different concentrations of F6P to determine apparent rate constants of AcThDP formation from progression of absorbance at 420 nm. As for the wild-type enzyme and XFPK<sub>N549D</sub>, apparent rate constants exhibited hyperbolic dependence on the substrate concentration that allowed determination of the apparent kinetic constants by fitting data with Equation 7. The apparent maximum rate constant  $k_{\text{obs}_1}^{\text{max}}$  of  $1.26 \pm 0.06 \text{ s}^{-1}$  is further reduced compared to XFPK<sub>N549D</sub>, but although formation of AcThDP occurs about 60 times distinctly slower than in the wild-type enzyme, the double variant still catalyzes dehydration of DHETHDP as typical catalytic feature of phosphoketolase.

The reaction of AcThDP with phosphate was analyzed in a sequential mixing experiment as described before (Sections 2.5.2 and 3.3.3). Due to considerably slower formation of AcThDP, aging time for accumulation of the post-dehydration after pre-mixing of XFPK<sub>Y501F/N549D</sub> with F6P was set to 30 s to ensure the steady-state phase was reached. Progress of the absorbance at 420 nm was monitored after rapid-mixing with different concentrations of Na<sub>2</sub>HPO<sub>4</sub> in a second mixing step, progress curves are depicted in Figure 44 A. Fitting with a single-term exponential Equation (Eq.8) yielded apparent rate constants  $k_{\text{obs}_3}$ . Surprisingly, they did not exhibit dependence on the Na<sub>2</sub>HPO<sub>4</sub> concentration (Figure 44B). With an average rate of about

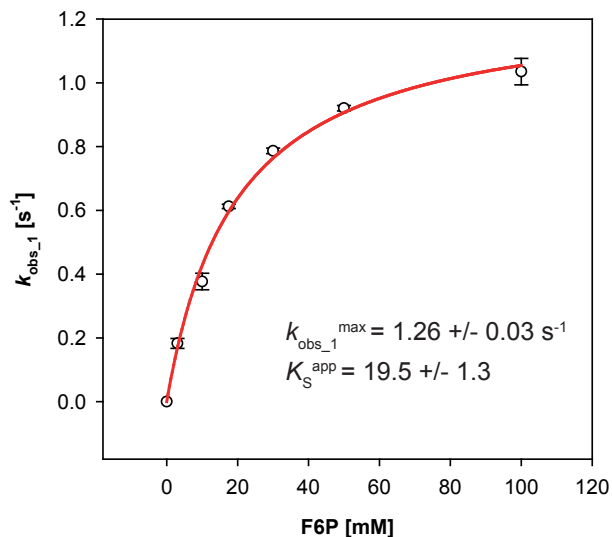


**Figure 43: Transient kinetic analysis of AcThDP formation in XFPK<sub>Y501F/N549D</sub>.** Apparent rate constants  $k_{\text{obs}_1}$ , were determined by fitting progression of absorbance at 420 nm after fast-mixing of 24  $\mu\text{M}$  XFPK<sub>Y501F/N549D</sub> with different concentrations of F6P in a stopped-flow device with a single-term exponential model (Eq.8). Apparent rate constants were plotted against the applied F6P concentration. Fitting with Equation 7 yielded the kinetic constants depicted in the diagram.

$0.5 \text{ s}^{-1}$  depletion of the absorbance signal occurs around 2000 times slower than in wild-type phosphoketolase, suggesting a strong impact of the active site mutations on the reaction between AcThDP and inorganic phosphate. In the crystal structure of phosphoketolase in complex with inorganic phosphate, both Tyr 501 and asparagine 549 were identified as part of the phosphate binding site<sup>73</sup>. Furthermore, the single mutants XFPK<sub>Y501F</sub> and XFPK<sub>N549D</sub> show a reduced  $K_M$  for the acceptor substrate. Thus, disturbance of reaction steps including the acceptor substrate seems a logical consequence.

With the additional introduction of the Glu437Leu mutation, phosphoketolase activity is lost completely. The triple variant did not show activity in form of E4P formation, neither could accumulation of AcThDP be detected, indicating one or more catalytic steps leading up to the formation of the post-dehydration intermediate being severely affected by the additional amino acid exchange.

In addition, XFPK<sub>Y501F/N549D</sub> and XFPK<sub>E437L/Y501F/N549D</sub> were tested for potential transketolase activity. Therefore, both variants were incubated with F6P as donor and R5P as acceptor substrate for 16 hours and analyzed for formation of sedoheptulose 7-phosphate, the product of a potential transketolase reaction. For XFPK<sub>Y501F/N549D</sub>, partly conversion from F6P to E4P was observed, whereas no E4P was detected in the reaction of F6P with XFPK<sub>E437L/Y501F/N549D</sub>, confirming phosphoketolase inactivity of the triple variant as predicted by the spectroscopic assays. S7P was detected in neither of the samples. The transketolase reaction is characterized by its reversibility. To shift the equilibrium towards product formation, the transketolase reaction can be coupled to two further enzymatic reactions as shown in Figure 15. G3P resulting from cleavage of X5P is used as substrate for triosephosphatisomerase (TIM) that catalyzes its conversion



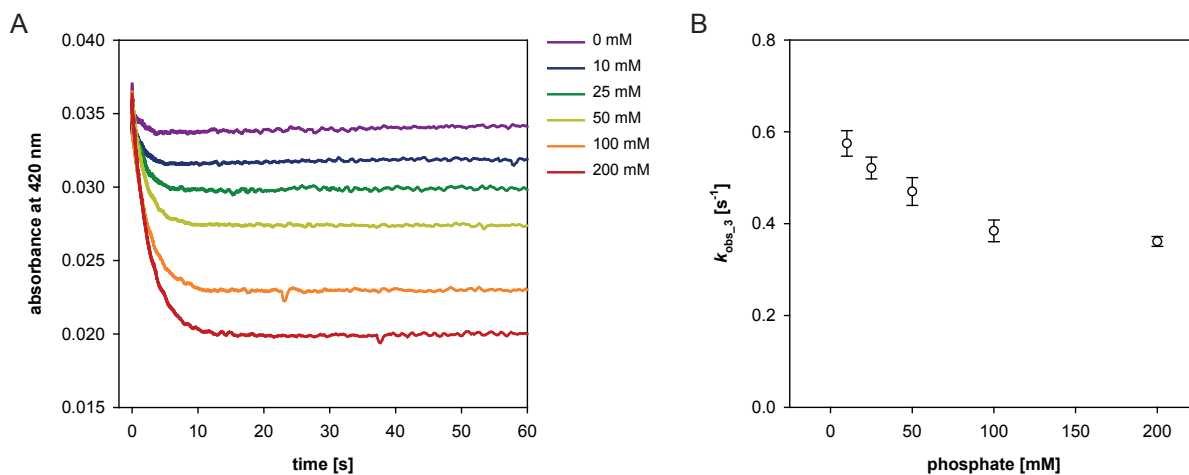


**Figure 44: Transient kinetic analysis of AcThDP depletion in XFPK<sub>Y501F/N549D</sub>.** (A) Progression of absorbance at 420 nm after sequential mixing of 24  $\mu$ M XFPK<sub>Y501F/N549D</sub> with 20 mM F6P and different concentrations of Na<sub>2</sub>HPO<sub>4</sub>. Applied phosphate concentrations are listed in the legend. (B) Apparent rate constants  $k_{obs\_3}$  determined by fitting of progress curves with Equation 8 were plotted against the applied Na<sub>2</sub>HPO<sub>4</sub> concentrations. They do not display substrate dependency.

to dihydroxyacetone phosphate, which is in turn irreversibly reduced by  $\alpha$ -glycerolphosphate dehydrogenase (GDH) to  $\alpha$ -glycerolphosphate. Thus, G3P is pulled out of the reaction preventing the transketolase back reaction. To test whether transketolase activity of XFPK<sub>Y501F/N549D</sub> and XFPK<sub>E437L/Y501F/N549D</sub> might be observable under conditions favoring the forward reaction, the variants were incubated with X5P as donor sugar and E4P or R5P as acceptor together with enzymes, coenzymes and substrates of the auxiliary reactions. Again, formation of products resulting from transketolase reactivity was analyzed by GC-MS, but also in this experimental setup no transketolase products were detected, excluding that XFPK<sub>Y501F/N549D</sub> or XFPK<sub>E437L/Y501F/N549D</sub> exhibit transketolase activity.

Overall, replacement of tyrosine 501 and asparagine 549 by their transketolase equivalents reduces the phosphoketolase turnover, mainly but not exclusively affecting catalytic steps involving the acyl-acceptor substrate phosphate. Nevertheless, the main catalytic feature of phosphoketolase, the dehydration of AcThDP, can still be observed. Thus, those residues seem not to be direct determinants for the catalytic differences between phosphoketolase and transketolase. Introduction of the third amino acid exchange resulting in the "transketolase-like" triple variant XFPK<sub>E437L/Y501F/N549D</sub> disrupts the phosphoketolase activity completely. Neither of the variants did display potential transketolase activity.

## 4 Discussion

### 4.1 New insights into the catalytic mechanism of phosphoketolase reveal coupling of tautomerization and acetyl-transfer by substrate-assisted catalysis

Recent kinetic, structural and computational studies on phosphoketolase from different *bifidobacteria* and *lactobacillus* species shed light on its molecular mode of action and led to the proposal of a detailed reaction mechanism<sup>71,73,75</sup>. However, the catalytic mechanism of phosphoketolase is far from being understood as well as that of other ThDP-dependent enzymes such as the closely related transketolase. Especially the chemical state of the post-dehydration intermediate AcThDP and the mechanism behind enol- to keto-tautomerization of the intermediate, have been subject of debate<sup>4,75</sup>. Hence, a combined approach of different spectroscopic and kinetic methods was applied to characterize the putative AcThDP intermediate and further elucidate the tautomerization step within the reaction cycle of *B. breve* phosphoketolase.

The main characteristic of ThDP catalyzed enzymatic reactions is the formation of covalent, cofactor-derived reaction intermediates<sup>28</sup>. In a first step towards a better understanding of the phosphoketolase catalytic mechanism, the phosphoketolase reaction was analyzed for the formation of covalent ThDP reaction intermediates by two complementary spectroscopic methods. In a combination of acid-quench isolation of cofactor derivatives and their subsequent analysis by <sup>1</sup>H-NMR<sup>45</sup>, the distribution of ThDP intermediates during the phosphoketolase reaction in absence and presence of the acceptor substrate phosphate was investigated. In agreement with the proposed reaction mechanism, the covalent adducts DHEThDP and AcThDP were detected next to unsubstituted cofactor. In the absence of phosphate as acetyl-group acceptor, AcThDP occurred as predominant intermediate together with a small fraction of the carbanion/enamine intermediate DHEThDP. AcThDP was not detected when inorganic phosphate was present as substrate next to F6P (Figure 17C). The <sup>1</sup>H-NMR results agree with observations from a crystallographic study, that reported trapping of DHEThDP and AcThDP after soaking of phosphoketolase crystals with F6P under phosphate free conditions<sup>73</sup>, confirming the ThDP derivatives as true intermediates of the phosphoketolase reaction. Furthermore, detection of the pre- and the post-dehydration intermediate in the absence of phosphate supports the finding of YEVENES AND FREY that the phosphoketolase reaction follows a ping-pong catalytic mechanism, in which substrate cleavage and dehydration of the carbanion/enamine intermediate occur independently of phosphate binding<sup>71</sup>.

In parallel to the intermediate analysis by acid-quench/ $^1\text{H-NMR}$ , the phosphoketolase reaction was investigated by UV-Vis spectroscopy. Spectral analysis confirmed a distinct absorbance band with a maximum at 420 nm that was detected during the reaction of phosphoketolase with F6P, but not with both substrates F6P and  $\text{Na}_2\text{HPO}_4$  (Figure 16). Time-resolved monitoring of the spectral signal revealed maximum absorbance after around 60 ms and a lifetime of 300 s and longer (Figure 17A+B and Figure 58). In a prior study on *B. breve* phosphoketolase, it was suggested that the absorbance signal is associated with the post-dehydration intermediate AcThDP in its enol-configuration<sup>89</sup>. The complementary approach of UV-Vis and  $^1\text{H-NMR}$  spectroscopy applied in the present study enabled an unambiguous assignment of the observed UV-Vis absorbance band to AcThDP. During the reaction of phosphoketolase with F6P, leading to formation of the absorbance band, DHETThDP and AcThDP were detected in the acid-quench/ $^1\text{H-NMR}$  analysis, whereas the reaction with both substrates only produced DHETThDP as detectable intermediate. Under the latter reaction conditions, the specific absorbance band at 420 nm was absent. Hence, DHETThDP can be excluded as its source, leaving AcThDP as intermediate responsible for the observed absorbance band. The prolonged life time of the spectral signal coincides with the presumption that AcThDP is accumulated in absence of an acceptor substrate and slowly degraded by hydrolysis to acetate and free cofactor. Abrupt depletion of the signal after addition of inorganic phosphate supports the assumption of a fast reaction between AcThDP and the acyl-acceptor.

With a  $\lambda_{max}$  of 420 nm the absorbance band of AcThDP occurs at a wavelength much longer than anticipated by the length of its conjugated system. Moreover, the keto-form of chemically synthesized AcThDP in aqueous solution shows absorbance at 310 nm<sup>81</sup>. This significant red shift of the observed signal compared to the published absorbance band has initiated the analysis of possible electronic excitations in the phosphoketolase intermediate AcThDP by computational methods, carried out by PROF. RICARDO MATA and MIRKO PAULIKAT, Department of Computational Chemistry and Biochemistry, University of Göttingen. As the chemical state of AcThDP stabilized at the phosphoketolase active site in the absence of phosphate is not clear yet, the theoretical examinations were performed for enol-, enolate- and keto-AcThDP. Their results predict charge transfer transitions for all three tautomers with transition energies between 340 and 431 nm. The transition energies of enolate-AcThDP (413 nm) and keto-AcThDP (431 nm) are close to  $\lambda_{max}$  of the observed absorbance band. Hence, MATA and colleagues proposed that both tautomers contribute to the spectral signal.

The group of FRANK JORDAN examined the spectral properties of AcThDP as intermediate in the E1 component of the *E. coli* pyruvate dehydrogenase complex, generated by the use of the non-natural substrate fluoropyruvate. They could assign a broad positive CD band at 390 - 395 nm to the intermediate, which they assume to represent a charge transfer transition<sup>84</sup>. The transition energies between 340 and 431 nm for AcThDP in phosphoketolase calculated by MATA and colleagues are in good accordance with observations from the aforementioned publication by PATEL *et al.*, agreeing with their hypothesis that the absorbance bands of enzyme bound AcThDP with  $\lambda_{max}$  around 400 nm result from charge transfer transitions. A similar band was also observed for an acryloyl-ThDP adduct in N<sub>2</sub>-(2-carboxyethyl)arginine synthase (CEAS) ( $\lambda_{max} = 433$  nm), an enzyme of the clavulanic acid biosynthetic pathway<sup>101</sup>.

Recent results from a computational study on the absorbance spectra of ThDP in pyruvate decarboxylase demonstrated that changes in the conformation of the cofactor contribute to the distinct differences in the absorbance spectra of free ThDP or its adducts to those observed for their enzyme bound equivalents, as a result of changes in the charged transfer between pyrimidine- and thiazolium-ring<sup>102</sup>. It can be presumed that the different conformations adopted by keto-AcThDP in solution (S-conformation) and AcThDP bound to phosphoketolase (V-conformation) at least partly account for their discrepancy in absorbance. Altogether, assignment of the 420 nm absorbance band to the AcThDP intermediate in phosphoketolase nicely fits in with the data obtained from equivalent intermediates in other ThDP-dependent enzymes.

Identification of an absorbance signal for the phosphoketolase post-dehydration intermediate AcThDP provided the framework for further analysis of the phosphoketolase reaction by kinetic methods. Time resolved monitoring of the spectral signal over time allowed determination of rate constants for AcThDP-formation and -depletion during the phosphoketolase reaction cycle. This enabled a dissection of the catalytic mechanism into individual observable reaction steps, allowing a detailed kinetic description of the phosphoketolase reaction.

Transient kinetic observation of AcThDP formation via its absorbance signal allowed the determination of an apparent rate constant of  $75.2 \pm 2.5$  s<sup>-1</sup> that summarizes all steps leading to the formation of the post-dehydration intermediate. Moreover, progression of AcThDP absorbance permitted further insight into the necessary conversion of the dehydration product enol-AcThDP to its keto-tautomer which serves as a substrate for the final reaction step with phosphate. Progress curves at F6P concentrations >3 mM exhibited a pronounced kinetic overshooting in the pre-steady-state of the reaction, best described by two exponential terms, followed by a

long steady-state phase with constant AcThDP concentration (Figure 22A+B). According to the model developed in this study, the first phase represents formation of enolate-AcThDP while the second phase, showing a rate constant of  $4.7 \pm 0.6 \text{ s}^{-1}$  that is not depended on substrate concentration, likely represents tautomerization from enolate- to keto-AcThDP. As the apparent rate constant  $k_{\text{obs}_2}$  of the tautomerization is smaller than that of enolate formation  $k_{\text{obs}_1}$ , enolate-AcThDP is formed in excess at the beginning of the reaction, accounting for the observed peak in absorbance, before an equilibrium between enolate-AcThDP formation, tautomerization and hydrolysis of keto-AcThDP is reached, that leads to a steady ratio between enolate- and keto-AcThDP and hence a constant absorbance signal (section 3.3.2).

This model is in accordance with the computational data on the electronic excitations in the different AcThDP tautomers and seems reasonable in terms of the phosphoketolase reaction mechanism. The calculations by MATA AND PAULIKAT suggested contribution of enolate- and keto-AcThDP to the observed absorbance band at 420 nm. Furthermore, their computed excitation energy showed a larger oscillator strength for the enolate-ThDP adduct compared to the keto-tautomer, correlating with the stronger absorbance in the initial phase of the reaction. An attempt to further increase the difference between the theoretical transition energies of keto- and enolate-AcThDP by single amino acid exchanges in the environment of the intermediate to enable individual monitoring of the tautomers was unfortunately not successful (section 3.2).

Dehydration of DHETThDP yields enol-AcThDP that needs to undergo tautomerization to keto-AcThDP before nucleophilic attack of phosphate can take place. The exact catalytic mechanism behind the tautomerization has not been resolved yet, but a computational study on phosphoketolase from *B. longum* proposed conversion of enol- to keto-AcThDP proceeds via the formation of an enolate-intermediate<sup>75</sup>, coinciding with data of the present study.

The mechanism proposed from transient kinetic observation of the AcThDP absorbance signal implies coexistence of enolate- and keto-AcThDP when the post-dehydration intermediate is accumulated at the phosphoketolase active site in absence of a suitable acyl-acceptor. Evidence for a dynamic equilibrium of the AcThDP tautomers in phosphoketolase was provided based on an H/D-exchange experiment. By <sup>1</sup>H-NMR analysis of acetate, the product of the hydrolytic side reaction, SCHNEIDER could show almost complete exchange of the acetate's methyl-protons to deuterium after only 10 minutes, when the phosphoketolase side reaction with F6P was carried out in D<sub>2</sub>O<sup>89</sup>. According to HALKIDES *et al.*<sup>103</sup>, the proton exchange at the methyl-group of keto-AcThDP in solution occurs with  $6 \times 10^{-5} \text{ s}^{-1}$ . Hence, the observed H/D-exchange has to

be the result of dynamic changing of the AcThDP intermediate between its enol/enolate- and keto-form. Although no ultimate conclusion about the chemical state of the post-dehydration intermediate can be drawn from those experiments, it seems that rather than accumulation of keto-AcThDP, an equilibrium between the AcThDP tautomers is maintained at the phosphoketolase active site in absence of phosphate. Presence of enol- or enolate-AcThDP seems contradictory at first, due to the general higher thermodynamic stability of ketones and the resulting negligible amount of the enol(ate)-species present in solution. However, stabilization of AcThDP in its enol- or enolate form would prevent off-pathway hydrolysis of the post-dehydration intermediate. Putative presence of a similar enol(ate) intermediate has been proposed for the ThDP-dependent  $N_2$ -(2-carboxyethyl)arginine synthase (CEAS) based on X-ray crystallographic data<sup>104</sup>. How phosphoketolase prevents spontaneous tautomerization of enol- or enolate-AcThDP to the keto-form is unclear.

Irrespective of the chemical state of the post-dehydration intermediate, the extended life time and slow depletion of the AcThDP absorbance signal confirms that hydrolysis of the AcThDP intermediate in the absence of phosphate is slow compared to its formation, coinciding with accumulation of the post-dehydration intermediate in the absence of phosphate, as observed in our NMR based intermediate analysis (Figure 17C) and *in crystallo*<sup>73</sup>. Presumably, the off-pathway hydrolysis of AcThDP is the rate limiting step of the phosphoketolase reaction in absence of an acyl-acceptor substrate. Addition of phosphate however leads to a rapid decline in AcThDP absorbance. In a sequential-mixing stopped-flow experiment, an apparent rate constant of  $1057 \pm 95 \text{ s}^{-1}$  could be determined for the reaction between AcThDP and phosphate (Figure 24). The reaction proceeds at a much higher rate than AcThDP formation, explaining why the AcThDP intermediate is not detected in the reaction of phosphoketolase with both substrates F6P and phosphate in NMR- or UV-Vis spectroscopy.

For completion of the kinetic characterization of the phosphoketolase reaction, a steady-state assay was established that allowed monitoring of the phosphoketolase catalyzed conversion of F6P and phosphate to E4P and acetyl phosphate as well as the hydrolytic side reaction. The assay proved suitable for studying steady-state kinetics of the phosphoketolase reaction (section 3.3.1). It demonstrated a low enzymatic activity also in the absence of phosphate, yielding a turnover of  $0.83 \pm 0.02 \text{ s}^{-1}$  for the hydrolytic side reaction. The kinetic parameters for the reaction with both substrates ( $k_{\text{cat}} = 14.3 \pm 0.3 \text{ s}^{-1}$ ,  $K_{\text{M(F6P)}} = 32 \pm 2 \text{ mM}$  and  $K_{\text{M(phosphate)}} = 3.8 \pm 0.7 \text{ mM}$ ) slightly differ to those published by SUZUKI *et al.* for *B. breve* phosphoketolase ( $k_{\text{cat}} = 26 \pm$

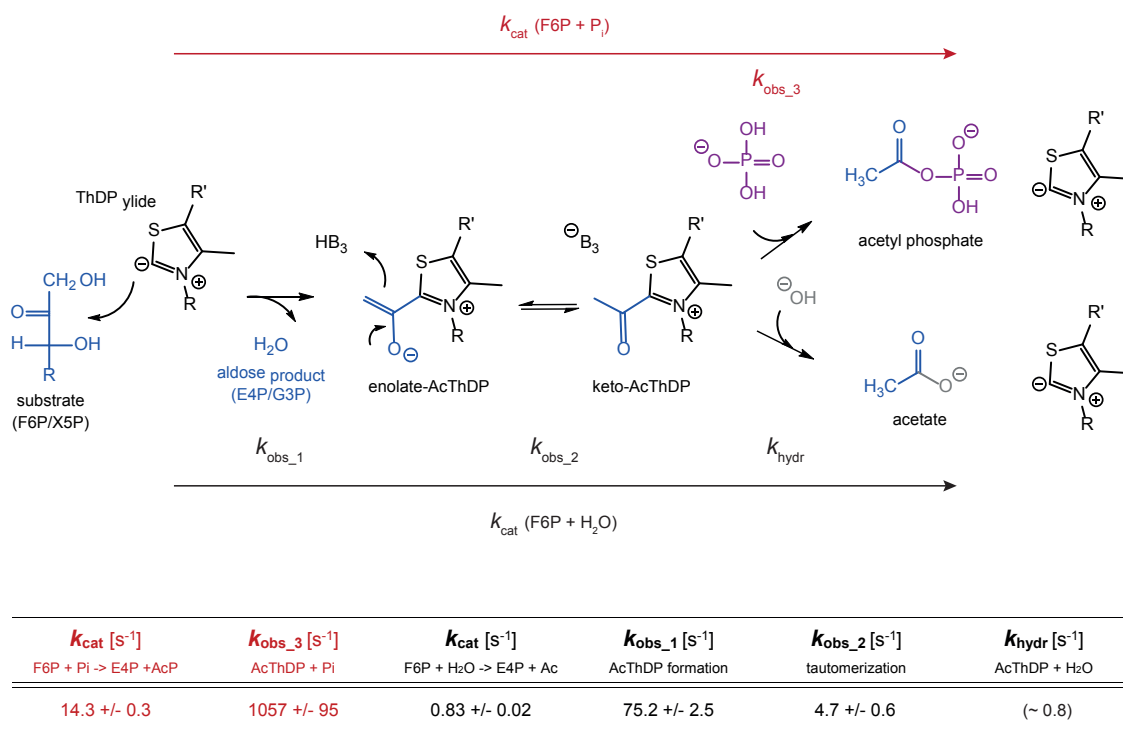


**Figure 45: Kinetic parameters of the phosphoketolase reaction.** Kinetic constants were determined for the overall phosphoketolase reaction and for individual catalytic steps in presence of absence of the acceptor substrate phosphate. Kinetic constants determined in presence of phosphate are represented in red, those obtained in absence of the acyl-acceptor are shown in black. Schematic representation of the phosphoketolase reaction illustrates assignment of the rate constants to the respective reaction(step). The rate for depletion of AcThDP by off-pathway hydrolysis  $k_{hydr}$  is presumably identical to the respective turnover number in absence of phosphate (see text).

$1 s^{-1}$ ,  $K_{M(F6P)} = 9.7 \pm 0.3 \text{ mM}$ ,  $K_{M(\text{phosphate})} = 1.2 \pm 0.2 \text{ mM}$ ). Those were obtained at different pH and temperature, though. For phosphoketolase from other *bifidobacteria* and *lactobacillus* species  $K_M$  values for F6P of 12 - 29 mM and 2.9 - 4.3 mM for phosphate were reported<sup>71,74,105</sup> which are in good accordance with our data.

Determination of the steady-state kinetic parameters completed the kinetic overview of the phosphoketolase reaction that is summarized in Figure 45. The apparent rate constants for AcThDP formation (approx.  $75 s^{-1}$ ) and the reaction of AcThDP with phosphate ( $>1000 s^{-1}$ ) are considerably higher than the overall turnover (approx.  $14 s^{-1}$ ). Thus, none of the reaction steps leading up to AcThDP formation (generation of substrate-ThDP complex, substrate-cleavage and dehydration of DHETHDP) seems to be rate-limiting. The very high apparent rate constant derived by monitoring depletion of AcThDP absorbance predicts fast formation of the AcThDP-phosphate adduct and the preceding tautomerization step in presence of the acceptor

substrate phosphate. This leaves the release of the final product acetyl phosphate as probable rate-determining step of the phosphoketolase reaction.

The experimental setup did not allow a determination of a first order rate constant for AcThDP hydrolysis, but the observed accumulation of AcThDP means that the hydrolytic cleavage presumably is the slowest step in the catalytic cycle. In this case, the rate of hydrolysis should be equal to the overall turnover of the reaction in absence of phosphate which is about  $0.8 \text{ s}^{-1}$ . Free AcThDP is hydrolyzed at rate of  $0.1 \text{ s}^{-1}$  under comparable conditions (pH 7,  $24 \text{ }^\circ\text{C}$ )<sup>81,82</sup>. The slightly higher hydrolysis rate of the enzyme-bound intermediate is most likely due to an activating effect of the enzymatic environment.

Altogether, transient and steady-state kinetic data indicate that the reaction of AcThDP and phosphate is favored over the hydrolysis of the post-dehydration intermediate. Similar observations were made for pyruvate oxidase from *Lactobacillus plantarum* (*Lp*POX). In a series of three publications, TITTMANN and coworkers elegantly demonstrated a coupling of AcThDP phosphorolysis to an electron transfer step in the reaction of *Lp*POX that ensures efficient acetyl-transfer from the cofactor adduct to the nucleophilic acceptor<sup>41,83,86</sup>. In a prior study on the reaction mechanism of phosphoketolase, it was hypothesized that phosphate might accelerate the phosphoketolase reaction by substrate-assisted catalysis<sup>89</sup>. So far, no experimental proof for an active participation of phosphate in mediation of any catalytical sub-steps of the phosphoketolase reaction was provided. Nevertheless, such an involvement could be the basis for coupling phosphorolytic cleavage to another reaction step of the phosphoketolases catalytic cycle, similar as observed in *Lp*POX. TITTMANN suggested chemical coupling of AcThDP tautomerization and phosphorolysis as a possible option for an efficient acetyl transfer<sup>4</sup>.

The detailed kinetic analysis of the phosphoketolase reaction undertaken in the present study revealed a discrepancy in the kinetic parameters of the phosphoketolase reaction that strongly supports this hypothesis. Spectrophotometric monitoring of AcThDP formation at the phosphoketolase active site in absence of phosphate revealed two phases in the pre-steady-state of intermediate formation. The second, non-substrate dependent phase was assigned to the tautomerization from enolate- to keto-AcThDP with an apparent rate constant of about  $4.7 \text{ s}^{-1}$  (3.3.2). Whereas this is in agreement with the turnover of the hydrolytic side reaction of  $0.8 \text{ s}^{-1}$ , it is slower than the  $k_{\text{cat}}$  of  $14 \text{ s}^{-1}$  determined for the phosphoketolase catalyzed conversion of F6P and phosphate to E4P and acetyl phosphate, apparently lacking competence for this reaction. However, transient kinetic examination of the reaction between AcThDP and phos-



phate and chemical-quench/ $^1\text{H}$ -NMR intermediate analysis demonstrated that in presence of the acceptor substrate this step is not relevant for rate limitation (3.1 and 3.3.2). Since all steps from tautomerization to the formation of the AcThDP-phosphate adduct happen very fast with a rate constant of  $> 1000 \text{ s}^{-1}$ , several magnitudes higher than  $k_{\text{cat}}$ , no accumulation of AcThDP could be observed. Consequently, the reaction rate of tautomerization must be enhanced in the presence of the acyl-acceptor phosphate. This rate enhancement could either be the result of a conformational change in the active site that facilitates tautomerization from enol- to keto-AcThDP induced by phosphate binding or it is caused by participation of the phosphate's functional groups itself in the tautomerization reaction.

Overlay of the X-ray crystal structures of *B. breve* phosphoketolase in its resting state and in complex with phosphate showed very little difference between the two structures (Figure 46A). Thus, a phosphate induced conformational change seems an unlikely option. Therefore, the phosphate molecule is assumed to act as a catalyst for the conversion from enol- to keto-AcThDP itself. The position of phosphate relative to the AcThDP adduct was estimated by superimposition of the phosphoketolase structures in complex with AcThDP and with phosphate. Illustration of the phosphate molecule within the structure of the phosphoketolase AcThDP complex shows that the acyl-acceptor's functional groups are in reasonable distance for proton transfer to and from the intermediates hydroxy- and methyl-group, fulfilling the requirements to act as a substrate catalyst in the enol- keto-tautomerization of AcThDP (Figure 46B).

Structural data on *B. breve* phosphoketolase in complex with AcThDP did not provide clear mechanistic information on the enol-keto tautomerization, but the active site residue His553 in hydrogen-bonding distance of the AcThDP, hydroxy-/carbonly-group was proposed as possible mediator for this reaction step<sup>4,75</sup>. Enzymatic inactivity and failure of the recombinant XFPK<sub>H553A</sub> phosphoketolase variant to form the AcThDP intermediate prevented experimental evaluation of the His553 side chain's role in the conversion from enol- to keto-AcThDP (section 3.4). In a computational model of the phosphoketolase reaction by ZHANG AND LIU, a high energy barrier was assigned to the proton-transfer step from His553 to enolate-AcThDP yielding keto-AcThDP<sup>75</sup>. Consequently, an alternative mechanism of phosphate directly taking part in AcThDP tautomerization seems likely.

Another observation supporting the idea of phosphate acting as direct catalyst in the phosphoketolase reaction stems from the pH-dependent kinetic analysis of the phosphoketolase reaction. Enzymatic activity, as determined by the E4P detecting CD spectroscopy assay was highest be-

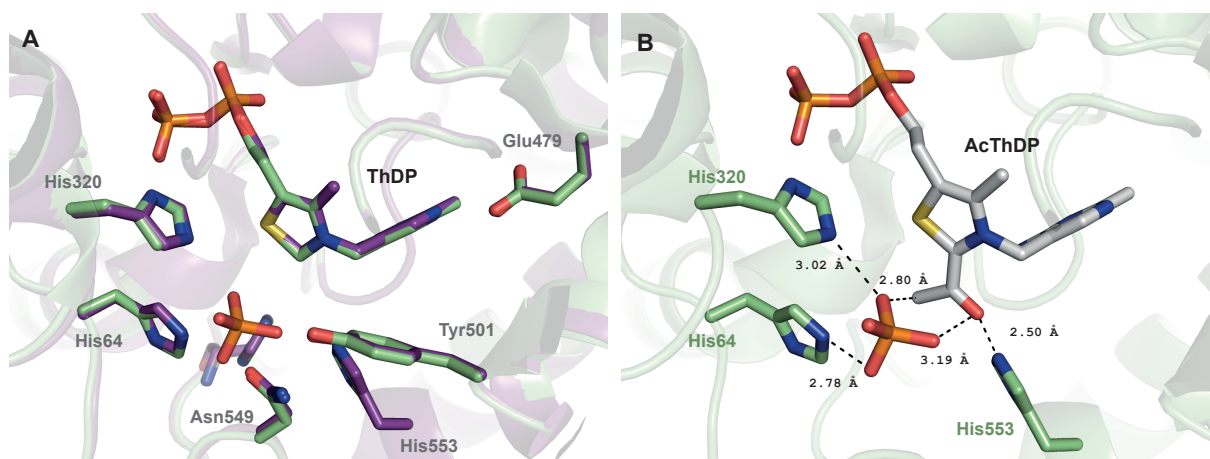


**Figure 46: Active site of *B. breve* phosphoketolase in complex with phosphate.**

(A) Superposition of XFPK in resting state (purple) and in complex with phosphate (green) shows little difference in the conformation of the ThDP cofactor or catalytically relevant residues. (B) Putative interactions of phosphate with AcThDP and selected active site residues. Structures of phosphoketolase in complex with AcThDP and with phosphate were superimposed and the phosphate molecule displayed in the structure of XFPK-AcThDP. The overlay suggests positioning of the phosphate's hydroxy groups in hydrogen bonding distance of the acetyl-moiety. Figure was prepared based on pdb files 3AHC, 3AHD and 3AHF (SUZUKI *et al.*<sup>73</sup>).

tween pH 6 and 7. A clear drop in activity was observed between pH 7 and 7.5 with further decrease in  $k_{cat}$  towards more alkaline conditions (Figure 26). From MD-simulations, dihydrogen-phosphate was assumed to be the catalytically relevant species (M. PAULIKAT, personal communication). The second  $pK_a$  of phosphoric acid is 7.21, coinciding with the observed drop in activity. Assuming dihydrogen-phosphate to be involved in catalysis of tautomerization from enol- to keto-AcThDP, the reduction in enzymatic activity could be explained by the decreasing amount of the single-deprotonated species with increasing pH. The effect was even more pronounced in the double-jump stopped-flow experiment, monitoring the reaction of AcThDP with phosphate. The apparent rate constant of this reaction step at 50 mM phosphate shows a 30 fold reduction in  $k_{obs\_3}$  to around  $15 \text{ s}^{-1}$  at pH 8.5 compared to  $471 \pm 27 \text{ s}^{-1}$  at pH 7.2. Thus, reduced concentration of dihydrogen-phosphate could play a role for rate reduction under alkaline conditions. However, influence of the  $\text{H}^+$ -concentration on the phosphoketolase reaction seems more complex than that, since formation of AcThDP is also affected by an increased pH (Figure 27A). Influence of the pH on the chemical state of the AcThDP has also to be considered due to changes in the spectral and kinetic behavior of the intermediate (section 3.2 and 3.3.4).

If the postulated substrate-assisted catalysis of the tautomerization step in the phosphoketolase reaction applies as general principle, other nucleophiles should be able to replace phosphate as acceptor-substrate and catalyst. Testing of different phosphate analogues identified arsenate as alternative reaction partner for AcThDP (section 3.3.3). Due to its similar physiochemical

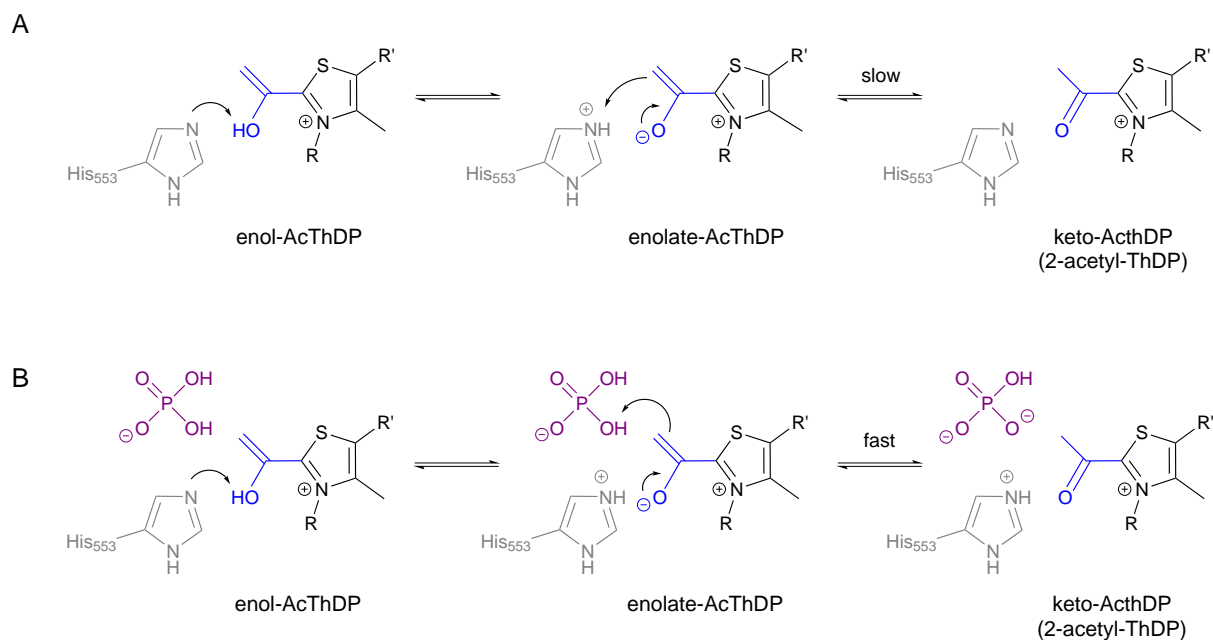


**Figure 47: Suggested mechanism for enol-keto tautomerization of AcThDP in phosphoketolase.** (A) In absence of phosphate, enol-keto tautomerization is mediated by His553. Abstraction of the hydroxy proton by His553 yields the enolate. A high free energy barrier for reprotonation of the ene-moiety by His553 is assumed. Accordingly, formation of keto-AcThDP occurs slow. (B) In presence of phosphate enol-AcThDP is deprotonated by His553, followed by fast protonation of the ene-moiety by dihydrogen-phosphate that yields keto-AcThDP.

properties, arsenate was shown to readily replace inorganic phosphate in several enzymatic reactions, for example in L-aspartate- $\beta$ -semialdehyde dehydrogenase<sup>106,107</sup> or purine nucleoside phosphorylase<sup>108,109</sup>. Early publications on phosphoketolase also reported enzymatic activity in the presence of arsenate instead of phosphate<sup>66–68</sup>. The apparent rate constant of  $822 \pm 179 \text{ s}^{-1}$  for the reaction between AcThDP and arsenate is only slightly reduced compared to phosphate ( $1057 \pm 95 \text{ s}^{-1}$ ) (Figure 25), indicating that arsenate does not only replace phosphate as acceptor substrate but can also take over its putative catalytic function. The remaining tested oxonium anions phosphite, sulfate and vanadate failed to replace phosphate. This was less surprising for phosphite and sulfate since they show distinct differences in geometry (phosphite) or  $\text{p}K_{\text{a}}$  profile (sulfuric acid). Vanadate however was described as substrate alternative for phosphate similar to arsenate<sup>98</sup>. Nevertheless, substrate-assisted catalysis seems not to be restricted to phosphate itself, but can be taken over by other nucleophiles, provided their chemical properties match those of the original acceptor substrate.

The assumption of substrate-assisted catalysis by phosphate is also supported by computational data on the tautomerization step of the phosphoketolase reaction pathway provided by MATA AND PAULIKAT, Department of Physical Chemistry, University of Göttingen. They performed molecular dynamic simulations to identify interactions in the phosphoketolase active site that

would possibly be involved in keto- enol-tautomerization of AcThDP. Their results propose hydrogen bond-interactions of His553 and dihydrogen-phosphate with the enol-group of AcThDP. Based on this observation they calculated free energies of intermediates and transition states for three possible pathways of the tautomerization reaction. Those calculations revealed a free energy barrier of 77.1 kJ/mol for the transition from enolate- to keto-AcThDP in case His553 acts as proton donor and acceptor in the absence of phosphate in this step of the reaction. This is in good agreement with the rate constant of about 4 s<sup>-1</sup> that was ascribed to the same reaction step based on the transient kinetic data which would correspond to a barrier of 70 kJ/mol. This reaction barrier is considerably reduced to 45 kJ/mol in case phosphate is assumed as proton donor to the ene-moiety, provided proton abstraction from the enol-AcThDP is still carried out by His553. In accordance with the kinetic data, the tautomerization step would then no longer be rate determining for the reaction. For a scenario where His553 acts as proton donor and acceptor when phosphate is present at the active site their calculations yielded a much higher barrier of around 120 kJ/mol, a value in the same range as calculated by ZHANG AND LIU<sup>75</sup>. Considering the results from the alternative pathways, this scenario seems highly unlikely, strongly supporting the conclusions drawn from the kinetic studies that phosphate acts as substrate catalyst in the tautomerization step of the phosphoketolase reaction.

Together, experimental and computational results strongly indicate active participation of the acceptor substrate phosphate in the enol-keto tautomerization of AcThDP, implying the following model for the phosphoketolase reaction: In absence of the second substrate, the conversion from enol- to keto-AcThDP is mediated by His553. Due to a high energy barrier for proton transfer from His553 to the ene-moiety of enolate-AcThDP, this step proceeds slow resulting in presence of enolate- and keto-AcThDP in this phase of the reaction and a slow overall tautomerization (Figure 47A). In case phosphate is bound at the active site, it provides the proton for this reaction step, which significantly enhances the rate of enol-keto conversion, enabling efficient acetyl-transfer for product formation (Figure 47B).

Substrate-assisted catalytic processes, in which a functional group of the substrate contributes to the catalytic mechanism were described for a number of enzymes, including some examples where a phosphate group acts as acid/base catalyst<sup>110</sup>. In the GTPase Ras p21, the  $\gamma$ -phosphate of the substrate was proposed to act as a general base for GTP hydrolysis<sup>111</sup>. Furthermore, proton donor/acceptor catalytic function of substrate phosphate groups were reported for aminoacyl tRNA synthetases<sup>112,113</sup> and restriction endonucleases<sup>114</sup>. However, the here described model

would be the first example for substrate-assisted catalysis in a ThDP-dependent enzyme and for a catalytic role of inorganic phosphate.

Participation of phosphate in the enol-keto tautomerization of AcThDP provides chemical coupling of the tautomerization step in the phosphoketolase reaction cycle to the subsequent acetyl-transfer from the keto-intermediate to the acceptor substrate. This way, the hydrolysis susceptible keto-intermediate is preferentially formed when the acceptor substrate is already bound to the active site, ensuring preference of the acetyl-transfer over the competing hydrolysis reaction. As already mentioned above, in *Lp*POX formation of the reactive keto-AcThDP intermediate is circumvented by coupling of AcThDP phosphorolysis to another step of the catalytic cycle, although by a very different molecular mechanism that involves single electron transfer reactions and the formation of radical ThDP adduct<sup>41,83</sup>. A similar coupling of oxidation-reduction and acyl-group transfer to the acceptor substrate coenzyme A is assumed to contribute to the reaction mechanism of the ThDP-dependent pyruvate:ferredoxin oxidoreductase (PFOR)<sup>87,88</sup>. Despite the mechanistic differences between the two latter enzymes and phosphoketolase, the principle by which efficient product formation is achieved over the competing hydrolysis, namely by linkage of the final acyl-transfer to the presence of the acceptor substrate, bears certain similarities.

Overall, new insights into the molecular mechanisms of phosphoketolase catalysis, obtained by spectroscopic and kinetic techniques supported by computational data, confirm AcThDP as intermediate of the phosphoketolase reaction and suggest a mechanism in which acyl-group transfer and enol-keto tautomerization of AcThDP is coupled by phosphate acting as acceptor substrate and acid/base catalyst for tautomerization.

## 4.2 Phosphoketolase exhibits carbonylase activity

The stereo-selective formation of new carbon-carbon bonds is of extreme importance and an everlasting challenge in organic synthesis. Known for their distinguished ability to catalyze C-C bond formations in natural processes, ThDP-dependent enzymes were investigated for their synthetic potential and found well suited for biocatalytic applications. They catalyze a wide range of carbonylation reactions with natural and non-natural carbonyl donor- and acceptor substrates, such as (crossed) acyloin/benzoin-condensations or 1,2- and 1,4- additions to  $\alpha, \beta$ -unsaturated aldehydes<sup>Mueller2009a, 59,60,65</sup>. Origin of those ligation reactions is without exception the nucleophilic character of the central C2 $\alpha$ -carbanion/enamine intermediate.

Due to the assumed transient character of its C2 $\alpha$ -carbanion/enamine intermediate DHEThDP<sup>73</sup>, phosphoketolase was so far not considered as candidate for chemoenzymatic synthesis, but data from this thesis predict presence of a second reactive nucleophile intermediate. Enolate-AcThDP, as the carbanion/enamine intermediate, should be capable to react with carbon electrophiles under formation of a new C-C bond. Consequently, phosphoketolase was analyzed for its ability to catalyze carboligation side reactions emerging from its reactive on-pathway intermediates.

In a model reaction with formaldehyde as acceptor, two ligation products dihydroxyacetone and 3-hydroxypropionic acid were observed whose origin from phosphoketolase bound DHEThDP and AcThDP could be verified by isotope-labeling experiments (section 3.5.2). Even though both products were obtained with only a very low yield, they provide proof of principle for a promiscuous carboligase activity of phosphoketolase.

Although commonly observed as native or promiscuous activity in a number of ThDP-dependent enzymes, the carboligation side reaction between the phosphoketolase carbanion/enamine intermediate DHEThDP and the aldehyde acceptor was a rather unexpected finding. The branching point in the reactions of phosphoketolase and transketolase lies in the fate of the DHEThDP adduct. Whereas it is dehydrated in phosphoketolase, it is donor for a ligation with an aldose phosphate sugar in transketolase. Since phosphoketolase does not show detectable transketolase activity, it was assumed that the DHEThDP in phosphoketolase is in general not accessible for ligation reactions, presumably due to fast and irreversible dehydration of the intermediate. Indeed, kinetic data obtained in this thesis indicate that dehydration of the carbanion/enamine proceeds with a rate of 75 s<sup>-1</sup> at least, relatively fast compared to the overall turnover of about 14 s<sup>-1</sup>. On the other hand, DHEThDP was detected in the intermediate analysis in presence of phosphate and during the slower hydrolytic site reaction. Regarding the presence of the pre-dehydration intermediate under steady-state conditions, we considered a reversibility of the dehydration reaction as a possibility, contrary to earlier studies<sup>71</sup>. This idea was addressed experimentally by performing the ligation reaction in <sup>18</sup>O-labeled water, but results from the experiment were ambiguous and did neither confirm nor exclude a possible rehydration of AcThDP. Whether enabled by a reversible dehydration or not, results from this work show that DHEThDP in phosphoketolase can be captured with an aldehyde acceptor. Hence, it can in principle undergo ligation reactions like in transketolase.

The even bigger discovery was however the detection of 3-hydroxypropionic acid as ligation product emerging from the post-dehydration intermediate AcThDP. The reaction between the

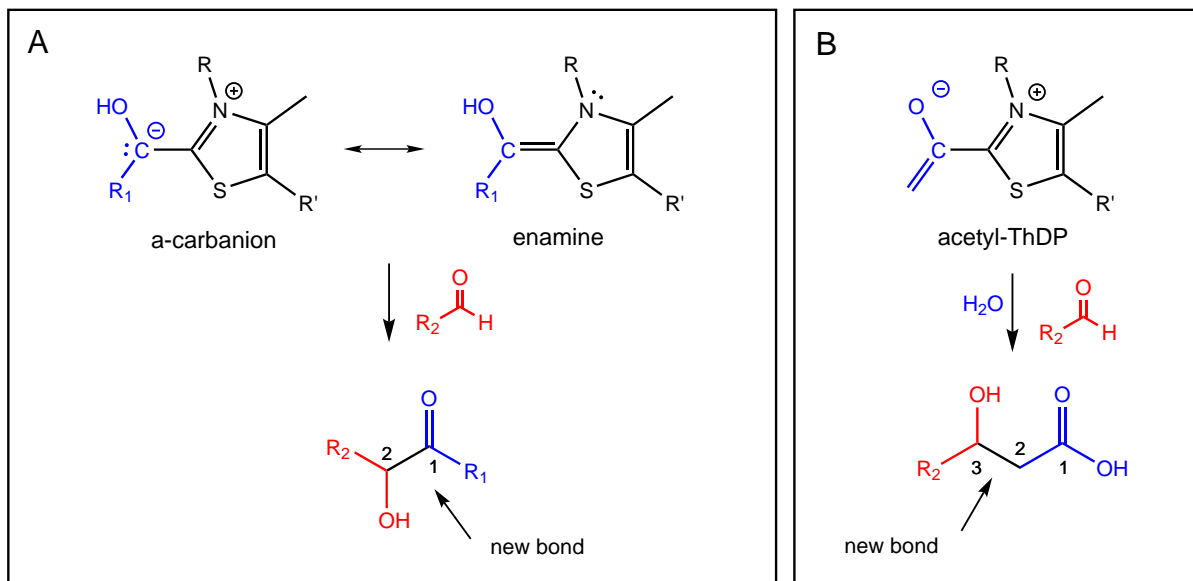


**Figure 48: Novel carboligase activity in ThDP-dependent enzymes.** (A) Most native or promiscuous C-C bond forming reactions in ThDP-dependent enzymes originate from the  $\alpha$ -carbanion/enamine intermediate yielding  $\alpha$ -hydroxy-ketones. (B) The novel promiscuous carboligation emerging from the enolate-AcThDP in phosphoketolase yields  $\beta$ -hydroxy carbon acids with the same acceptor substrate.

phosphoketolase bound AcThDP and formaldehyde as acceptor substrate clearly confirms the assumption that AcThDP exists (at least partially) as enolate-intermediate during the phosphoketolase reaction cycle, since only the nucleophilic enolate-species would undergo the observed aldol-reaction with formaldehyde, but not the keto-intermediate. Presence of the proposed enolate-AcThDP in turn strongly supports the mechanism for the enol-keto-tautomerization of AcThDP in phosphoketolase as suggested in the previous chapter of this thesis.

Furthermore does the observed reaction of the enolate-AcThDP intermediate represent a novel promiscuous activity among the ThDP enzyme family. All carboligase main- or side activities reported for ThDP-dependent enzymes emerge from the  $C2\alpha$ -carbanion/enamine intermediate and lead in most cases to the formation of  $\alpha$ -hydroxy-ketones or derivatives thereof. In the ligation reaction originating from enolate-AcThDP described here, an aldol addition between the ThDP-bound acetyl-group and an aldehyde acceptor yields a  $\beta$ -hydroxy carbon acid. Aldol reactions in biological processes are mostly carried out by aldolases which catalyze the reversible formation of  $\beta$ -hydroxyl carbonyl products from dihydroxyacetone(phosphate), pyruvate or acetaldehyde and a wide range of acceptor substrates. Aldol addition or cleavage in aldolases proceeds either via the formation of an Schiff-base intermediate between the donor substrate and an active site lysine residue (type I aldolases) or via an enediolate stabilized by an bivalent cation cofactor (type II aldolases)<sup>115</sup> (Figure 49). Hence, the ThDP-catalyzed aldol side reaction of phosphoketolase

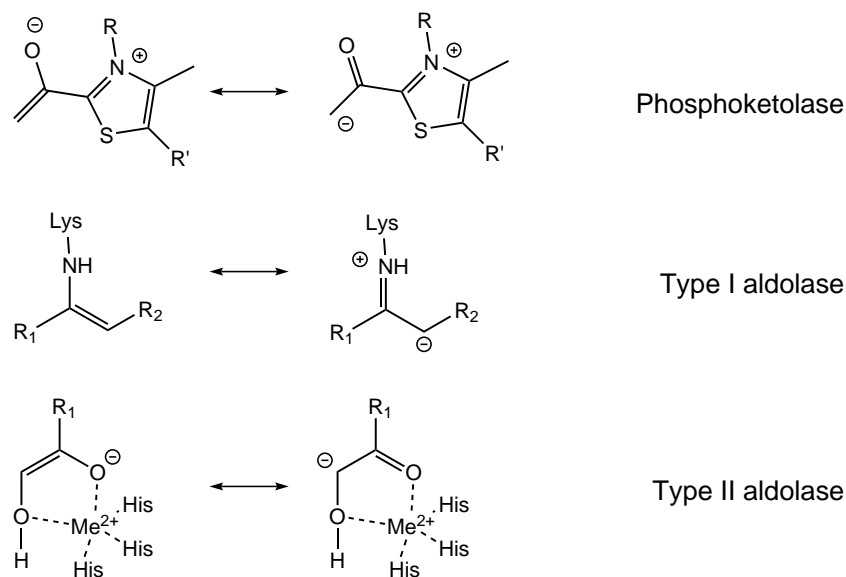


**Figure 49: Nucleophilic reaction intermediates in aldolases and phosphoketolase.** C-C bond forming reactions emerge from different nucleophilic intermediates in type I and II aldolases and phosphoketolase. In type I aldolases, an enamine/Schiff-base intermediate is formed. In type II aldolases, an enediolate is stabilized by a divalent metal ion. A ThDP-enolate is origin of the carboligase side reactivity in phosphoketolase.

not only expands the already versatile reaction range of ThDP-dependent enzymes by a new C-C bond forming reaction, but also represents a mechanistically new type of a biocatalyzed aldol-addition.

Naturally, aldolases are the first choice for biosynthetic purposes that include aldol couplings or condensations. Their application in stereoselective synthesis is investigated extensively with the result that wild-type and engineered aldolases are today used for the synthesis of natural and unnatural monosaccharides, deoxy-, thio- and iminosugars,  $\beta$ -hydroxyaminoacids or precursors for pharmaceutically important compounds<sup>54,116</sup>. However, enzymes that catalyze aldol additions as promiscuous activity, and hence via a different molecular mechanism, might be a valuable complementary tool offering for example different substrate range or enantioselectivity or irreversible product formation. Some enzymes that catalyze aldol additions as promiscuous activity such as lipases, proteases and tautomerases were described<sup>117,118</sup>, but the promiscuous aldol-reactivity of phosphoketolase is the first that involves a ThDP-dependent mechanism.

Next to aldol-reactions with aldehyde or ketone acceptors, the enolate-AcThDP intermediate could potentially also act as reaction partner in other biocatalyzed reactions important in natural product synthesis like Claisen-condensations, Mannich-reactions or even [4+2] cycloadditions, as they have been achieved with N-heterocyclic carbene catalysts<sup>119</sup> (Figure 50). The  $\beta$ -hydroxy carbon



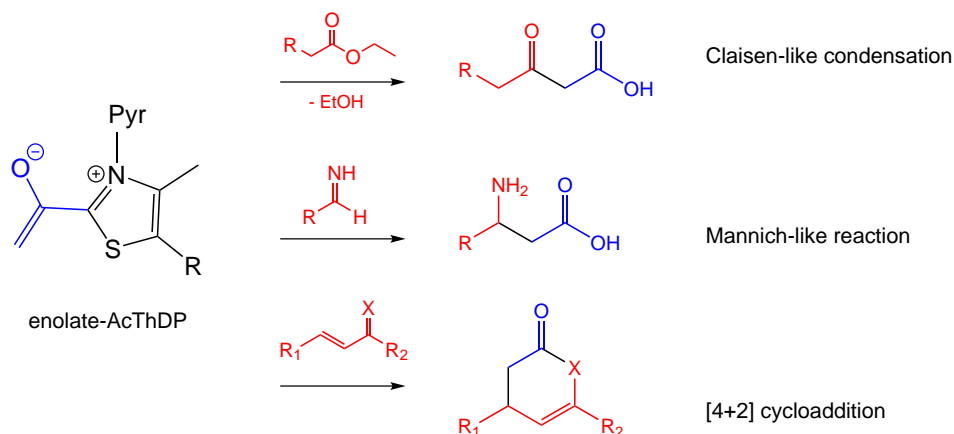


**Figure 50: Possible applications of phosphoketolase in organic synthesis.** Enolate-AcThDP could serve as nucleophile in C-C bond forming reactions with the potential acceptor substrates shown in red. (X = N, O)

acids 3-hydroxypropionic acid and 3-hydroxybutyric acid as possible ligation products of enolate-AcThDP with formaldehyde and acetaldehyde are building blocks for polyhydroxyalkanoate polymers that have been explored as biodegradable plastics<sup>120</sup>.

Potential applications for carboligations emerging from the enolate-AcThDP intermediate, although attractive, are not practical yet. So far, the reaction between phosphoketolase bound enolate-AcThDP and an aldehyde acceptor was only achieved as minor side reaction with extremely low yields (Table 2). The main obstacle towards an increased conversion rate is the limited acceptance of the enzyme for aldehyde acceptor substrates. Only the reaction with formaldehyde as acceptor resulted in detectable amounts of ligation products emerging from DHETHDP or enolate-AcThDP, but formaldehyde led to a fast inactivation of phosphoketolase that was not observed in the presence of other aldehyde substrates (sections 3.5.2 and 3.5.4). Why no reaction between the phosphoketolase intermediates and the other tested aldehydes acetaldehyde, glycolaldehyde or trifluoroacetaldehyde was observed is unclear. Of all the tested aldehyde acceptors, formaldehyde is the smallest and most reactive. One could speculate whether a reaction with the larger aldehydes, especially glycolaldehyde and trifluoroacetaldehyde, is hindered by the geometry of the active site. According to the BÜRGI-DUNNITZ trajectory, the ideal angle for a nucleophilic attack on a  $sp^2$  electrophile is 100 to 110 ° between the nucleophile and the plane defined by the carbonyl group<sup>121,122</sup>. Possibly, the architecture of the active site prohibits ideal orientation of the aldehyde substrates for adduct formation with the phosphoketolase bound intermediate. Using the an active site variant XFPK<sub>H64S</sub>, that was designed to decrease steric restriction, this problem could not be solved (section 3.5.4).

In order to use phosphoketolase in the biological synthesis of chemical compounds, substrate scope and product yield of the desired ligation clearly need to be increased tremendously. The use of acceptor aldehydes other than formaldehyde would also inform about a potential stereospecificity of the C-C bond formation. Also, steering between the ligation reactions emerging from phosphoketolase bound DHEThDP and enolate-AcThDP would be a desirable option. For several ThDP-dependent enzymes, new substrate specificities, changes of catalytic properties or alteration and optimization of enantioselectivity could be created by rational re-design of the enzymes active site. For example, pyruvate decarboxylase from *Zymomonas mobilis* was converted into an efficient carboligase by exchange of a single active site glutamic acid residue to glutamine<sup>123</sup>. WESTPHAL ET. AL combined active site properties of pyruvate decarboxylase from *Acetobacter pasteurianus* and benzaldehyde lyase from *Pseudomonas fluorescens* to achieve benzoin condensation of two aromatic aldehydes with (*S*)-selectivity<sup>124</sup>. Unfortunately, phosphoketolase appears to be a less well suited candidate for rational design approaches. All active site variants analyzed in this thesis show no (His553Ala) or drastically decreased (His64Ser, Glu156Gln, Asn549Asp) catalytic activity. Especially, the conserved histidine network seems extremely susceptible to any disturbances as shown in mutagenesis studies by SUZUKI *et al.*<sup>73</sup>. In this regard, high-throughput methods and directed evolution approaches might be a promising options to optimize carboligase activity and acceptor substrate range in phosphoketolase. The advantage (and drawback at the same time) of directed evolution based enzyme (re)-design or optimization is that a complete understanding of the relationship between enzyme sequence/structure and function is not necessary. Hence, these approaches often identify mutations outside of the active site that are beneficial for the desired function, as they slightly alter geometry, dynamics or electrostatic interactions in the active site<sup>125</sup>. Directed evolution has proven especially useful in enhancing and fine-tuning already existing promiscuous activities and for broadening the substrate range<sup>126,127</sup>. In transketolase, high-throughput screening in combination with saturation mutagenesis was successfully used to expand the substrate range towards non-phosphorylated acceptors, non- $\alpha$ -hydroxylated aldehydes or aromatic substrates<sup>60</sup>.

Although phosphoketolase is far away from being an efficient carboligase, the detection of carboligase side activity emerging from its reactive intermediates serves as proof of principle and shows again the catalytic variety of ThDP-dependent enzymes. Furthermore, successful trapping of enolate-AcThDP with formaldehyde confirms presence of the predicted enolate species in the catalytic cycle of phosphoketolase, supporting the molecular mechanism that was proposed for

the enol-keto tautomerization based on kinetic and spectroscopic data. The reaction between enolate-AcThDP and formaldehyde adds a new type of C-C bond forming reactions to the catalytic portfolio of ThDP-dependent enzymes.

### 4.3 Amino-acid exchanges between the active sites of phosphoketolase and transketolase do not account directly for their different catalytic activities

The ThDP-dependent enzymes phosphoketolase and transketolase closely resemble each other in substrate specificity, cofactor requirements and even partly in their catalytic mechanism. The extraordinary structural resemblance of the two enzymes that was revealed upon determination of the phosphoketolase structure was therefore not completely unexpected. Despite these striking similarities, the catalytic outcomes of phosphoketolase and transketolase are quite different. Whereas phosphoketolase catalyzes the irreversible cleavage of its ketose-phosphate substrates to provide the high-energy metabolite acetyl phosphate as part of a catabolic pathway, transketolase catalyzes the reversible interconversion of phosphate sugars by transfer of a C2 fragment in different metabolic contexts.

Mechanistically, these different catalytic activities originate in the diverging reactivity of the  $\alpha$ -carbanion/enamine intermediate DHEThDP that adds onto an acceptor substrate in transketolase but undergoes dehydration to AcThDP in phosphoketolase. It is assumed that dehydration is the result of a phosphoketolase specific acid/base catalyst responsible for protonation of the O1-hydroxy group prior to water elimination<sup>4</sup>. However, the active site environment of the intermediate is almost identical in the two enzymes and a specific acid/base catalyst or other factors that would explain why dehydration exclusively occurs in phosphoketolase could not be identified based on X-ray crystallographic data of phosphoketolase and transketolase in complex with DHEThDP. The only apparent difference between the active sites of phosphoketolase and transketolase can be found at the phosphoketolase positions Glu437, Y501, and Asn549 that are replaced in transketolase by a leucine, phenylalanine and aspartic acid residues respectively. Although it is unlikely that any of these residues is directly involved in the dehydration mechanism, in a step-wise approach a "transketolase-like" phosphoketolase variant was generated in which these residues were replaced by their transketolase counterparts to determine how they contribute to phosphoketolase's catalytic characteristic.

Of special interest was the examination of Asn549. In transketolase, this position is occupied by a strictly conserved aspartic acid residue (Asp469 in *E. coli* transketolase, Asp477 in *Sac-*

*Saccharomyces cerevisiae* transketolase). The crucial role of this side chain in the transketolase catalytic mechanism was confirmed by a mutagenesis study that showed a reduction in  $k_{\text{cat}}/K_{\text{M}}$  for an aspartate to alanine variant of *Saccharomyces cerevisiae* transketolase by three orders of magnitude<sup>128</sup>. The side chain lies in hydrogen bonding distance to the substrate-ThDP adduct and is assumed to be part of a proton shuttle that leads to ionization of the 3-OH group in course of C2-C3 donor substrate bond cleavage<sup>4</sup>. Furthermore, it determines specificity for the donor substrate and is therefore essential for enantioselectivity of the transketolase reaction<sup>128</sup>. Whereas the latter function is not of importance in the phosphoketolase reaction, its role in C2-C3 bond cleavage must be compensated by other active site residues in phosphoketolase. It was assumed that the asparagine-aspartic acid exchange between phosphoketolase and transketolase mostly accounts for the necessity to accommodate the additional charge of the phosphoketolase acceptor substrate phosphate<sup>4,72</sup>. Indeed, the XFPK<sub>N549D</sub> phosphoketolase variant showed a slight increase in  $K_{\text{M}}$  for phosphate ( $3.8 \pm 0.7$  mM in XFPK<sub>WT</sub> to  $7.9 \pm 0.9$  mM in XFPK<sub>N549D</sub>) (Figure 40). Moreover, the apparent maximum rate constant for the reaction of phosphate and AcThDP was reduced 60 fold compared to the wild-type enzyme (Figure 41B). Although the effect of the amino acid exchange on phosphate binding/affinity appears only moderate, the reaction of acceptor substrate and the AcThDP intermediate is significantly impaired. Presumably, electrostatic repulsion between the introduced negatively charged aspartate side chain and the acceptor substrate prohibits correct orientation of phosphate for the nucleophilic attack and, considering its proposed role as substrate catalyst (section 4.1), for protonation of the AcThDP intermediate during enol-keto tautomerization. Activity of XFPK<sub>N549D</sub> for the overall phosphoketolase reaction was reduced about 95%, in accordance with the results for the equivalent enzyme variant from *Bifidobacterium longum*<sup>72</sup>.

The double variant XFPK<sub>Y501F/N549D</sub> still catalyzes dehydration of DHETThDP as characteristic step of the phosphoketolase reaction, but the interaction between AcThDP and phosphate seems further impaired, resulting in only residual phosphoketolase activity of the enzyme variant. The hydrogen bond between the Tyr501 hydroxy-group and phosphate appears to play a major role in binding, proper orientation or reactivity of the acceptor substrate. For the single variant XFPK<sub>Y501F</sub> a twentyfold increase in  $K_{\text{M}}$  for phosphate was reported<sup>73</sup>. Furthermore, the additional introduction of the Tyr501Phe mutation into XFPK<sub>N549D</sub> led to considerable changes in the behavior of the enzyme in the double-jump stopped-flow experiment that analyzes reaction of AcThDP with phosphate. Addition of phosphate still leads to decrease in AcThDP absorbance

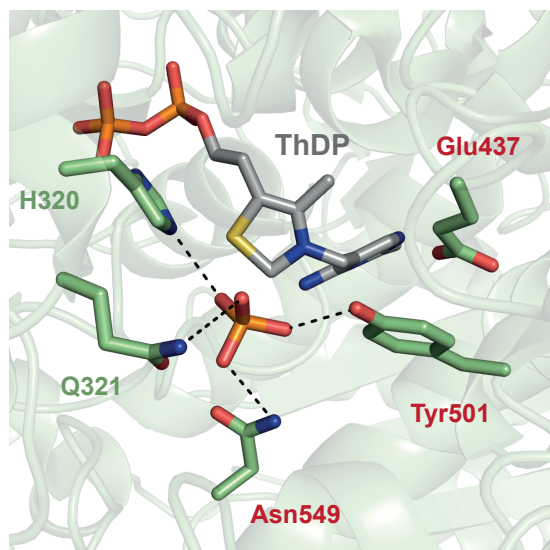


**Figure 51: Phosphate binding site of *B. breve* phosphoketolase.** Tyr501 and Asn549 are part of the phosphate binding site. Replacement by the equivalent transketolase side chains severely impairs the reaction between phosphate and AcThDP. Glu437 does not directly interact with phosphate or potential ThDP-C2-adducts. Figure was prepared based on pdb file 3AHF (SUZUKI *et al.*<sup>73</sup>).

that increases in amplitude towards higher phosphate concentrations, indicating the reaction between AcThDP and phosphate, although distinctly slowed down, still occurs faster than formation of the post-dehydration intermediate. However, the rate of signal decrease was constant, independently of the applied phosphate concentration, suggesting that it is not determined by substrate binding but by some uni-molecular reaction step. Although it is not possible to give a precise mechanistic explanation for this observations at this point, it is clear that the exchange of Tyr501 and Asn549 to their transketolase equivalents severely disturbs the molecular mechanism of the reaction between the acceptor substrate and AcThDP, as was expected from their location of the active site residues in the phosphate binding site (Figure 51).

Nevertheless, impact of the mutations is not restricted to the second-half reaction with phosphate. Formation of the AcThDP intermediate occurs about 15 fold slower in XFPK<sub>N549D</sub> than in wild-type phosphoketolase and is further slowed down in the double variant, indicating additional function of both residues in steps leading to formation of the post-dehydration intermediate. Asn549 is located in the substrate channel of phosphoketolase, presumably interacting with the hydroxy-groups of the substrate-ThDP adduct<sup>73</sup>, which would suggest a role in substrate binding or recognition. Disturbance of the interaction by introduction of the equivalent transketolase residue suggests slight differences in the hydrogen-bonding network of phosphoketolase and transketolase.

Further introduction of the Glu437Leu mutation caused complete loss of phosphoketolase activity. The role of Glu437 in phosphoketolase is somewhat unclear. It is conserved in phosphoketolase<sup>73</sup>, in transketolase the position is, with exception of the human enzyme (threonin), always occupied by a hydrophobic leucine residue, suggesting Glu437 is necessary for electrostatic interactions

or acid-base catalysis in phosphoketolase. A Glu437Gln single variant gave contradictory experimental results. It was reported to be inactive and not to exhibit the AcThDP spectral signal upon F6P addition in accordance with the results that were obtained for the triple mutant XFPK<sub>E437L/Y501F/N549D</sub> in this thesis, but trapping of the post-dehydration intermediate could be achieved after soaking XFPK<sub>E437Q</sub> with F6P<sup>89</sup>. From the crystallographic data, the author assumed a role for Glu437 in coordinating the Tyr501 side chain and as such acting indirectly on phosphate binding and/or coordination<sup>89</sup>. Whatever the precise function of Glu437 in phosphoketolase is, it is absolutely essential for the reaction mechanism.

The "transketolase-like" phosphoketolase variant XFPK<sub>E437L/Y501F/N549D</sub> showed complete loss of phosphoketolase catalytic activity. As judged by spectroscopic detection, the triple mutant no longer catalyzes formation of the AcThDP intermediate. Thus, it seems no longer able to catalyze the characteristic dehydration. Whether it still catalyzes substrate binding and cleavage has to be analyzed by chemical quench/<sup>1</sup>H-NMR intermediate analysis. No new information on the mechanism of DHETThDP dehydration was derived from the mutagenesis study. Also, exchange of Glu437, Tyr501 and Asn549 to their transketolase counterparts did not lead to gain of transketolase activity.

Similar to the absence of the dehydration step in transketolase, no transketolase activity in form of ligation between phosphoketolase bound DHETThDP and a transketolase acceptor substrate can be detected in phosphoketolase. Prevention of a possible re-ligation between DHETThDP and the cleavage products G3P or E4P is absolutely essential for phosphoketolase's biological function in energy provision. It was assumed that this necessary irreversibility of the phosphoketolase reaction is achieved by very fast and irreversible dehydration of DHETThDP. In this thesis it was shown that there is after all DHETThDP present under steady-state reaction conditions that could even be trapped in a carboligation reaction with formaldehyde, demonstrating that a ligation reaction emerging from phosphoketolase bound DHETThDP as required for transketolase activity is possible in principle. Hence, there might be another or additional mechanistic feature that prohibits (re-)ligation with E4P or similar acceptor substrates. It has been discussed whether stabilization of the DHETThDP intermediate in different chemical states could account for their differing reactivities of the intermediate in transketolase and phosphoketolase. Whereas DHETThDP in transketolase adapts a planar conformation with predominant enamine character<sup>90</sup>, X-ray crystallographic data on the phosphoketolase-DHETThDP complex indicated potential *sp*<sup>3</sup> character of the DHETThDP C2-atom, implying a protonated state of the  $\alpha$ -carbanion<sup>73</sup>.

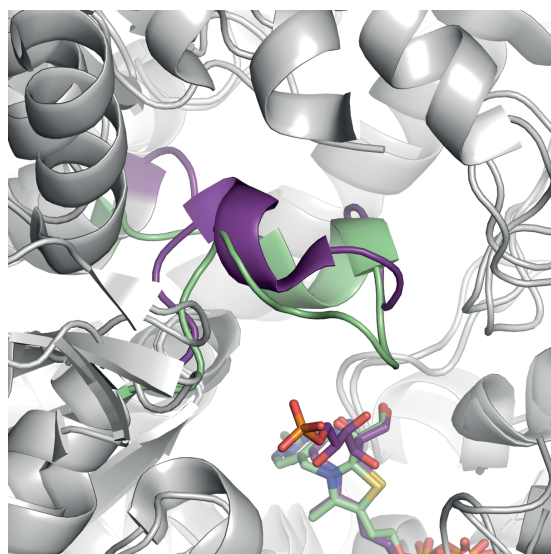


**Figure 52: Different orientation of a substrate channel loop in phosphoketolase and transketolase.** Superposition of *B. breve* phosphoketolase in complex with DHEThDP (green) and *E. coli* transketolase in complex with the substrate cofactor adduct F6P-ThDP (purple). The loops containing the phosphoketolase residue 540 - 557 or the transketolase residues 460 - 477 (displayed in color) show a slightly different orientation. Structure alignment based on pdb files 2R8P (ASZTALOS *et al.*, 2007<sup>43</sup>) and 3AHE (SUZUKI *et al.*, 2010<sup>73</sup>).

Temporary protonation of the  $\alpha$ -carbanion would prevent religation with the G3P or E4P product<sup>4</sup>, but bears the risk of off-pathway aldehyde formation and does contradict our observation that phosphoketolase-bound DHEThDP can in principle undergo a ligation with an electrophilic acceptor. However, for a reliable determination of the chemical state of DHEThDP in both phosphoketolase and transketolase X-ray crystallographic structures of higher resolution than currently available would be necessary. Furthermore, dynamic processes should be considered. A reorganization of the active site after substrate cleavage could for example promote liberation of the aldose product or prevent the back reaction otherwise. In this regard, an active site loop in the substrate binding channel (residues 540 - 557 in *B. breve* PK and residues 460 - 477 in *E. coli* TK) might play a role. It contains the catalytically important residues Asn549 and His553 (Asp469 and His437 in TK) and shows a slightly different orientation in the two enzymes (Figure 52). Introduction of the "transketolase-like" mutations did not induce a change in the carboligase abilities of phosphoketolase, as neither XFPK<sub>Y501F/N549D</sub> nor XFPK<sub>E437L/Y501F/N549D</sub> showed a reaction with the transketolase acceptor substrates.

Although highly important for the catalytic mechanism of phosphoketolase, the analyzed active site residues Glu437, Tyr501 and N549 are no direct determinants for phosphoketolase or transketolase activity of the enzyme. The differences to the transketolase active site mainly, but not exclusively account for accommodation of the phosphoketolase acceptor substrate phosphate. Hence, the molecular mechanism behind the different catalytic activities of phosphoketolase and transketolase and the identity of the putative acid/base catalyst that mediates dehydration of DHEThDP remains elusive. Presumably, it is a complex interplay of subtle differences in (or even outside) the active sites of both enzymes that causes differences in the hydrogen bonding network or

acid/base properties of side chains, which in the end lead to the individual catalytic outcomes. The present case demonstrates once again the complexity of enzymatic systems that can not always be rationalized purely based on obvious structural differences.

#### 4.4 Conclusion and outlook

One major goal in enzyme research is to find and understand fundamental mechanistic principles and strategies of enzymatic catalysis that can be applied in the synthesis of organic molecules or for the design of novel biocatalysts. Results from the present study propose a catalytic mechanism for the enol-keto tautomerization of AcThDP in phosphoketolase in which tautomerization is linked to the final product forming acyl-transfer from the intermediate onto the nucleophilic acceptor substrate phosphate. This coupling avoids formation of the hydrolysis susceptible keto-AcThDP intermediate in the absence of an acceptor substrate and subsequent uncoupling of the reaction by off-pathway hydrolysis. Linkage of the final acyl-transfer to the presence of the acceptor substrate seems to be a general strategy in ThDP dependent enzymes whose catalytic pathways involve formation of an AcThDP intermediate, as a similar principles can be found in *Lp*POX or PFOR. In this regard it would be interesting to examine whether similar mechanisms exist in further ThDP-dependent enzymes such as the E1 component of the *E. coli* pyruvate dehydrogenase complex. Anyway, it provides an elegant example of how to protect reactive reaction intermediates that could be applied as strategy in engineered enzymatic reactions. Confirmation of the underlying molecular mechanism that involves substrate-assisted catalysis by the acceptor substrate phosphate and the tautomerization via a (stabilized) enolate-intermediate might be provided by X-ray crystal structures of phosphoketolase in complex with AcThDP at resolutions close to 1 Å that would allow determination of the chemical state of the intermediate. Moreover, structural information of the enzyme in complex AcThDP and one of the non-reactive phosphate analogues could allow further insight into the interactions between post-dehydration intermediate and acceptor substrate.

Furthermore, the enzymatic system studied in this thesis is an excellent example of promiscuous enzymatic activity emerging from reactive reaction intermediates. Evidence could be provided for carbonylation reactions of the nucleophilic phosphoketolase reaction intermediates DHETThDP and enolate-AcThDP with an aldehyde acceptor. Especially the latter non-natural reaction was of great interest as it confirms the presence of the putative enolate-intermediate and represents a novel ThDP-catalyzed C-C bond forming reaction. To make use of this reaction in biocatalytic



synthesis, the so far minor carbonylase activity of phosphoketolase has to be greatly improved towards a broader acceptor substrate range and higher yields by enzyme engineering approaches. In this regard, the application of high throughput methods should be considered.

No mechanistic explanation could be found for the catalytic differences between the related ThDP-dependent enzymes phosphoketolase and transketolase. In a stepwise mutagenesis approach a "transketolase like" phosphoketolase variant was generated which demonstrated the importance of the three phosphoketolase specific active site-residues for the phosphoketolase reaction mechanism, but did not lead to identification of the phosphoketolase specific acid/base catalyst which mediates dehydration of the AcThDP intermediate or gain of transketolase activity. Although the three active site residues seem not to be direct determinants of phosphoketolase or transketolase activity, analysis of the reverse "phosphoketolase-like" transketolase variant might be informative. Also, rather than just replacing single residues one could exchange larger secondary structure elements like the substrate channel loop shown in Figure 52. Moreover, it would be interesting to see how "phosphoketolase-transketolase hybrid" variants that contain a phosphoketolase PYR and a transketolase PP domain, or vice versa, would behave catalytically. With the new opportunity to analyze the ability of phosphoketolase variants to catalyze dehydration of DHEThDP fast and easy by spectroscopic detection of the post-dehydration intermediate AcThDP, it might also be worth to revisit some of the active site mutants that were generated to identify the phosphoketolase active site residue that mediates acid/base catalysis in the dehydration of DHEThDP, like the His97 or His142 variants.

Taken together, this thesis provides a mechanistic update on AcThDP tautomerization within the catalytic cycle of the ThDP-dependent enzyme phosphoketolase that involves substrate-assisted catalysis by the acceptor substrate phosphate and the formation of an enolate-AcThDP intermediate. Presence of the enolate-AcThDP could be confirmed by trapping the intermediate in a reaction with an aldehyde acceptor substrate. At the same time, this ligation reaction represents a novel thiamine diphosphate-catalyzed C-C bond forming reaction.

## Appendix

His <sub>6</sub> -tag	Linker				
HHHHHH	SSGL	VPRGSHMTN			
	<u>10</u>	<u>20</u>	<u>30</u>	<u>40</u>	<u>50</u>
MTNPFVIGTPW	QKLDRPVSEE	AIEGMDKYWR	VTNYMSIGQI	YLRSNPLMKE	PFTRDDVKHR
	<u>70</u>	<u>80</u>	<u>90</u>	<u>100</u>	<u>110</u>
LVGHWGTTTPG	LNFLLAHINR	LIADHQQNTV	FIMGPGHGGP	AGTSQSYVDG	TYTEYYPNIT
	<u>130</u>	<u>140</u>	<u>150</u>	<u>160</u>	<u>170</u>
KDEAGLQKFF	RQFSYPPGIP	SHFAPETPGS	IHEGGELGYA	LSHAYGAVMN	NPSLRFVPCII
	<u>190</u>	<u>200</u>	<u>210</u>	<u>220</u>	<u>230</u>
GDGEAETGPL	ATGWQSNKLV	NPRTDGIVLP	ILHLNGYKIA	NPTILARISD	EELHDFFRGM
	<u>250</u>	<u>260</u>	<u>270</u>	<u>280</u>	<u>290</u>
GYHPYEFVAG	FDNEDHMSIH	RRFAELFETI	FDEICDIKAA	AQTDDMTRPF	YPMLIFRTPK
	<u>310</u>	<u>320</u>	<u>330</u>	<u>340</u>	<u>350</u>
GWTCPKFIDG	KKTEGSWRAH	QVPLASARDT	EEHFEVLKGW	MESYKPEELF	NADGSIKDDV
	<u>370</u>	<u>380</u>	<u>390</u>	<u>400</u>	<u>410</u>
TAFMPKGE LR	IGANPNANGG	VIREDLKLP E	LDQYEVTVGK	EYGHGWGQVE	APRALGAYCR
	<u>430</u>	<u>440</u>	<u>450</u>	<u>460</u>	<u>470</u>
DIIKNNPDSF	RIFGPDE TAS	NRLNATYEVT	DKQWDNGYLS	GLVDEHMAVT	GQVTEQLSEH
	<u>490</u>	<u>500</u>	<u>510</u>	<u>520</u>	<u>530</u>
QCEGFLEAYL	LTGRHGIWSS	YESFVHVIDS	MLNQHAKWLE	ATVREIPWRK	PISSVNL LVS
	<u>550</u>	<u>560</u>	<u>570</u>	<u>580</u>	<u>590</u>
SHVWRQDHNG	FSHQDPGVTS	LLINKTFNND	HVTNIYFATD	ANMLLAISEK	CFKSTNKINA
	<u>610</u>	<u>620</u>	<u>630</u>	<u>640</u>	<u>650</u>
IFAGKQPAPT	WVTLD EARAE	LEAGAAEWK W	ASNAENNDEV	QVVLASAGDV	PTQELMAASD
	<u>670</u>	<u>680</u>	<u>690</u>	<u>700</u>	<u>710</u>
ALNKMGIKFK	VVNVVDLLKL	QSRENNDEAL	TDEEFTELEF T	ADKPVLFA YH	SYAQDVRGLI
	<u>730</u>	<u>740</u>	<u>750</u>	<u>760</u>	<u>770</u>
YDRPNHDNFH	VVGYKEQGST	TTPFDMVRVN	DMDRYALQAA	ALKLIDADKY	ADKIDELNAF
	<u>790</u>	<u>800</u>	<u>810</u>	<u>820</u>	
RKKAFAQFAVD	NGYDIPEFTD	WVYDPVKVDE	TQMLSATAAT	AGDNE	

molecular weight: 94837.13 Da

**Figure 53: Amino acid sequence of the recombinant *B. breve* phosphoketolase.** Amino acid sequence of the recombinant *B. breve* phosphoketolase construct including the N-terminal His<sub>6</sub>-tag and linker. Amino acid residues are color-coded according to the respective domain PP = green, PYR = purple, C-terminal = grey. The residues analyzed in this thesis by mutagenesis are marked in red. The molecular weight was determined by the ExPASy ProtParam tool.

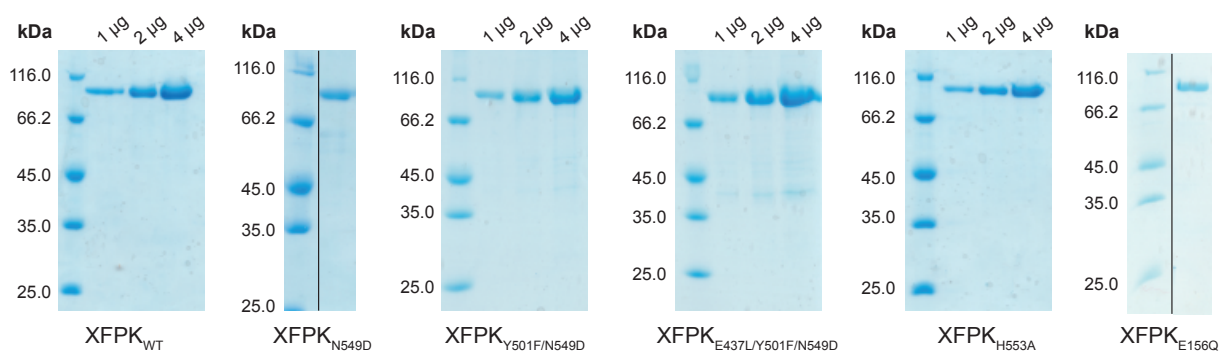


**Figure 54: SDS-PAGE analysis of purified XFPK<sub>WT</sub> and variants.** Recombinant XFPK<sub>WT</sub> or variants were obtained in milligram amounts, purified up to 95% homogeneity.

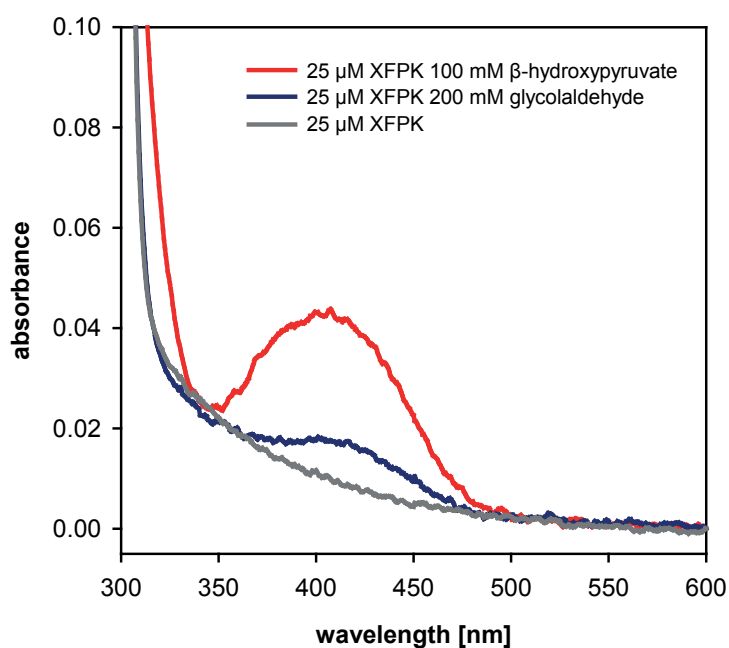


**Figure 55: UV-Vis absorbance spectra of phosphoketolase with alternative substrates.** Spectra of 25  $\mu\text{M}$  phosphoketolase with 100 mM  $\beta$ -hydroxyypyruvate (red) or 200 mM glycolaldehyde (blue) after subtraction of the respective substrate spectrum are shown. Comparison to the resting state spectrum (gray) shows formation of absorbance band with  $\lambda_{max}$  at 420 nm after substrate addition as observed for the natural substrate F6P.

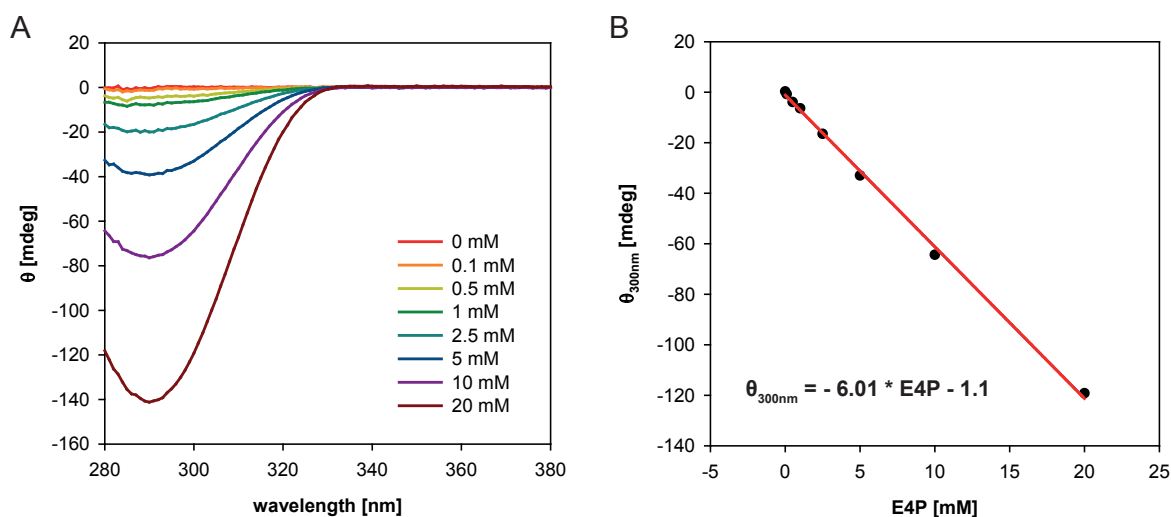


**Figure 56: Erythrose 4-phosphate calibration curve.** (A) CD spectra were recorded for different E4P concentrations. (B) Molar ellipticity at 300 nm was plotted against the applied respective E4P concentration and fitted with a linear term (red line) that allowed conversion of initial changes in CD signal measured in the CD steady state assay into initial reaction rates.

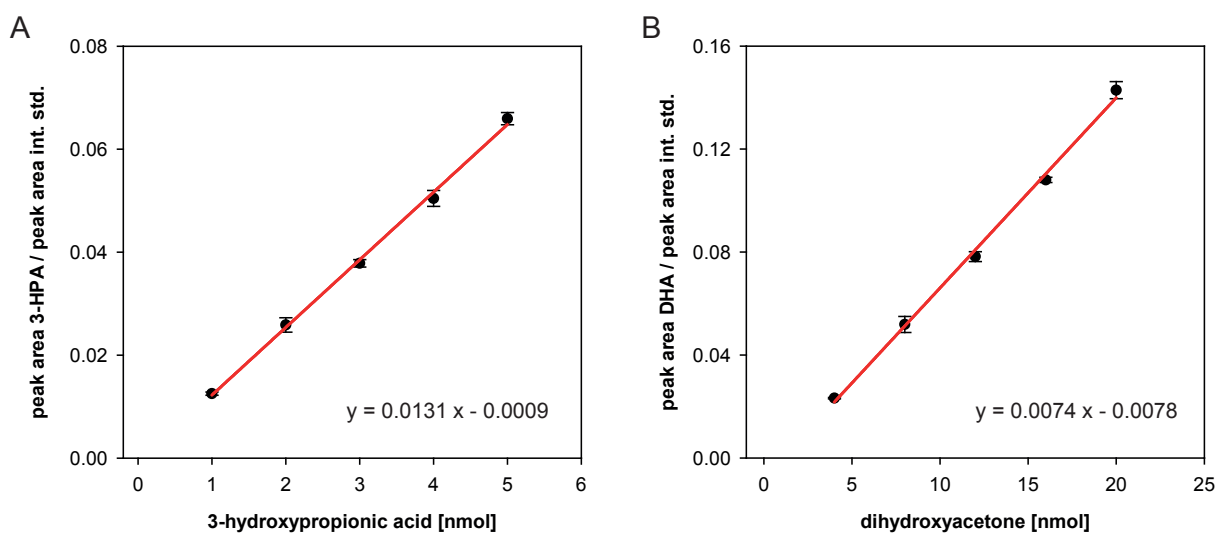


**Figure 57: Calibration curves for quantification of carboligation products.** Reference samples containing defined amounts of (A) 3-hydroxypropionic acid (3-HPA) or (B) dihydroxyacetone (DHA) and an internal standard (allo-inositol) were analyzed in GC-MS. Integrated peak areas of selected masses were related to those of the internal standard and plotted against the respective amount of reference substance and fitted with a linear term (red lines).

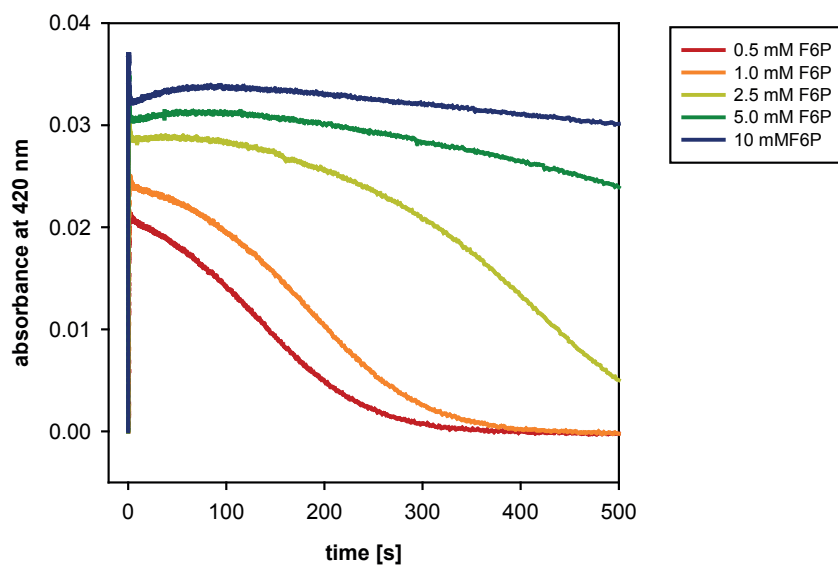


**Figure 58: Progression of AcThDP absorbance over time.** XFPK ( $24 \mu\text{M}$ ) was fast-mixed with different concentrations of F6P in stopped-flow mixing device. Absorbance at 420 nm was recorded over time. Already at low substrate concentrations signal depletion requires  $> 300$  s.

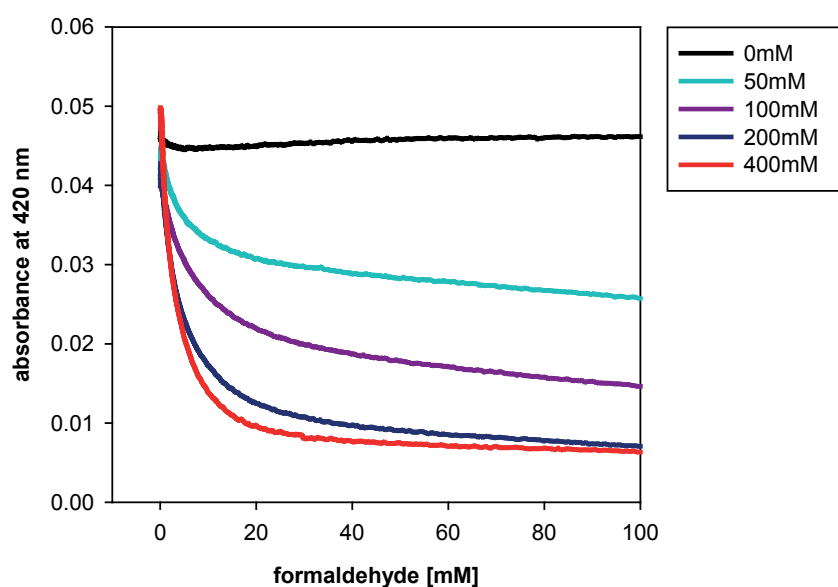


**Figure 59: Depletion of the AcThDP absorbance after mixing with formaldehyde.** XFPK ( $24 \mu\text{M}$ ) was fast-mixed with 20 mM F6P in a stopped-flow mixing device set to sequential mixing mode. The reaction mix was aged for 5 s to ensure population of the AcThDP intermediate. In a second mixing step the aged solution was fast-mixed with different concentrations of formaldehyde, depletion of AcThDP was detected via decrease of absorbance at 420 nm over time. Applied concentrations of formaldehyde are listed in the legend.

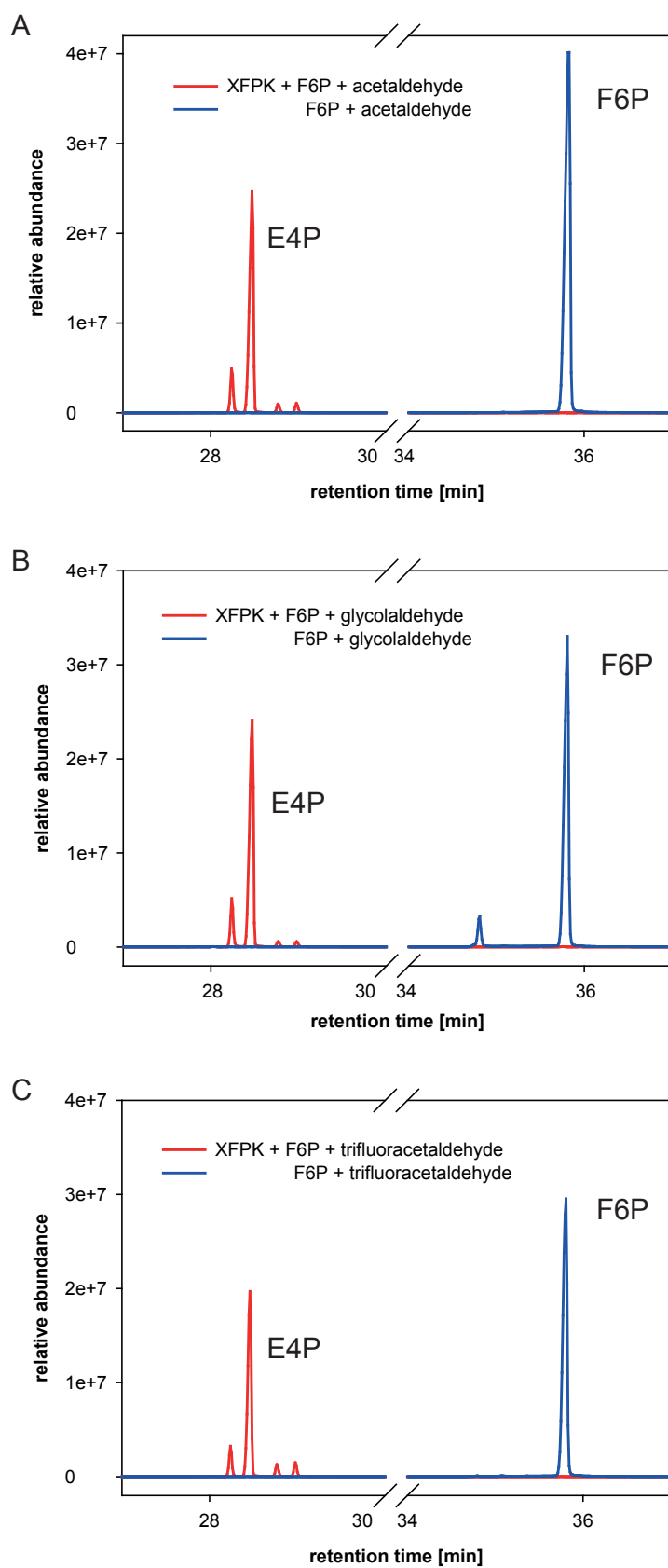


**Figure 60: Analysis of F6P conversion by GC-MS.** GC-MS chromatograms after reaction of XFPK with F6P and (A) 100 mM acetaldehyde, (B) 100 mM glycolaldehyde or (C) 100 mM trifluoroacetaldehyde are shown in red. GC-MS chromatograms of respective control reactions without enzyme are shown in blue. In all cases complete conversion of F6P to E4P was observed.

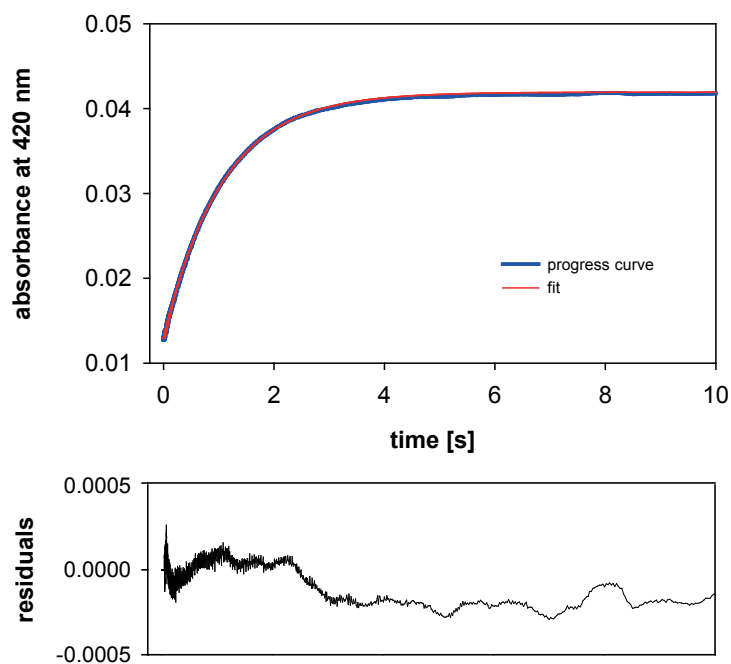


**Figure 61: Exemplary progress curve of AcThDP formation in XFPK<sub>N549D</sub>.** Progression of absorbance at 420 nm after rapid-mixing of 24  $\mu$ M XFPK<sub>N549D</sub> with 10 mM F6P is shown as red line. Progress curves did not exhibit kinetic overshooting and were fitted with a single term exponential equation (Eq. 7) (blue line) to determine first order rate constants. Deviation of the applied fit from the represented data is shown as residuals plot.

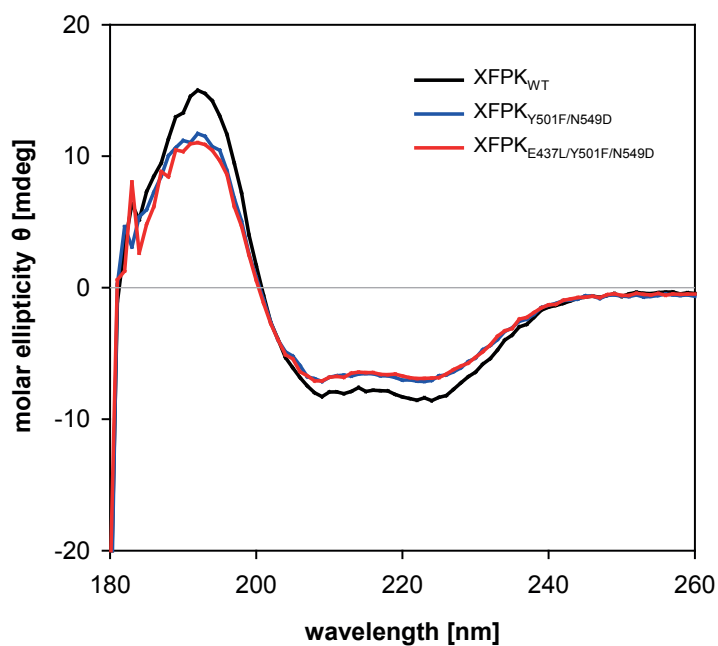


**Figure 62: Far-UV CD spectra of phosphoketolase wild type and "transketolase-like" variants.** CD spectra between 180 - 260 nm were recorded for XFPK<sub>WT</sub>, XFPK<sub>Y501F/N549D</sub> and triple. CD spectra of both variants are similar to the spectrum of XFPK<sub>WT</sub>, indicating introduction of the active site mutations did not cause a change in secondary structure.

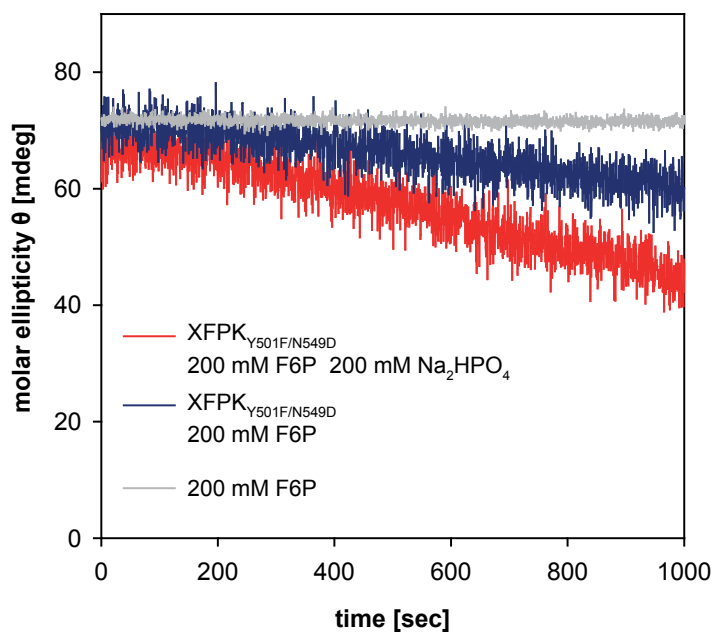


**Figure 63: Phosphoketolase activity of XFPK<sub>Y501F/N549D</sub>.** Increase of the negative E4P CD signal at 300 nm over time after mixing of 105  $\mu$ M XFPK<sub>Y501F/N549D</sub> with 200 mM F6P (red curve) or 200 mM F6P and 200 mM Na<sub>2</sub>HPO<sub>4</sub> (blue curve) shows residual phosphoketolase activity of XFPK<sub>Y501F/N549D</sub>.



## References

- [1] E. C. Heath, J. Hurwitz, and B. L. Horecker. “Acetyl phosphate formation in the phosphorytic cleavage of pentose phosphate”. In: *Journal of the American Chemical Society* 78.20 (1956), pp. 5449–5449.
- [2] Michael Widmann, Robert Radloff, and Jürgen Pleiss. “The Thiamine diphosphate dependent Enzyme Engineering Database: a tool for the systematic analysis of sequence and structure relations.” In: *BMC biochemistry* 11 (Feb. 2010), p. 9.
- [3] Thiamine diphosphate dependent Enzyme Engineering Database. <https://teed.biocatnet.de>, accessed 17.08.2017.
- [4] Kai Tittmann. “Sweet siblings with different faces: The mechanisms of FBP and F6P aldolase, transaldolase, transketolase and phosphoketolase revisited in light of recent structural data”. ENG. In: *Bioorganic Chemistry* (Sept. 2014).
- [5] Otto Kandler. “Carbohydrate metabolism in lactic acid bacteria”. en. In: *Antonie van Leeuwenhoek* 49.3 (May 1983), pp. 209–224.
- [6] W. de Vries and A. H. Stouthamer. “Pathway of glucose fermentation in relation to the taxonomy of bifidobacteria.” In: *Journal of bacteriology* 93 (2 Feb. 1967), pp. 574–576.
- [7] W. de Vries, S.J. Gerbrandy, and A.H. Stouthamer. “Carbohydrate metabolism in *Bifidobacterium bifidum*”. In: *Biochimica et Biophysica Acta (BBA) - General Subjects* 136.3 (1967), pp. 415–425.
- [8] M. J. Wolin, Y. Zhang, S. Bank, S. Yerry, and T. L. Miller. “NMR detection of  $^{13}\text{CH}_3^{13}\text{COOH}$  from 3- $^{13}\text{C}$ -glucose: a signature for *Bifidobacterium* fermentation in the intestinal tract.” In: *The Journal of nutrition* 128 (1 Jan. 1998), pp. 91–96.
- [9] Baltasar Mayo and Douwe Van Sinderen, eds. *Bifidobacteria: genomics and molecular aspects*. Horizon Scientific Press, 2010.
- [10] Anastasia Krivoruchko, Yiming Zhang, Verena Siewers, Yun Chen, and Jens Nielsen. “Microbial acetyl-CoA metabolism and metabolic engineering”. In: *Metabolic Engineering* 28 (2015), pp. 28–42.
- [11] Calvin Andrew Henard, Emily Frances Freed, and Michael Thomas Guarnieri. “Phosphoketolase pathway engineering for carbon-efficient biocatalysis”. In: *Current Opinion in Biotechnology*. Pathway engineering 36 (Dec. 2015), pp. 183–188.

- [12] Marco Sonderegger, Michael Schümperli, and Uwe Sauer. “Metabolic engineering of a phosphoketolase pathway for pentose catabolism in *Saccharomyces cerevisiae*.” In: *Applied and environmental microbiology* 70 (5 May 2004), pp. 2892–2897.
- [13] Marta Papini, Intawat Nookaew, Verena Siewers, and Jens Nielsen. “Physiological characterization of recombinant *Saccharomyces cerevisiae* expressing the *Aspergillus nidulans* phosphoketolase pathway: validation of activity through  $^{13}\text{C}$ -based metabolic flux analysis.” In: *Applied microbiology and biotechnology* 95 (4 Aug. 2012), pp. 1001–1010.
- [14] Akito Chinen, Yuri I. Kozlov, Yoshihiko Hara, Hiroshi Izui, and Hisashi Yasueda. “Innovative metabolic pathway design for efficient l-glutamate production by suppressing  $\text{CO}_2$  emission”. In: *Journal of Bioscience and Bioengineering* 103.3 (2007), pp. 262–269.
- [15] Bouke Wim de Jong, Shuobo Shi, Verena Siewers, and Jens Nielsen. “Improved production of fatty acid ethyl esters in *Saccharomyces cerevisiae* through up-regulation of the ethanol degradation pathway and expression of the heterologous phosphoketolase pathway.” In: *Microbial cell factories* 13 (1 Mar. 2014).
- [16] Kanokarn Kocharin, Verena Siewers, and Jens Nielsen. “Improved polyhydroxybutyrate production by *Saccharomyces cerevisiae* through the use of the phosphoketolase pathway.” In: *Biotechnology and bioengineering* 110 (8 Aug. 2013), pp. 2216–2224.
- [17] Gianni Panagiotou, Mikael R Andersen, Thomas Grotkjaer, Torsten B Regueira, Jens Nielsen, and Lisbeth Olsson. “Studies of the production of fungal polyketides in *Aspergillus nidulans* by using systems biology tools.” In: *Applied and environmental microbiology* 75 (7 Apr. 2009), pp. 2212–2220.
- [18] Igor W. Bogorad, Tzu-Shyang Lin, and James C. Liao. “Synthetic non-oxidative glycolysis enables complete carbon conservation.” In: *Nature* 502.7473 (Oct. 2013), pp. 693–697.
- [19] Igor W. Bogorad, Chang-Ting Chen, Matthew K. Theisen, Tung-Yun Wu, Alicia R. Schlenz, Albert T. Lam, and James C. Liao. “Building carbon-carbon bonds using a biocatalytic methanol condensation cycle.” In: *Proceedings of the National Academy of Sciences of the United States of America* (Oct. 2014).
- [20] Ronald G. Duggleby. “Domain relationships in thiamine diphosphate-dependent enzymes”. eng. In: *Accounts of Chemical Research* 39.8 (Aug. 2006), pp. 550–557.

- [21] Seán J Costelloe, John M Ward, and Paul A Dalby. “Evolutionary analysis of the TPP-dependent enzyme family.” In: *Journal of molecular evolution* 66 (1 Jan. 2008), pp. 36–49.
- [22] M. Schramm, V. Klybas, and E. Racker. “Phosphorolytic cleavage of fructose-6-phosphate by fructose-6-phosphate phosphoketolase from *Acetobacter xylinum*”. In: *The Journal of Biological Chemistry* 233.6 (Dec. 1958), pp. 1283–1288.
- [23] Ronald Breslow. “Rapid deuterium exchange in thiazolium salts”. In: *Journal of the American Chemical Society* 79.7 (1957), pp. 1762–1763.
- [24] Ronald Breslow. “On the Mechanism of Thiamine Action. IV.1 Evidence from Studies on Model Systems”. In: *Journal of the American Chemical Society* 80.14 (1958), pp. 3719–3726.
- [25] R. A. W. Frank, F. J. Leeper, and B. F. Luisi. “Structure, mechanism and catalytic duality of thiamine-dependent enzymes.” In: *Cellular and molecular life sciences* 64 (7-8 Apr. 2007), pp. 892–905.
- [26] R. R. Williams. “Structure of Vitamin B<sub>1</sub>”. In: *Journal of the American Chemical Society* 58.6 (1936), pp. 1063–1064.
- [27] K. Lohmann and Ph. Schuster. “Über die Co-Carboxylase”. In: *Naturwissenschaften* 25.2 (1937), pp. 26–27.
- [28] Ronald Kluger and Kai Tittmann. “Thiamin diphosphate catalysis: enzymic and nonenzymic covalent intermediates.” In: *Chemical Reviews* 108.6 (June 2008), pp. 1797–1833.
- [29] D. S. Kemp and J. T. O’Brien. “Base catalysis of thiazolium salt hydrogen exchange and its implications for enzymatic thiamine cofactor catalysis.” In: *Journal of the American Chemical Society* 92 (8 Apr. 1970), pp. 2554–2555.
- [30] Michael W. Washabaugh and William P. Jencks. “Thiazolium C(2)-proton exchange: structure-reactivity correlations and the pK<sub>a</sub> of thiamin C(2)-H revisited.” In: *Biochemistry* 27.14 (1988), pp. 5044–5053.
- [31] Dorothee Kern, Gunther Kern, Holger Neef, Kai Tittmann, Margrit Killenberg-Jabs, Christer Wikner, Gunter Schneider, and Gerhard Hübner. “How thiamine diphosphate is activated in enzymes.” In: *Science* 275.5296 (Mar. 1997), pp. 67–70.

- [32] Y. Lindqvist, G. Schneider, U. Ermler, and M. Sundström. “Three-dimensional structure of transketolase, a thiamine diphosphate dependent enzyme, at 2.5 Å resolution.” In: *The EMBO Journal* 11.7 (July 1992), pp. 2373–2379.
- [33] Alfred Schellenberger. “Die Funktion der 4-Aminopyrimidin-Komponente im Katalysemechanismus von Thiaminpyrophosphat-Enzymen aus heutiger Sicht”. In: *Chemische Berichte* 123.7 (1990), pp. 1489–1494.
- [34] Y. A. Muller, Y. Lindqvist, W. Furey, G. E. Schulz, F. Jordan, and G. Schneider. “A thiamin diphosphate binding fold revealed by comparison of the crystal structures of transketolase, pyruvate oxidase and pyruvate decarboxylase.” In: *Structure* 1 (2 Oct. 1993), pp. 95–103.
- [35] Frank Jordan and Yitbarek H. Mariam. “N1'-Methylthiaminium diiodide. Model study on the effect of a coenzyme bound positive charge on reaction mechanisms requiring thiamin pyrophosphate.” In: *Journal of the American Chemical Society* 100.8 (1978), pp. 2534–2541.
- [36] A. Schellenberger. “Sixty years of thiamin diphosphate biochemistry.” In: *Biochimica et biophysica acta* 1385 (2 June 1998), pp. 177–186.
- [37] Alexander Kaplun, Elad Binshtein, Maria Vyazmensky, Andrea Steinmetz, Ze'ev Barak, David M Chipman, Kai Tittmann, and Boaz Shaanan. “Glyoxylate carboligase lacks the canonical active site glutamate of thiamine-dependent enzymes.” In: *Nature chemical biology* 4 (2 Feb. 2008), pp. 113–118.
- [38] Danilo Meyer, Piotr Neumann, Ralf Ficner, and Kai Tittmann. “Observation of a stable carbene at the active site of a thiamin enzyme.” In: *Nature chemical biology* 9 (8 Aug. 2013), pp. 488–490.
- [39] August Turano, William Furey, James Pletcher, Martin Sax, David Pike, and Ronald Kluger. “Synthesis and crystal structure of an analog of 2- $\alpha$ -lactyl-thiamin, racemic methyl 2-hydroxy-2-(2-thiamin)-ethylphosphonate chloride trihydrate. A conformation for a least-motion, maximum-overlap mechanism for thiamin catalysis.” In: *Journal of the American Chemical Society* 104.11 (June 1982), pp. 3089–3095.
- [40] Danilo Meyer, Piotr Neumann, Christoph Parthier, Rudolf Friedemann, Natalia Nemeria, Frank Jordan, and Kai Tittmann. “Double duty for a conserved glutamate in pyruvate decarboxylase: evidence of the participation in stereoelectronically controlled decarboxyla-

- tion and in protonation of the nascent carbanion/enamine intermediate .” In: *Biochemistry* 49 (37 Sept. 2010), pp. 8197–8212.
- [41] Georg Wille, Danilo Meyer, Andrea Steinmetz, Erik Hinze, Ralph Golbik, and Kai Tittmann. “The catalytic cycle of a thiamin diphosphate enzyme examined by cryocrystallography”. In: *Nature Chemical Biology* 2.6 (June 2006), pp. 324–328.
- [42] Stefan Lüdtke, Piotr Neumann, Karl M Erixon, Finian Leeper, Ronald Kluger, Ralf Ficner, and Kai Tittmann. “Sub-Ångström-resolution crystallography reveals physical distortions that enhance reactivity of a covalent enzymatic intermediate.” In: *Nature chemistry* 5 (9 Sept. 2013), pp. 762–767.
- [43] Peter Asztalos, Christoph Parthier, Ralph Golbik, Martin Kleinschmidt, Gerhard Hübner, Manfred S. Weiss, Rudolf Friedemann, Georg Wille, and Kai Tittmann. “Strain and Near Attack Conformers in Enzymic Thiamin Catalysis: X-ray Crystallographic Snapshots of Bacterial Transketolase in Covalent Complex with Donor Ketoses Xylulose 5-phosphate and Fructose 6-phosphate, and in Noncovalent Complex with Acceptor Aldose Ribose 5-phosphate”. In: *Biochemistry* 46.43 (Oct. 2007), pp. 12037–12052.
- [44] Danilo Meyer, Piotr Neumann, Eline Koers, Hanno Sjuts, Stefan Lüdtke, George M. Sheldrick, Ralf Ficner, and Kai Tittmann. “Unexpected tautomeric equilibria of the carbanion-enamine intermediate in pyruvate oxidase highlight unrecognized chemical versatility of thiamin.” In: *Proceedings of the National Academy of Sciences of the United States of America* 109.27 (July 2012), pp. 10867–10872.
- [45] Kai Tittmann, Ralph Golbik, Kathrin Uhlemann, Ludmila Khailova, Gunter Schneider, Mulchand Patel, Frank Jordan, David M. Chipman, Ronald G. Duggleby, and Gerhard Hübner. “NMR Analysis of Covalent Intermediates in Thiamin Diphosphate Enzymes”. In: *Biochemistry* 42.26 (July 2003), pp. 7885–7891.
- [46] Natalia S. Nemeria, Sumit Chakraborty, Anand Balakrishnan, and Frank Jordan. “Reaction mechanisms of thiamin diphosphate enzymes: defining states of ionization and tautomerization of the cofactor at individual steps”. In: *The FEBS journal* 276.9 (May 2009), pp. 2432–2446.
- [47] Frank Jordan and Natalia S. Nemeria. “Progress in the experimental observation of thiamin diphosphate-bound intermediates on enzymes and mechanistic information derived from these observations”. In: *Bioorganic Chemistry* 57 (Dec. 2014), pp. 251–262.

- [48] Constantin Vogel and Jürgen Pleiss. “The modular structure of ThDP-dependent enzymes.” eng. In: *Proteins* 82.10 (Oct. 2014), pp. 2523–2537.
- [49] C. F. Hawkins, A. Borges, and R. N. Perham. “A common structural motif in thiamin pyrophosphate-binding enzymes.” In: *FEBS letters* 255 (1 Sept. 1989), pp. 77–82.
- [50] Kathryn M. Koeller and Chi-Huey Wong. “Enzymes for chemical synthesis”. en. In: *Nature* 409.6817 (Jan. 2001), pp. 232–240.
- [51] U. T. Bornscheuer, G. W. Huisman, R. J. Kazlauskas, S. Lutz, J. C. Moore, and K. Robins. “Engineering the third wave of biocatalysis.” In: *Nature* 485 (7397 May 2012), pp. 185–194.
- [52] Georg A. Sprenger and Martina Pohl. “Synthetic potential of thiamin diphosphate-dependent enzymes”. In: *Journal of Molecular Catalysis B: Enzymatic* 6.3 (Mar. 1999), pp. 145–159.
- [53] Michael Müller, Dörte Gocke, and Martina Pohl. “Thiamin diphosphate in biological chemistry: exploitation of diverse thiamin diphosphate-dependent enzymes for asymmetric chemoenzymatic synthesis.” en. In: *FEBS Journal* 276.11 (June 2009), pp. 2894–2904.
- [54] Margarita Brovetto, Daniela Gamemara, Patricia Saenz Mendez, and Gustavo A. Seoane. “C-C bond-forming lyases in organic synthesis”. In: *Chemical Reviews* 111.7 (July 2011), pp. 4346–4403.
- [55] Christopher K. Prier and Frances H. Arnold. “Chemomimetic Biocatalysis: Exploiting the Synthetic Potential of Cofactor-Dependent Enzymes To Create New Catalysts”. In: *Journal of the American Chemical Society* 137.44 (2015), pp. 13992–14006.
- [56] Martina Pohl, Bettina Lingen, and Michael Müller. “Thiamin diphosphate-dependent enzymes: new aspects of asymmetric C-C bond formation.” In: *Chemistry (Weinheim an der Bergstrasse, Germany)* 8 (23 Dec. 2002), pp. 5288–5295.
- [57] G. Hildebrandt and Klavehn W. *Verfahren zur Herstellung von 1-1-Phenyl-2-methylaminopropan-1-ol*. Deutsches Reichspatent 549 459. 1932.
- [58] B. Hauer, M. Breuer, P. Rogers, V. Sandford, and B. Rosche. *Verfahren zur Herstellung von R-Phenylacetylcarbinol durch ein enzymatisches verfahren in einem Zweiphasensystem*. DE Patent App. DE2,001,142,574. Mar. 2003.
- [59] Martina Pohl, Georg A. Sprenger, and Michael Müller. “A new perspective on thiamine catalysis.” In: *Current Opinion in Biotechnology* 15.4 (Aug. 2004), pp. 335–342.

- [60] Helen C. Hailes, Dörte Rother, Michael Müller, Robert Westphal, John M. Ward, Jürgen Pleiss, Constantin Vogel, and Martina Pohl. “Engineering stereoselectivity of ThDP-dependent enzymes.” In: *The FEBS journal* 280 (24 Dec. 2013), pp. 6374–6394.
- [61] Pascal Dünkemann, Doris Kolter-Jung, Adam Nitsche, Ayhan S. Demir, Petra Siegert, Bettina Lingen, Martin Baumann, Martina Pohl, and Michael Müller. “Development of a donor-acceptor concept for enzymatic cross-coupling reactions of aldehydes: the first asymmetric cross-benzoin condensation.” In: *Journal of the American Chemical Society* 124 (41 Oct. 2002), pp. 12084–12085.
- [62] Patrizia Lehwald, Michael Richter, Caroline Röhr, Hung-Wen Liu, and Michael Müller. “Enantioselective intermolecular aldehyde-ketone cross-coupling through an enzymatic carbonylation reaction.” In: *Angewandte Chemie International Edition* 49 (13 Mar. 2010), pp. 2389–2392.
- [63] Carola Dresen, Michael Richter, Martina Pohl, Steffen Lüdeke, and Michael Müller. “The Enzymatic Asymmetric Conjugate Umpolung Reaction.” In: *Angewandte Chemie International Edition* 49.37 (Sept. 2010), pp. 6600–6603.
- [64] Anja Kurutsch, Michael Richter, Volker Brecht, Georg A. Sprenger, and Michael Müller. “MenD as a versatile catalyst for asymmetric synthesis.” In: *Journal of Molecular Catalysis B: Enzymatic* 61.1 (2009). *Chemical Biology of Thiamine*, pp. 56–66.
- [65] Michael Müller, Georg A. Sprenger, and Martina Pohl. “C-C bond formation using ThDP-dependent lyases.” In: *Current Opinion in Chemical Biology* 17.2 (Apr. 2013), pp. 261–270.
- [66] E. C. Heath, Jerard Hurwitz, B. L. Horecker, and A. Ginsburg. “Pentose Fermentation by *Lactobacillus Plantarum* I. The Cleavage of Xylulose 5-Phosphate by Phosphoketolase”. In: *Journal of Biological Chemistry* 231.2 (Jan. 1958), pp. 1009–1029.
- [67] M. Schramm and E. Racker. “Formation of erythrose-4-phosphate and acetyl phosphate by a phosphorolytic cleavage of fructose-6-phosphate.” In: *Nature* 179 (4574 June 1957), pp. 1349–1350.
- [68] Melvin L. Goldberg and Efraim Racker. “Formation and Isolation of a Glycolaldehyde-Phosphoketolase Intermediate”. In: *Journal of Biological Chemistry* 237.12 (Jan. 1962), pp. 3841–3842.

- [69] W. Schröter and H. Holzer. “Zum Wirkungsmechanismus der Phosphoketolase II. Umsatz von Thiaminpyrophosphat aktivierte Glycolaldehyde”. In: *Biochimica et biophysica acta* 77 (Nov. 1963), pp. 474–481.
- [70] L. O. Krampitz. “Catalytic functions of thiamin diphosphate.” In: *Annual review of biochemistry* 38 (1969), pp. 213–240.
- [71] Alejandro Yevenes and Perry A. Frey. “Cloning, expression, purification, cofactor requirements, and steady state kinetics of phosphoketolase-2 from *Lactobacillus plantarum*”. In: *Bioorganic Chemistry* 36.3 (June 2008), pp. 121–127.
- [72] Kazutoshi Takahashi, Uno Tagami, Nobuhisa Shimba, Tatsuki Kashiwagi, Kohki Ishikawa, and Ei-ichiro Suzuki. “Crystal structure of *Bifidobacterium Longum* phosphoketolase; key enzyme for glucose metabolism in *Bifidobacterium*.” In: *FEBS letters* 584.18 (Sept. 2010), pp. 3855–3861.
- [73] Ryuichiro Suzuki, Takane Katayama, Byung-Jun Kim, Takayoshi Wakagi, Hirofumi Shoun, Hisashi Ashida, Kenji Yamamoto, and Shinya Fushinobu. “Crystal structures of phosphoketolase: Thiamine diphosphate dependent dehydration mechanism.” In: *Journal of Biological Chemistry* 285.44 (Oct. 2010), pp. 34279–34287.
- [74] Leo Meile, Lukas M. Rohr, Thomas A. Geissmann, Monique Herensperger, and Michael Teuber. “Characterization of the D-xylulose 5-phosphate/D-fructose 6-phosphate phosphoketolase gene *xfp* from *Bifidobacterium lactis*”. In: *Journal of Bacteriology* 183.9 (Jan. 2001), pp. 2929–2936.
- [75] Jing Zhang and Yongjun Liu. “Computational studies on the catalytic mechanism of phosphoketolase.” In: *Computational and Theoretical Chemistry* 1025 (Dec. 2013), pp. 1–7.
- [76] Kai Tittmann. “Reaction mechanisms of thiamine diphosphate enzymes: redox reactions.” In: *The FEBS journal* 276 (9 May 2009), pp. 2454–2468.
- [77] Ronald Breslow and Edward McNelis. “On the mechanism of thiamine action: VI. 2-Acetylthiazolium salts as active acetate.” In: *Journal of the American Chemical Society* 82.9 (1960), pp. 2394–2395.
- [78] Fred G. White and Lloyd L. Ingraham. “On the mechanism of thiamine action.” In: *Journal of the American Chemical Society* 82.15 (1960), pp. 4114–4115.
- [79] Koji Daigo and Lester J. Reed. “Synthesis and Properties of 2-Acetyl-3,4-dimethylthiazolium Iodide.” In: *Journal of the American Chemical Society* 84.4 (1962), pp. 659–662.



- [80] Gustav E. Lienhard. “Kinetics and Mechanism of the Hydrolysis of 2-Acetyl-3,4-dimethylthiazolium Ion”. In: *Journal of the American Chemical Society* 88.23 (1966), pp. 5642–5649.
- [81] K. J. Gruys, C. J. Halkides, and P. A. Frey. “Synthesis and properties of 2-acetylthiamin pyrophosphate: an enzymatic reaction intermediate.” In: *Biochemistry* 26 (24 Dec. 1987), pp. 7575–7585.
- [82] K J Gruys, A Datta, and P A Frey. “2-Acetylthiamin pyrophosphate (acetyl-TPP) pH-rate profile for hydrolysis of acetyl-TPP and isolation of acetyl-TPP as a transient species in pyruvate dehydrogenase catalyzed reactions.” In: *Biochemistry* 28 (23 Nov. 1989), pp. 9071–9080.
- [83] Kai Tittmann, Georg Wille, Ralph Golbik, Annett Weidner, Sandro Ghisla, and Gerhard Hübner. “Radical phosphate transfer mechanism for the thiamin diphosphate- and FAD-dependent pyruvate oxidase from *Lactobacillus plantarum*. Kinetic coupling of intercofactor electron transfer with phosphate transfer to acetyl-thiamin diphosphate via a transient FAD semiquinone/hydroxyethyl-ThDP radical pair.” In: *Biochemistry* 44 (40 Oct. 2005), pp. 13291–13303.
- [84] Hetalben Patel, Natalia S. Nemeria, Forest H. Andrews, Michael J. McLeish, and Frank Jordan. “Identification of charge transfer transitions related to thiamin-bound intermediates on enzymes provides a plethora of signatures useful in mechanistic studies.” In: *Biochemistry* 53 (13 Apr. 2014), pp. 2145–2152.
- [85] D. S. Flournoy and P. A. Frey. “Pyruvate dehydrogenase and 3-fluoropyruvate: chemical competence of 2-acetylthiamin pyrophosphate as an acetyl group donor to dihydroliipoamide.” In: *Biochemistry* 25 (20 Oct. 1986), pp. 6036–6043.
- [86] K. Tittmann, R. Golbik, S. Ghisla, and G. Hübner. “Mechanism of elementary catalytic steps of pyruvate oxidase from *Lactobacillus plantarum*.” In: *Biochemistry* 39 (35 Sept. 2000), pp. 10747–10754.
- [87] George H. Reed, Stephen W. Ragsdale, and Steven O. Mansoorabadi. “Radical reactions of thiamin pyrophosphate in 2-oxoacid oxidoreductases.” In: *Biochimica et biophysica acta* 1824 (Nov. 2012), pp. 1291–1298.
- [88] Cristina Furdul and Stephen W Ragsdale. “The roles of coenzyme A in the pyruvate:ferredoxin oxidoreductase reaction mechanism: rate enhancement of electron transfer from a radical intermediate to an iron-sulfur cluster.” In: *Biochemistry* 41 (Aug. 2002), pp. 9921–9937.

- [89] Stefan Schneider. “Functional characterization of transketolase-like proteins and related model systems with respect to thiamine diphosphate mediated chemistry.” PhD thesis. Georg-August-Universität Göttingen, 2013.
- [90] Erik Fiedler, Stina Thorell, Tatyana Sandalova, Ralph Golbik, Stephan König, and Gunter Schneider. “Snapshot of a key intermediate in enzymatic thiamin catalysis: Crystal structure of the  $\alpha,\beta$ -carbanion of ( $\alpha,\beta$ -dihydroxyethyl)-thiamin diphosphate in the active site of transketolase from *Saccharomyces cerevisiae*.” In: *Proceedings of the National Academy of Sciences* 99.2 (Jan. 2002), pp. 591–595.
- [91] H. Inoue, H. Nojima, and H. Okayama. “High efficiency transformation of *Escherichia coli* with plasmids.” In: *Gene* 96 (1 Nov. 1990), pp. 23–28.
- [92] Ryuichiro Suzuki, Byung-Jun Kim, Tsuyoshi Shibata, Yuki Iwamoto, Takane Katayama, Hisashi Ashida, Takayoshi Wakagi, Hirofumi Shoun, Shinya Fushinobu, and Kenji Yamamoto. “Overexpression, crystallization and preliminary X-ray analysis of xylulose-5-phosphate/fructose-6-phosphate phosphoketolase from *Bifidobacterium breve*”. In: *Acta Crystallographica Section F: Structural Biology and Crystallization Communications* 66.Pt 8 (July 2010), pp. 941–943.
- [93] M. M. Bradford. “A rapid and sensitive method for the quantitation of microgram quantities of protein utilizing the principle of protein-dye binding.” In: *Analytical biochemistry* 72 (May 1976), pp. 248–254.
- [94] U. K. Laemmli. “Cleavage of structural proteins during the assembly of the head of bacteriophage T4.” In: *Nature* 227 (5259 Aug. 1970), pp. 680–685.
- [95] Q. H. Gibson, B. E. Swoboda, and V. Massey. “Kinetics and mechanisms of action of glucose oxidase.” In: *The Journal of biological chemistry* 239 (Nov. 1964), pp. 3927–3934.
- [96] G. A. Kochetov. “Transketolase from yeast, rat liver, and pig liver.” In: *Methods in enzymology* (1982), pp. 209–223.
- [97] Fritz Lipmann and L. Constance Tuttle. “A specific micromethod for the determination of acyl phosphates.” In: *Journal of Biological Chemistry* 159.1 (1945), pp. 21–28.
- [98] Dan S. Tawfik and Ronald E. Viola. “Arsenate replacing phosphate - alternative life chemistries and ion promiscuity.” In: *Biochemistry* 50.7 (Feb. 2011), pp. 1128–1134.

- [99] Bernard Metz, Gideon F. A. Kersten, Peter Hoogerhout, Humphrey F. Brugghe, Hans A. M. Timmermans, Ad de Jong, Hugo Meiring, Jan ten Hove, Wim E. Hennink, Daan J. A. Crommelin, and Wim Jiskoot. "Identification of formaldehyde-induced modifications in proteins: reactions with model peptides". In: *The Journal of Biological Chemistry* 279.8 (Feb. 2004), pp. 6235–6243.
- [100] Gunter Schneider and Ylva Lindqvist. "Crystallography and mutagenesis of transketolase: mechanistic implications for enzymatic thiamin catalysis." In: *Biochimica et Biophysica Acta (BBA) - Protein Structure and Molecular Enzymology* 1385.2 (June 1998), pp. 387–398.
- [101] Matthew Merski and Craig A. Townsend. "Observation of an Acryloyl-Thiamin Diphosphate Adduct in the First Step of Clavulanic Acid Biosynthesis". In: *Journal of the American Chemical Society* 129.51 (2007). PMID: 18052280, pp. 15750–15751.
- [102] Mirko Paulikat, Cindy Wechsler, Kai Tittmann, and Ricardo A. Mata. "Theoretical Studies of the Electronic Absorption Spectra of Thiamin Diphosphate in Pyruvate Decarboxylase." In: *Biochemistry* 56.13 (2017). PMID: 28296385, pp. 1854–1864.
- [103] Christopher J. Halkides, Perry A. Frey, and John B. Tobin. "Rapid hydrogen exchange at the acetyl (C2) methyl group of acetylthiamine pyrophosphate". In: *Journal of the American Chemical Society* 115.8 (1993), pp. 3332–3333.
- [104] Matthew E.C. Caines, John L. Sorensen, and Christopher J. Schofield. "Structural and mechanistic studies on N2-(2-carboxyethyl)arginine synthase". In: *Biochemical and Biophysical Research Communications* 385.4 (2009), pp. 512–517.
- [105] Jean-Pierre Grill, Joel Crociani, and Jean Ballongue. "Characterization of fructose 6 phosphate phosphoketolases purified from *Bifidobacterium* species". In: *Current Microbiology* 31.1 (July 1995), pp. 49–54.
- [106] Michelle M. Kish and Ronald E. Viola. "Oxyanion Specificity of Aspartate-beta-semialdehyde Dehydrogenase." In: *Inorganic chemistry* 38 (4 Feb. 1999), pp. 818–820.
- [107] Christopher R. Faehnle, Julio Blanco, and Ronald E. Viola. "Structural basis for discrimination between oxyanion substrates or inhibitors in aspartate-beta-semialdehyde dehydrogenase." In: *Acta crystallographica. Section D, Biological crystallography* 60 (Pt 12 Pt 2 Dec. 2004), pp. 2320–2324.

- [108] Apirat Chaikuad and R. Leo Brady. “Conservation of structure and activity in Plasmodium purine nucleoside phosphorylases.” In: *BMC structural biology* 9 (July 2009), p. 42.
- [109] Paul C. Kline and Vern L. Schramm. “Purine nucleoside phosphorylase. Catalytic mechanism and transition-state analysis of the arsenolysis reaction”. In: *Biochemistry* 32.48 (1993). PMID: 8241176, pp. 13212–13219.
- [110] W. Dall’Acqua and P. Carter. “Substrate-assisted catalysis: molecular basis and biological significance”. In: *Protein Science: A Publication of the Protein Society* 9.1 (Jan. 2000), pp. 1–9.
- [111] T. Schweins, R. Langen, and A. Warshel. “Why have mutagenesis studies not located the general base in ras p21.” In: *Nature structural biology* 1 (7 July 1994), pp. 476–484.
- [112] J. J. Perona, M. A. Rould, and T. A. Steitz. “Structural basis for transfer RNA aminoacylation by Escherichia coli glutaminyl-tRNA synthetase”. In: *Biochemistry* 32.34 (Aug. 1993), pp. 8758–8771.
- [113] J. Cavarelli, G. Eriani, B. Rees, M. Ruff, M. Boeglin, A. Mitschler, F. Martin, J. Gangloff, J. C. Thierry, and D. Moras. “The active site of yeast aspartyl-tRNA synthetase: structural and functional aspects of the aminoacylation reaction”. In: *The EMBO journal* 13.2 (Jan. 1994), pp. 327–337.
- [114] A Jeltsch, M Pleckaityte, U Selent, H Wolfes, V Siksnys, and A Pingoud. “Evidence for substrate-assisted catalysis in the DNA cleavage of several restriction endonucleases.” In: *Gene* 157 (1-2 May 1995), pp. 157–162.
- [115] B.L. Horecker, Orestes Tsolas, and C.Y. Lai. “6 Aldolases”. In: *The Enzymes* 7 (1972), pp. 213–258.
- [116] Pere Clapés, Wolf-Dieter Fessner, Georg A. Sprenger, and Anne K. Samland. “Recent progress in stereoselective synthesis with aldolases.” In: *Current opinion in chemical biology* 14 (2 Apr. 2010), pp. 154–167.
- [117] Claire L. Windle, Marion Müller, Adam Nelson, and Alan Berry. “Engineering aldolases as biocatalysts.” In: *Current opinion in chemical biology* 19 (Apr. 2014), pp. 25–33.
- [118] Yufeng Miao, Mehran Rahimi, Edzard M. Geertsema, and Gerrit J. Poelarends. “Recent developments in enzyme promiscuity for carbon-carbon bond-forming reactions.” In: *Current opinion in chemical biology* 25 (Apr. 2015), pp. 115–123.

- [119] Xiaodan Zhao, Kyle E. Ruhl, and Tomislav Rovis. “N-Heterocyclic-Carbene-Catalyzed Asymmetric Oxidative Hetero-Diels–Alder Reactions with Simple Aliphatic Aldehydes”. In: *Angewandte Chemie* 124.49 (2012), pp. 12496–12499.
- [120] Y. Poirier, C. Nawrath, and C. Somerville. “Production of polyhydroxyalkanoates, a family of biodegradable plastics and elastomers, in bacteria and plants.” In: *Nature Biotechnology* 13 (2 Feb. 1995), pp. 142–150.
- [121] H. B. Bürgi, J. D. Dunitz, and Eli Shefter. “Geometrical reaction coordinates. II. Nucleophilic addition to a carbonyl group”. In: *Journal of the American Chemical Society* 95.15 (1973), pp. 5065–5067.
- [122] H.B. Bürgi, J.D. Dunitz, J.M. Lehn, and G. Wipff. “Stereochemistry of reaction paths at carbonyl centres”. In: *Tetrahedron* 30.12 (1974), pp. 1563–1572.
- [123] Danilo Meyer, Lydia Walter, Geraldine Kolter, Martina Pohl, Michael Müller, and Kai Tittmann. “Conversion of Pyruvate Decarboxylase into an Enantioselective Carboligase with Biosynthetic Potential”. In: *Journal of the American Chemical Society* 133.10 (Mar. 2011), pp. 3609–3616.
- [124] Robert Westphal, Constantin Vogel, Carlo Schmitz, Jürgen Pleiss, Michael Müller, Martina Pohl, and Dörte Rother. “A Tailor-Made Chimeric Thiamine Diphosphate Dependent Enzyme for the Direct Asymmetric Synthesis of (S)-Benzoin”. In: *Angewandte Chemie International Edition* 53.35 (Aug. 2014), pp. 9376–9379.
- [125] Cara A. Tracewell and Frances H. Arnold. “Directed enzyme evolution: climbing fitness peaks one amino acid at a time.” In: *Current opinion in chemical biology* 13 (1 Feb. 2009), pp. 3–9.
- [126] Karl Hult and Per Berglund. “Enzyme promiscuity: mechanism and applications”. In: *Trends in Biotechnology* 25.5 (May 2007), pp. 231–238.
- [127] Olga Khersonsky, Cintia Roodveldt, and Dan S. Tawfik. “Enzyme promiscuity: evolutionary and mechanistic aspects”. In: *Current Opinion in Chemical Biology. Analytical techniques / Mechanisms* 10.5 (Oct. 2006), pp. 498–508.
- [128] Ulrika Nilsson, Laurence Hecquet, Thierry Gefflaut, Christine Guerard, and Gunter Schneider. “Asp477 is a determinant of the enantioselectivity in yeast transketolase”. In: *FEBS Letters* 424.1-2 (Mar. 1998), pp. 49–52.

## Acknowledgment

First and most of all, I want to thank my supervisor PROF. DR. KAI TITTMANN for introducing me into the fascinating world of enzymology, for his never-ending wealth of scientific ideas, for patiently answering all of my question, for solving every big and small (kinetic) problem I encountered during my experiments and for providing the infrastructure and great working atmosphere that allowed me to prepare this thesis over the last three years.

Furthermore I want to thank PROF. DR. RALF FICNER not only for taking over the duty as second reviewer and member of my thesis committee, but also for support in all organizational issues in Kai's absence and for generous access to the facilities in his department.

My special thanks also go to PROF. DR. RICARDO MATA for being member of my thesis committee and for a very fruitful collaboration on the phosphoketolase project for which he and his PhD student MIRKO PAULIKAT provided extensive computational data that really are a cornerstone of the present work.

I am grateful to PROF. DR. HOLGER STARK, DR. MANFRED KONRAD and DR. FABIAN COMMICHAU for being part of the extended examination board.

I would like to thank DR. TILL ISCHEBECK and SABINE FREITAG for greatly supporting me with the GC-MS analysis. In this regard I also want to thank PROF. DR. IVO FEUSSNER for generous access to the facilities of his department.

I am extremely grateful to my colleagues from the Department of Molecular Enzymology for three fantastic years in the lab. Special thanks go to VIKTOR SAUTNER for valuable advice and input on the draft of this thesis and for profound and fun scientific discussions. Thank you FABIAN RABE VON PAPPENHEIM and SABIN PRAJAPATI for proofreading the thesis. Thanks SÖREN RINDFLEISCH also for proofreading and for solving all LaTeX problems. I furthermore would like to thank ELKE PENKA and LISA-MARIE FUNK for technical assistance and keeping up gender equality. Thanks also to my Bachelor and lab rotation students DAVID KUHS and GEORG VON MASSOW for their help in characterizing some of the phosphoketolase variants. Moreover I am very thankful to my former colleague DR. FLORIAN BRODHUN for his support in all sorts of

things at the beginning of my PhD, I would always share an office and a Spotify account with you again.

Furthermore I want to thank SVEN J., FLO, MARCEL, JOHANNES, ACHIM, DIMITRIJ, SVEN H., ELLEN and all other members of the Department of Molecular Structural Biology and the Department of Plant Biochemistry for uncomplicated "neighborly help" at all times.

Many thanks go to the members of the DFG Research Group 1296 for fruitful scientific discussion, special thanks on this way to PROF. DR. MICHAEL MÜLLER who provided valuable input on the carboligation project.

I especially want to acknowledge the awesome work of the GGNB Team.

In the end I want to express my deepest gratitude to my family. Without your moral and financial support none of this would have been possible.

Last but not least, thank you JULIA, LENA H., SEBI, all other members of the KöWo 30 gang, HANNAH, LENA B., SONJA and SVEN for your friendship, your endless encouragement and for provision of coffee, redwine and a home whenever needed.

## Curriculum vitae

### PERSONAL DATA

---

Name : Fabienne Libuda  
Date of birth : 08.12.1987  
Place of birth : Ostercappeln  
Address : Rosdorfer Weg 19a, 37073 Göttingen  
Email : flibuda@gwdg.de

### EDUCATION

---

09/2014 - present      PhD student, University of Göttingen, GGNB graduate program  
Thesis: "Phosphoketolase - A mechanistic update"  
Department of Molecular Enzymology, University of Göttingen,  
Prof. Dr. Kai Tittmann

10/2010 - 06/2013      Master of Science in Biochemistry, Hannover Medical School  
Thesis: "Heterologous expression of different variants of the  
apoptotic protein Apaf-1"  
Department of Biophysical Chemistry, Hannover medical school,  
Prof. Dr. Dietmar Mannstein, Dr. Susanne Eschenburg

10/2007 - 09/2010      Bachelor of Science in Biochemistry, University of Hannover  
Thesis: "Mesenchymal differentiation of adult stem cells"  
Department for Trauma Surgery, Hannover Medical School, Prof.  
Dr. Andrea Hoffmann

07/2000 - 06/2007      Abitur, Gymnasium Bad Essen

### PROFESSIONAL EXPERIENCE

---

09/2014 - present      Research Assistant  
Department of Molecular Enzymology, University Göttingen, Prof.  
Dr. Kai Tittmann



- 
- 11/2013 – 07/2014      Research Assistant  
Department of Microbiology and Immunology, University of Otago,  
New Zealand, Prof. Andrew Mercer, Dr. Lyn Wise
- 11/2011 - 02/2012      Research Intern  
Department of Microbiology and Immunology, University of Otago,  
Prof. Roslyn Kemp
- 06/2009 – 03/2013      Student Research Assistant  
Department of Physiological Chemistry and Department of  
Cellular Chemistry, Hannover Medical School

#### OTHER

---

- 09/2014 - present      Member of GGNB graduate programm *Biomolecules: Structure -  
Function - Dynamics*
- 09/2014 - 03/2017      Member of DFG research group 1296 *Diversity of Asymmetric  
Thiamine Catalysis*